Doctoral theses at NTNU, 2013:112

Severin Sadjina

Spin-Orbit-Induced Transport in Metals and Superconductors

Doctoral Thesis

Severin Sadjina

ISBN 978-82-471-4324-7 (printed version)
ISBN 978-82-471-4325-4 (electronic version)
ISSN 1503-8181

NTNU – Trondheim
Norwegian University of
Science and Technology

Doctoral theses at NTNU, 2013:112

NTNU
Norwegian University of Science and Technology
Thesis for the degree of Philosophiae Doctor
Faculty of Natural Sciences and Technology
Department of Physics

NTNU – Trondheim
Norwegian University of
Science and Technology

Severin Sadjina

Spin-Orbit-Induced Transport in Metals and Superconductors

Thesis for the degree of Philosophiae Doctor

Trondheim, March 2013

Norwegian University of Science and Technology
Faculty of Natural Sciences and Technology
Department of Physics

NTNU – Trondheim
Norwegian University of
Science and Technology

NTNU
Norwegian University of Science and Technology

Thesis for the degree of Philosophiae Doctor

Faculty of Natural Sciences and Technology
Department of Physics

ISBN 978-82-471-4324-7 (printed version)
ISBN 978-82-471-4325-4 (electronic version)
ISSN 1503-8181

Doctoral theses at NTNU, 2013:112

Printed by Skipnes Kommunikasjon as

Abstract

This thesis is devoted to the theoretical study of spin-orbit-induced transport in diffusive normal metals and superconductors. The spin-orbit interaction plays a vital role in the aspiring field of spintronics, which aims to utilize the electron spin with the ambition to enable a new generation of efficient and powerful electronic devices. It provides a link between the spin and charge degrees of freedom, couples spin currents of different polarizations, and leads to the dephasing of spin information.

We elucidate the nature of the spin swapping effect, where the spin polarization and the direction of flow are interchanged due to spin-orbit coupling, and demonstrate that an intrinsic analog to the previously predicted extrinsic spin swapping effect can be induced by Rashba spin-orbit coupling in two-dimensional diffusive metals. Unlike its extrinsic counterpart, intrinsic spin swapping is a strong effect and results in a nontrivial relation between the injected spin flow and the spin polarization. Moreover, a long-range spin swapping effect takes place in narrow strips with intrinsic spin-orbit coupling.

Rich and interesting physics emerge when the useful properties of superconductors are combined with spin generation and manipulation. We study in detail spin relaxation due to magnetic impurity scattering and spin-orbit coupling, skew scattering, the side-jump mechanism, and the spin swapping effect. Employing the quasiclassical theory of superconductivity, we derive kinetic equations describing the transport of spin, charge, and energy in diffusive superconductors, and investigate how the various mechanisms are influenced by superconducting correlations. We find that the spin Hall angle is renormalized by the superconducting density of states and that the spin swapping constant is renormalized implicitly through generalized diffusion coefficients.

Additionally, we consider an inverse spin Hall effect occurring due to the

interplay between Rashba spin-orbit coupling and Zeeman fields in S|N|S Josephson junctions in thermal equilibrium. This combination induces an effective vector potential in the normal conductor and gives rise to a supercurrent, in analogy to the Meissner effect. Spin-orbit coupling also diminishes the depairing effects of strong Zeeman fields and leads to a long-range propagation of ± 1 triplet components on the scale of the spin-orbit precession length, providing a link between the two superconducting terminals.

It is the aim of this thesis to contribute to a fundamental understanding of the physical properties of nanoscaled condensed matter systems, obtain results that may inspire further research, and thereby aid the development of novel and improved technologies in the promising field of spintronics.

Preface

This thesis is submitted to the Norwegian University of Science and Technology (NTNU) as part of the requirements for the degree of Philosophiae Doctor. It concludes the work conducted during four years at the Department of Physics at NTNU under the supervision of Professor Arne Brataas. This period includes the equivalent of one year of full-time teaching work and the equivalent of half a year of full-time coursework. The research has been funded by the Research Council of Norway (NFR) through the project "Magnetodynamics of Nanostructured Metal Oxides" (grant no. 182037).

This thesis consists of two parts: In the first part, we will provide a short introduction to the research field and a discussion of the motivation for our research. In addition, we present some of the results we obtained and give an overview of the underlying theoretical concepts that were used. The main part of our research is then presented in the second part, where the papers resulting from my Ph.D. work are appended.

Severin Sadjina

Trondheim, February 2013

Acknowledgements

Not only does this thesis conclude my doctoral studies at NTNU, it also marks the end of four exciting and challenging years in Trondheim. I have enjoyed the company of people whose support and kindness made my Ph.D. work and my life in general as inspirational and delightful as I could imagine.

First and foremost, I wish to express my gratitude to my supervisor Arne Brataas for his dedicated and invaluable guidance and inspiration. I am deeply indebted to him for the opportunity to attend interesting conferences and schools in Norway and abroad, to meet leading scientists in our field, and to work on interesting and challenging problems. I also wish to thank Anatoly Malshukov for a very fruitful collaboration. His enthusiasm, knowledge, and patience have been highly beneficial to me. In addition, my colleagues and friends at the department of physics have provided me with a most pleasant working environment. I would especially like to thank Håvard Haugen, Swarnali Bandopadhyay, Lars Husdal, Alireza Qaiumzadeh, William Naylor, and Hans Skarsvåg, with whom I have had the great pleasure of sharing offices with, Lars Erlend Leganger, Lars Tandle Kyllingstad, Arturo Amador Cruz, Peder Notto Galteland, and Erlend Grytli Tveten. All the lunch and coffee breaks, the discussions, the cabin trips, and the conference experiences I have shared with you are greatly appreciated!

I am also deeply grateful to my parents, Christine Sadjina-Höfer and Kurt Sadjina, who have inspired and encouraged me to follow my path in life and who have constantly provided me with sustained love, support, and nourishment. Fond appreciation is due also to my brother and my parents-in-law. Thanks for all your support and love!

Last, but not least, I thank my best friend and partner, Emily Christin Kershaw, whose omnipresent love, support, and patience I will forever cherish. I consider myself very glad and lucky to have you in my life!

List of Papers

Paper [1]
A. G. Mal'shukov, S. Sadjina, and A. Brataas.
Inverse spin hall effect in superconductor/normal-metal/superconductor josephson junctions.
Phys. Rev. B, 81:060502, 2010.

Paper [2]
S. Sadjina, A. Brataas, and A. G. Mal'shukov.
Intrinsic spin swapping.
Phys. Rev. B, 85:115306, 2012.

Paper [3]
S. Sadjina, A. Brataas, and A. G. Mal'shukov.
Extrinsic spin-orbit induced spin, charge, and energy transport in diffusive superconductors.
Preprint, 2013.

My Contribution to the Papers

I have contributed substantially to all parts of the two papers where I am listed as the first author, i.e. Papers [2] and [3]. In these papers, I have carried out the analytical and the numerical calculations, generated the figures, and I am the main author of the text. The analytical calculations in Section III of Paper [2] were carried out by the third author. In Paper [1], where I am listed as the second author, I was involved in parts of the calculations and I generated the figures. The model formulation and the interpretation of the results is mainly the work of the first author.

Contents

List of Figures

1 Introduction

Developments and discoveries in science and technology have been following a steep, for most parts exponential, path for a long time. This is illustrated well by the history of modern electronics. In 1965, Moore [4] postulated that the number of transistors and resistances on integrated circuits per unit area would double every two years. This seemingly bold prediction has proven to be uncannily accurate ever since, and has set the frame for fast-paced research and development in the electronics industry. The density with which elementary components are being crammed into computer chips or memory storage devices has reached mind-boggling proportions, with more than six million transistors[1] fitting in the period at the end of this sentence. Obviously, growth at an exponential rate is impossible to maintain, and in the case of Moore's law the semiconductor industry should expect to be facing serious issues of elementary nature sometime within the next ten to fifteen years [5]. Most notably, the miniaturization of components to boost performance has apparent physical limits, under which electron motion can not be controlled any longer due to quantum mechanical effects, such as tunneling. On the other hand, Joule heating sets an upper bound to component lifetime and viability. A surprising observation in light of impending difficulties is the excessive focus on the electron *charge*.

In 1928, Dirac [6] showed that the electron does not only possess a mass and a charge, but also an intrinsic angular momentum, which has its roots in relativistic quantum mechanics: the *spin*. That this is not just an abstract mathematical concept, but has the potential to establish a new generation of electronics, is manifested in the emerging field of *spintronics*.

[1] Recent Intel 22 nm tri-gate manufacturing process.

1.1 Spintronics

Spintronics is a relatively new area of condensed matter physics that studies the properties of electron spin and aims to exploit them with the promise of increased speed, decreased power consumption, and further miniaturization of electronic devices. The birth of spintronics is often linked to the observation that the electric resistance of alternating layers of magnetic and nonmagnetic metals can change by a large amount when a magnetic field is applied. This giant magnetoresistive effect (GMR) was independently discovered by Fert and Grünberg in 1988, who shared the 2007 Nobel Prize in Physics for their discovery [5]. It was realized shortly after that the GMR was controllable through the thickness of the interlayers [7], which would pave the way for a commercial use and help store vast amounts of data on mobile electronic devices, such as music players and notebooks. In 1990, Datta and Das [8] presented their concept of a spin field effect transistor, which serves as a well-suited example for the potential of spintronic devices: The spin transistor's structure is quite similar to a conventional transistor, but while the latter utilizes the gate voltage to influence electron motion, its spintronic analog uses its gate voltage to modify electron spin through a controlled spin precession. This spin manipulation holds the promise of being far less energy costly, more efficient, and providing faster switching times. Recently, Walser *et al.* [9] observed an increase in the spin lifetime of synchronized electrons in a persistent spin helix (PSH) by a factor of 30, preserving the spin-encoded information for longer than one nanosecond.[2]

To think that spintronics is purely an application-based field, however, would be a fallacy. It also relies heavily on a fundamental understanding of the properties of the electron spin and its transport, and provides new chances to explore the quantum character of matter.

1.2 Spin-Orbit Coupling

One mechanism that is essential by nature to the development of spintronics is the *spin-orbit interaction*, because it links the charge and spin degrees of freedom. In its presence, an initially unpolarized current acquires a spin polarization, but it also leads to the dephasing of spin information. It

[2] One nanosecond is a billionth of a second and might not appear overly impressive to a reader not familiar with the physics of the nanoworld. But it is about the time it takes the processor of a modern mobile phone to cycle.

therefore plays an important role in all of the three main fields of spintronics research: spin injection, spin control and manipulation, and spin detection. Following the convention used by Engel *et al.* [10], the mechanisms of spin-orbit coupling can be classified into two categories:[3] i) *Extrinsic* effects are due to the presence of extrinsic impurities, while ii) *intrinsic* effects are inherent in the band structure and remain finite even in the absence of extrinsic impurities.

The aforementioned coupling between charge and spin is provided by the *spin Hall effect*, and is a remarkable demonstration of the influence of spin-orbit coupling on electron transport. It was predicted in 1971 by Dyakonov and Perel [11, 12], who realized that an unpolarized electric current leads to a transverse spin-polarized current in systems with extrinsic spin-orbit coupling. Similarly, a spin current gives rise to a transverse electric current in the inverse effect. Over 30 years later, Murakami *et al.* [13] and Sinova *et al.* [14] predicted the intrinsic spin Hall effect, which results from intrinsic spin-orbit coupling, and triggered an intense theoretical debate, see Refs. [10, 15, 16] and references therein. The number of experimentally realized spin Hall devices has increased considerably in recent years.[4] This helped to establish the relevance of the spin Hall effect in the field of spintronics, demonstrating its utility as an electric or optical spin injector and detector in nonmagnetic systems. Metal-based spin Hall devices [18, 19] have demonstrated that nonmagnetic electrodes can be used for spin generation and detection [20]. In semiconductors, the attention has been focused on optical detection [21, 22, 23], and it was realized that the inverse spin Hall effect facilitates the direct electric detection of the polarization of light by generating electric currents from optically induced pure spin currents [24, 25]. Some devices combine electric spin detection through the inverse spin Hall effect with an electric manipulation of the spin-orbit interaction [26, 27], which could constitute an important step towards the realization of a spin field effect transistor.

Recently, graphene layer systems and surface-state systems in three-dimensional topological insulators have caught the attention of spintronics research.[5] The electron properties in these systems are closely related, but while spin-orbit coupling is weak in graphene, it is strong in topological in-

[3] We shall use this classification throughout this thesis for consistency.

[4] For a recent overview of spin Hall effect devices and experimental realizations, see Jungwirth *et al.* [17] for instance.

[5] A recent account of past and ongoing research in these systems can be found in Refs. [28, 29] and references therein.

sulator surface systems. The spintronics potential for graphene is given as an unusually efficient spin conservator, providing extreme long-range propagation of spin information [30, 31]. Topological insulator surface systems, on the other hand, hold the promise of efficient tools for spin generation via the spin Hall effect [32], for example.

Aside from the coupling of charge and spin provided by the spin Hall effect, the spin-orbit interaction also creates a link between spin currents of different polarizations. This so-called 'spin swapping' effect was first predicted by Lifshits and Dyakonov [33] in systems with extrinsic spin-orbit coupling. In its simplest manifestation, spin swapping interchanges the spin current flow direction and its polarization direction. In a sample, this gives rise to the accumulation of 'swapped' spin polarizations at the lateral edges when a spin current is injected. A deeper understanding of the spin-orbit coupling also motivated the research presented in Paper [2], where we demonstrate that the spin swapping effect also exists in two-dimensional metals with intrinsic Rashba spin-orbit coupling, and in Paper [3], where we study the spin Hall effect and spin swapping in superconductors in detail.

1.3 Superconductivity

In 1911, the same year in which Rutherford discovered the atomic nucleus, Onnes [34] made the remarkable observation that the electric resistance of solid mercury completely vanishes[6] below a sharply defined temperature of around 4.2 K. Soon after, lead and tin joined the list of materials to exhibit this strange and intriguing behavior below a certain temperature, and many more would follow. This property of *perfect conductance* is one of nature's most fascinating phenomena, because it so fundamentally contradicts our common sense conception of the characteristics of macroscopic physical systems. Electric currents set up inside *superconducting* rings have been observed to persist for one year without any measurable decay [36], implying that the time it would take for the current to completely vanish could be as long as, or even longer than, the estimated age of the universe [35]. The next breakthrough in understanding superconductivity occurred in 1933, when Meissner and Ochsenfeld [37] discovered that magnetic field lines are spon-

[6] Strictly speaking, it is impossible to measure zero resistance or, alternatively, infinite conductance. Rather, a drop of several orders of magnitude in the resistance was detected. Onnes himself held on to the belief that a tiny resistance would remain below the superconducting critical temperature [35].

taneously expelled from the interior of a superconducting material when it is cooled below its critical temperature. This meant that superconductivity could no longer be attributed to perfect conductance alone, but instead constitutes a new thermodynamic state characterized also by *perfect diamagnetism*.

The first theoretical description of superconductivity emerged in 1935, when London and London [38] showed that the Meissner effect discovered two years earlier is due to a minimization of the free energy carried by superconducting current. What was lacking, however, was a theory formulated from first principles. Based on important insights gained by Maxwell [39] and Reynolds *et al.* [40], a complete microscopic theory of superconductivity was finally presented 46 years after Onnes' discovery of perfect conductance by Bardeen, Cooper and Schrieffer [41], who were able to explain the phenomenon in terms of an effective attractive interaction between electrons mediated by phonons. According to their theory, the ground state becomes unstable below the critical temperature, and electrons of opposite spins start forming so-called Cooper pairs, which experience a gap in their energy spectrum. For sufficiently low temperatures, the thermal energy of the lattice is smaller than this energy gap, and no interaction between the Cooper pairs and the lattice can take place. Consequently, the condensate becomes a superfluid and all traces of electric resistance vanish. Superconductivity is thus a purely quantum mechanical phenomenon on a macroscopic scale, based on the phase coherence of the many-body wave function. In 1959, Gor'kov [42] formulated the theory of superconductivity in terms of Green's functions and further helped the BCS model to become a powerful tool for the theoretical study of superconductivity. Eilenberger [43] contributed with important improvements, introducing a quasiclassical scheme based on the realization that the energies involved are typically much smaller than the Fermi energy. This allowed for a greatly simplified treatment of a wide range of phenomena and resulted in more intuitive transport-like equations.

In 1962, Josephson [44] discovered that when two superconductors are connected by a weak link, they are able to sustain a supercurrent, induced by a difference in the phases of their macroscopic wave functions, without any applied voltage. A weak link can, for instance, consist of an insulating material (S|I|S) or a normal metal (S|N|S). This discovery, for which Josephson was awarded the 1973 Nobel Prize in Physics, lead to a wide range of applications for Josephson junctions. Nowadays, superconductors are able to provide significant improvements over alternative methods, or enable applications that would not even be possible without superconduc-

tivity. One of the most notable implementations of *Josephson junctions* are superconducting quantum interference devices (SQUIDs), which offer the most accurate detection and measurement of magnetic fields. SQUIDs are, for instance, used in mobile phone base stations or to conduct noninvasive studies of brain activity [35]. On large scales, superconductors facilitate high-capacity power lines and the use of large magnetic fields for medical, scientific, and industrial purposes.

1.4 Superspintronics

Interesting and rich physics occurs when superconductors, in which the movement of electrons is dissipationless and the ground state exhibits macroscopic coherence, and nonsuperconducting materials are combined. Within the field of spintronics, superconductors offer possibilities to enhance effects, utilize novel phenomena, or retrieve information on physical processes that would not be accessible in the normal state.

There has been a growing interest in spin injection into superconductors in order to investigate the interplay between superconductivity and spin accumulation [45, 46, 47, 48]. Superconducting correlations cause various spin transport mechanisms to become temperature dependent. In nonlocal geometries, which allow the study of spin transport properties in the absence of charge currents, a great enhancement in the spin signal below the superconducting critical temperature has been reported [49, 50]. In the elastic transport regime, the nature of spin-flip processes determines their temperature dependence in the superconducting state and facilitates a spin-flip spectroscopy [49], in order to determine which mechanism is more efficient.

The interplay of magnetism and superconductivity also has attracted considerable attention. The *proximity effect* arises when magnetic materials are brought in contact with superconductors and cause the suppression of superconductivity through the exchange interaction. These exchange effects can be mitigated by the insertion of ultrathin tunnel junctions, allowing an efficient injection of spin-polarized currents into superconductors [51, 46]. Aluminum layers sandwiched between ferromagnetic electrodes with magnetic tunnel junctions exhibit a giant increase in the spin lifetime below the critical superconducting temperature, as demonstrated recently by Yang *et al.* [48]. In superconducting spin switches, where a superconductor is sandwiched between two ferromagnet, the critical temperature is determined by the magnetization configuration [52]. On the other hand, a strong size

and temperature dependence of the magnetization-dependent resistance is found in F|S|F spin valves [53]. The contest between the ferromagnetic and superconducting order parameters also leads to some unusual effects in S|F structures. While singlet components of the Cooper condensate decay fast inside the adjacent ferromagnet, the triplet components exhibit a long-range propagation and lead to a significant increase of the ferromagnet conductance below the superconducting critical temperature [54].

Some superconductivity-induced features of the spin Hall effect originating from intrinsic spin-orbit coupling were studied theoretically in s-wave bulk superconductors [55], and in S|N|S Josephson junctions [56]. Another example of the coupling between charge and spin that the spin Hall effect provides is the generation of supercurrents through the interplay of spin-orbit coupling and magnetic fields in thermal equilibrium in S|N|S Josephson junctions. In addition, this interplay also facilitates a long-range propagation of spins through the system. Paper [1] is devoted to the study of these effects.

In the inelastic transport regime, a great enhancement of the extrinsic spin Hall effect signal in nonlocal geometries has been predicted by Takahashi and Maekawa [57, 47, 50]. It is interesting to examine how the extrinsic spin Hall effect is renormalized by superconductivity in the elastic transport regime, and whether a spin swapping effect also exists in the superconducting state. This problem inspired the research in Paper [3], where we derive spin, charge, and energy transport equations based on a quasiclassical approach and study the superconducting renormalizations of the spin Hall effect and the spin swapping effect in the presence of extrinsic spin-orbit coupling.

1.5 Outline

This thesis is organized as follows: We first give an overview of the quasiclassical theory of superconductivity in Chapter 2 which is our most important theoretical tool for studying spin transport. In Chapter 3, we then introduce and discuss relevant spin transport mechanisms. The ensuing chapters are devoted to the effects and systems that we consider and present some of the main results: In Chapter 4, we discuss spin transport in diffusive superconductors and study how the spin swapping effect and the spin Hall effect are influenced by superconducting correlations. Next, we elucidate the intrinsic spin swapping effect and compare it to its extrinsic analog in Chapter 5. Lastly, we investigate how the interplay of intrinsic spin-orbit

coupling and magnetic fields gives rise to an equilibrium inverse spin Hall effect in S|N|S Josephson junctions in Chapter 6. A conclusion and some personal thoughts on the outlook of the research is appended to the end of each chapter.

2 Theoretical Formalism

The main theoretical tool that we employ in this thesis, is the quasiclassical theory of superconductivity in terms of nonequilibrium Keldysh Green's functions. While the presence of disorder and impurities practically prohibits the exact quantum mechanical description of transport in nanoscale systems, the traditional semiclassical approach centered around the Boltzmann equation fails to describe coherence-dependent phenomena, such as superconductivity. Green's functions, on the other hand, are exact quantum mechanical objects containing information on coherence, while disregarding small-scale information that is irrelevant for the calculation of macroscopic properties. The present chapter is meant to provide an overview of the quasiclassical theory of superconductivity, to introduce relevant concepts, and to lay the groundwork for subsequent chapters. More comprehensive reviews can be found in, for example, Refs. [58, 59, 60, 61, 62] and references therein.

2.1 Quasiclassical Theory of Superconductivity

In order to describe a nonequilibrium system, the distribution of nonequilibrium excitations and their spectra need to be known. With respect to the Green's function formalism, all the different tasks for studying nonequilibrium transport boil down to finding the time-dependent Green's function of the system. A general difficulty is the lack of a proper time-ordering procedure in the definition of the real-time Green's functions for superconducting systems. So far, two equivalent methods have been worked out to resolve this issue and obtain real-time Green's functions: the theory developed by Gor'kov and Eliashberg [63, 64] utilizes the Matsubara technique and an analytic continuation from imaginary to the real-time frequencies,

while the method due to Keldysh [65] uses real-time Green's functions directly together with special ordering rules and provides a relatively simple and transparent description of nonequilibrium superconductivity. Both are well suited to the study of nonequilibrium transport in mesoscopic superconductors. Here, we shall focus on the Keldysh Green's function formalism for dirty superconductors, where strong elastic impurity scattering renders the Green's function almost isotropic.

2.1.1 Green's Functions

The starting point when deriving kinetic equations for a dirty superconductor is the definition of Green's functions in terms of quantum statistical averages of field operators in the Nambu-Gor'kov formalism. To this end, it is convenient to introduce a 4-component vector notation,

$$\hat{\psi}^\dagger(1) = (\psi_\uparrow^\dagger(1), \psi_\downarrow^\dagger(1), \psi_\uparrow(1), \psi_\downarrow(1)), \tag{2.1}$$

where ψ_σ is the field annihilation operator for spin σ, and $1 = (\boldsymbol{r}_1, t_1)$ is comprised of the spatial and temporal coordinates. This allows us to define superconducting Green's functions in a similar fashion as the Green's functions for a conventional conductor [59]. In this sense, a natural[1] definition of the retarded Green's function is

$$\hat{G}^{\mathrm{R}}_{ij}(1, 1') = -\mathrm{i}\Theta(t_1 - t_{1'}) \sum_k (\hat{\tau}_3)_{ik} \big\langle \big[\hat{\psi}_k(1\,),\, \hat{\psi}_j^\dagger(1')\big]_+ \big\rangle, \tag{2.2a}$$

where $\Theta(t)$ is the Heaviside step function, $\langle \dots \rangle$ denotes a quantum statistical average, and $[A, B]_\pm = AB \pm BA$. Furthermore, we introduced a generalization of the third Pauli matrix $\hat{\tau}_3 = \mathrm{diag}(1, 1, -1, -1)$. Similarly, the advanced Green's function is defined as

$$\hat{G}^{\mathrm{A}}_{ij}(1, 1') = \mathrm{i}\Theta(t_{1'} - t_1) \sum_k (\hat{\tau}_3)_{ik} \big\langle \big[\hat{\psi}_k(1\,),\, \hat{\psi}_j^\dagger(1')\big]_+ \big\rangle. \tag{2.2b}$$

These Green's functions are 4×4 matrices in spin $\otimes$ particle-hole space. We denote such matrices with a 'hat' superscript (see Appendix A.4). Generally speaking, the retarded and the advanced Green's functions contain information on the spectral properties of the system. For example, they

[1] Our choice of definition for the Green's functions is by no means unique, and numerous other definitions exist. Physical observables are, of course, independent of this choice, which boils down to personal preference and convenience with regard to the system one aims to study.

determine the energy dependence of the density of states in the superconducting state and how various transport mechanisms, such as diffusion or spin relaxation, are renormalized below the superconducting critical temperature, as we shall see in later chapters. The Keldysh Green's function is defined as

$$\hat{G}^{\mathrm{K}}_{ij}(1,1') = -\mathrm{i}\sum_k (\hat{\tau}_3)_{ik}\langle[\hat{\psi}_k(1), \hat{\psi}^\dagger_j(1')]_-\rangle \tag{2.2c}$$

and determines the kinetic properties of the system, such as the currents and the distribution functions.

Using the Heisenberg equation of motion for the field operators ψ_σ and $\psi^\dagger_\sigma$, an equation of motion is derived for the pseudo-spinor $\hat{\psi}$:

$$(\hat{\tau}_3 \mathrm{i}\partial_{t_1} - \hat{\mathcal{H}}(1))\hat{\psi}(1) = 0. \tag{2.3}$$

The Hamiltonian for a diffusive superconductor is

$$\hat{\mathcal{H}}(1) = -\hat{1}\frac{1}{2m}\partial^2_{\boldsymbol{r}_1} - \hat{1}\mu + \hat{\Delta}(1) + \hat{U}_{\mathrm{tot}}(\boldsymbol{r}_1), \tag{2.4}$$

where μ is the electrochemical potential, $\hat{U}_{\mathrm{tot}}$ is the local potential, and we introduced the identity matrix in particle-hole space $\hat{1}$. It is beneficial to choose a gauge where the superconducting order parameter

$$\Delta(1) = \lambda(\boldsymbol{r}_1)\langle\psi_\downarrow(1)\psi_\uparrow(1)\rangle \tag{2.5a}$$

is a real quantity. Here, λ is the interaction strength. Superconducting correlations are then described via the gap matrix

$$\hat{\Delta}(1) = \begin{pmatrix} 0 & 0 & 0 & \Delta(1) \\ 0 & 0 & -\Delta(1) & 0 \\ 0 & \Delta(1) & 0 & 0 \\ -\Delta(1) & 0 & 0 & 0 \end{pmatrix}. \tag{2.5b}$$

We include the effects of elastic impurity scattering

$$\hat{U}(\boldsymbol{r}) = \hat{1}\sum_i u(\boldsymbol{r} - \boldsymbol{r}_i) \tag{2.6}$$

in the local potential $\hat{U}_{\mathrm{tot}}$. Here, $u(\boldsymbol{r} - \boldsymbol{r}_i)$ is the i^{th} elastic scattering potential at position $\boldsymbol{r}_i$. In Chapter 3, we will in addition include magnetic impurity scattering and spin-orbit coupling.

By constructing an 8×8 Green's function matrix in spin $\otimes$ particle-hole $\otimes$ Keldysh space,

$$\check{G} = \begin{pmatrix} \hat{G}^{\mathrm{R}} & \hat{G}^{\mathrm{K}} \\ \hat{0} & \hat{G}^{\mathrm{A}} \end{pmatrix}, \tag{2.7}$$

and using Eqs. (2.2) and (2.3), the equation of motion for the thus defined Green's function matrix can be cast in a rather compact form:

$$(\hat{\tau}_3 \mathrm{i}\partial_{t_1} - \hat{\mathcal{H}}(1))\check{G}(1,1') = \check{1}\delta(1-1'). \tag{2.8}$$

Here, $\check{1}$ is the identity matrix in Keldysh space. Such matrices are denoted with a 'check' superscript. This equation of motion provides an exact quantum mechanical description of nonequilibrium transport down to the atomic level. Using it directly to treat real systems, though not impossible, usually proves rather cumbersome due to the unessential and redundant information it contains. Moreover, the presence of impurities causes the Green's function to oscillate rapidly on length scales of the Fermi wavelength λ_{F} as a function of the relative coordinate $\boldsymbol{r} = \boldsymbol{r}_1 - \boldsymbol{r}_{1'}$. Eq. (2.8) is, however, a natural starting point for approximations in order to obtain simplified equations.

2.1.2 The Quasiclassical Approximation

Fortunately, the short-ranged oscillations contained in the relative coordinate $\boldsymbol{r}$, which are due to the specific microscopic properties of a given system, are irrelevant for the calculation of the macroscopic properties, which are governed by the features of the nonequilibrium state. This means that we can make use of the so-called gradient approximation and expand the Green's function in terms of a Taylor series in the relative coordinates $\boldsymbol{r}$ and $t = t_1 - t_{1'}$ around the center-of-mass coordinates $\boldsymbol{R} = (\boldsymbol{r}_1 + \boldsymbol{r}_{1'})/2$ and $T = (t_1 + t_{1'})/2$. To this end, it is convenient to shift the frame of reference to the center-of-mass coordinates and perform a Fourier transformation in the relative coordinates (see Appendix A.1). In order to study stationary transport in bulk superconductors and superconducting hybrid structures, it is generally sufficient to keep only zeroth order terms in the expansion. In addition, to describe nonequilibrium superconductivity one is interested in quasiparticles with a momentum around the Fermi momentum $\boldsymbol{p}_{\mathrm{F}}$. Consequently, the Green's function's weak dependence on the magnitude of the momentum can be eliminated by integrating over the kinetic energy $\xi_p = p^2/2m$ while preserving the relevant dependence on the direction of the velocity $\boldsymbol{v}_{\mathrm{F}} = \boldsymbol{p}_{\mathrm{F}}/m$. This is known as the quasiclassical

approximation. It allows for a greatly simplified treatment of a wide range of phenomena and results in more intuitive transport-like equations, as we shall see in Chapter 4.

2.1.3 Impurity Average and Self-Energy

In developing a quasiclassical theory in which quantities do not depend on the properties of a specific sample, we need to replace the Green's function and the local potential by average quantities that are defined on length scales much larger than the impurity mean free path l_{tr} and independent of a particular impurity configuration. The effects of the local potential are then included in the self-energy. Within the self-consistent Born approximation it is calculated from, see Fig. 2.1(a),

$$\check{\Sigma}(1,1') = \langle \hat{U}_{\mathrm{tot}}(\boldsymbol{r}_1)\check{G}_{\mathrm{c}}(1,1')\hat{U}_{\mathrm{tot}}(\boldsymbol{r}_{1'})\rangle_{\mathrm{c}}, \tag{2.9}$$

where $\langle \dots \rangle_{\mathrm{c}}$ denotes averaging over all possible impurity configurations, and $\check{G}_{\mathrm{c}} = \langle \check{G} \rangle_{\mathrm{c}}$ is the impurity-averaged Green's function matrix of Eq. (2.7). The self-energy (2.9) only includes irreducible diagrams, in other words, we assume that scattering potentials are uncorrelated and demand that $\langle \hat{U}_{\mathrm{tot}} \rangle_{\mathrm{c}} = 0$.

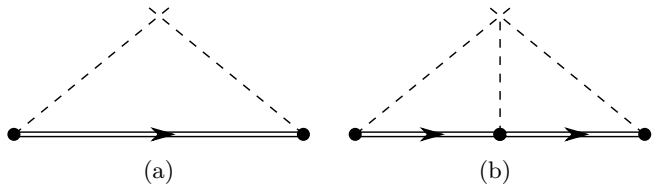

Figure 2.1: Self-energy diagrams. (a) Self-consistent Born approximation. (b) Third order contribution which determines skew scattering.

Some effects need to be treated outside the framework of the self-consistent Born approximation (2.9). An example is skew scattering which contributes to the spin Hall effect. In order to include it, the calculations need to be extended to at least third order in the scattering potential [66, 10], see Fig. 2.1(b).

2.1.4 Eilenberger Equation

By subtracting the equation of motion (2.8) from its conjugate and incorporating the quasiclassical approximation, the Eilenberger equation is obtained. For a stationary state it is, to lowest order in the gradient approximation,

$$0 = \mathrm{i}\boldsymbol{v}_\mathrm{F} \cdot \boldsymbol{\nabla}\check{g} + \left[\hat{\tau}_3\epsilon, \check{g}\right]_- - \left[\hat{\Delta}, \check{g}\right]_- - \left[\check{\sigma}, \check{g}\right]_-, \tag{2.10}$$

where ϵ denotes the quasiparticle energy,

$$\check{g}(\boldsymbol{R}, \boldsymbol{p}_\mathrm{F}, \epsilon) = \frac{\mathrm{i}}{\pi} \int_\Gamma \mathrm{d}\xi_p \int \mathrm{d}\boldsymbol{r}\ \mathrm{e}^{-\mathrm{i}\boldsymbol{p}\cdot\boldsymbol{r}} \int \mathrm{d}t\ \mathrm{e}^{\mathrm{i}\epsilon t} \check{G}_\mathrm{c}(\boldsymbol{R}, \boldsymbol{r}, t)\Big|_{\boldsymbol{p}=\boldsymbol{p}_\mathrm{F}}, \tag{2.11}$$

is the quasiclassical Green's function, and the self-energy $\check{\Sigma}$ was replaced by its quasiclassical approximation $\check{\sigma}$, in order to have a closed set of equations and a complete quasiclassical theory. Following Eilenberger [43], the integration contour in Eq. (2.11) is given in terms of two closed semicircles representing the physically relevant low-energy contribution Γ. Alternatively, a high-energy cutoff can be used in the integration, as done by Serene and Rainer [58]. The Eilenberger equation does not determine the quasiclassical Green's function uniquely and we therefore also need to introduce the normalization condition[2]

$$\check{g}^2 = \check{1}. \tag{2.12}$$

We have thus traded the complexity and some of the unessential information that Eq. (2.8) contains in for the simpler and more intuitive Eilenberger equation (2.10), which is a counterpart of the Boltzmann equation.

2.1.5 The Dirty Limit

The quasiparticles' momentum direction is randomized by elastic scattering events. In diffusive systems, where elastic impurity scattering is strong, the corresponding contribution to the self-energy is the dominating term in the Eilenberger equation. As a consequence, the quasiclassical Green's function becomes almost isotropic and can be conveniently expanded in spherical harmonics up to first order,

$$\check{g}(\boldsymbol{R}, \boldsymbol{p}_\mathrm{F}, \epsilon) \approx \check{g}_\mathrm{s}(\boldsymbol{R}, \epsilon) + \boldsymbol{e}_p \cdot \check{\boldsymbol{g}}(\boldsymbol{R}, \epsilon), \tag{2.13a}$$

[2] A detailed proof of the normalization condition can be found, for example, in Ref. [67].

where $\check{g}_\mathrm{s}$ and $\check{\boldsymbol{g}}$ are the isotropic and anisotropic Green's functions, respectively, and $\boldsymbol{e}_p = \boldsymbol{p}_\mathrm{F}/|\boldsymbol{p}_\mathrm{F}|$. This is known as the dirty limit. From the normalization condition (2.12), we obtain

$$\check{g}_\mathrm{s}^2 = 1, \quad \left[\check{g}_\mathrm{s}, \check{\boldsymbol{g}}\right]_+ = 0. \tag{2.13b}$$

The self-energy contribution from elastic impurity scattering (2.6) can be computed within the self-consistent Born approximation in terms of Eq. (2.9) from

$$\check{\Sigma}_\mathrm{imp}(1, 1') = n \int \mathrm{d}\boldsymbol{r}_i \, u(\boldsymbol{r}_1 - \boldsymbol{r}_i) \check{G}_\mathrm{c}(1, 1') u(\boldsymbol{r}_{1'} - \boldsymbol{r}_i), \tag{2.14a}$$

where n is the impurity concentration. Using Eq. (2.13a), in the quasiclassical approximation it reads

$$\check{\sigma}_\mathrm{imp}(\boldsymbol{R}, \boldsymbol{p}_\mathrm{F}, \epsilon) = -\frac{\mathrm{i}}{2\tau} \check{g}_\mathrm{s}(\boldsymbol{R}, \epsilon) - \frac{\mathrm{i}}{2}\Big(\frac{1}{\tau} - \frac{1}{\tau_\mathrm{tr}}\Big)\Big(\boldsymbol{e}_p \cdot \check{\boldsymbol{g}}(\boldsymbol{R}, \epsilon)\Big), \tag{2.14b}$$

where

$$\frac{1}{\tau} = 2\pi n N_0 \Big\langle \big|u(\boldsymbol{e}_p \cdot \boldsymbol{e}_q)\big|^2 \Big\rangle_\mathrm{F} \tag{2.14c}$$

and

$$\frac{1}{\tau_\mathrm{tr}} = 2\pi n N_0 \Big\langle \big|u(\boldsymbol{e}_p \cdot \boldsymbol{e}_q)\big|^2 (1 - \boldsymbol{e}_p \cdot \boldsymbol{e}_q) \Big\rangle_\mathrm{F} \tag{2.14d}$$

are the elastic scattering rate and the inverse transport relaxation time, respectively. Here, N_0 is the density of states at the Fermi level in the normal state and $\langle \ldots \rangle_\mathrm{F} = \int \frac{\mathrm{d}\boldsymbol{e}_q}{4\pi} \ldots$ denotes taking the angular average with respect to $\boldsymbol{e}_q$.

This now allows for a decomposition of the Eilenberger equation into an even and an odd part with respect to the momentum by carrying out angular averages over the momentum direction. The anisotropic Green's function is determined by the odd part,

$$\check{\boldsymbol{g}} = -l_\mathrm{tr} \check{g}_\mathrm{s} \boldsymbol{\nabla} \check{g}_\mathrm{s}, \tag{2.15}$$

where $l_\mathrm{tr} = v_\mathrm{F} \tau_\mathrm{tr}$ is the impurity mean free path. Contributions involving the energy ϵ and the superconducting order parameter Δ are neglected in Eq. (2.15) compared to the dominating elastic impurity scattering (2.14). The spin, charge, and energy currents are computed from the anisotropic Green's function, as we shall see shortly. Using Eq. (2.15) in the Eilenberger

equation after inserting the Green's function expansion (2.13a) and performing the angular average yields an equation that determines the isotropic Green's function and is a counterpart of the drift-diffusion equation. This is known as the Usadel equation and it is given by

$$0 = D\boldsymbol{\nabla}\cdot(\check{g}_\mathrm{s}\boldsymbol{\nabla}\check{g}_\mathrm{s}) + \mathrm{i}\big[\hat{\tau}_3\epsilon,\check{g}_\mathrm{s}\big]_- - \mathrm{i}\big[\hat{\Delta},\check{g}_\mathrm{s}\big]_-, \tag{2.16}$$

where $D = v_\mathrm{F} l_\mathrm{tr}/3$ is the diffusion constant. The presence of magnetic impurities and spin-orbit coupling results in additional contributions to the Usadel equation (2.16) and to the expression for the anisotropic Green's function (2.15). We shall discuss these and their influence on spin transport in Chapter 4.

2.1.6 Parameterization

The Usadel equation describes the flow of spin, charge, and energy in diffusive superconducting hybrid structures. However, it is still an 8×8 matrix equation in spin $\otimes$ particle-hole $\otimes$ Keldysh space and thus rather unwieldy. In order to derive scalar equations from it, we observe that the normalization condition (2.12) allows to express the Keldysh isotropic Green's function in terms of the distribution matrix $\hat{h}$:

$$\hat{g}_\mathrm{s}^\mathrm{K} = \hat{g}_\mathrm{s}^\mathrm{R}\hat{h} - \hat{h}\hat{g}_\mathrm{s}^\mathrm{A}. \tag{2.17}$$

The advanced isotropic Green's function can in general be expressed in terms of the retarded isotropic Green's function,

$$\hat{g}_\mathrm{s}^\mathrm{A}(\boldsymbol{R},\epsilon) = -\big(\hat{\tau}_3\hat{g}_\mathrm{s}^\mathrm{R}(\boldsymbol{R},\epsilon)\hat{\tau}_3\big)^\dagger, \tag{2.18a}$$

and symmetry considerations allow to write the retarded isotropic Green's function as

$$\hat{g}_\mathrm{s}^\mathrm{R}(\boldsymbol{R},\epsilon) = \begin{pmatrix} g_\mathrm{s}^\mathrm{R}(\boldsymbol{R},\epsilon) & 0 & 0 & f_\mathrm{s}^\mathrm{R}(\boldsymbol{R},\epsilon) \\ 0 & g_\mathrm{s}^\mathrm{R}(\boldsymbol{R},\epsilon) & -f_\mathrm{s}^\mathrm{R}(\boldsymbol{R},\epsilon) & 0 \\ 0 & f_\mathrm{s}^\mathrm{R}(\boldsymbol{R},\epsilon) & g_\mathrm{s}^\mathrm{R}(\boldsymbol{R},\epsilon) & 0 \\ -f_\mathrm{s}^\mathrm{R}(\boldsymbol{R},\epsilon) & 0 & 0 & g_\mathrm{s}^\mathrm{R}(\boldsymbol{R},\epsilon) \end{pmatrix} \tag{2.18b}$$

if a singlet superconducting state is assumed. The matrix elements g_s^R and f_s^R depend on position and energy and determine how the various transport mechanisms renormalize below the superconducting critical temperature.

They are obtained from the retarded (upper-left) matrix block of the Usadel equation together with the normalization condition,

$$\left(g_{\mathrm{s}}^{\mathrm{R}}(\boldsymbol{R},\epsilon)\right)^2 - \left(f_{\mathrm{s}}^{\mathrm{R}}(\boldsymbol{R},\epsilon)\right)^2 = 1. \tag{2.18c}$$

For energies far above the gap, the functions approach their normal state limits ($g_{\mathrm{s}}^{\mathrm{R}} \to 1$ and $f_{\mathrm{s}}^{\mathrm{R}} \to 0$) while they diverge for energies close to the superconducting order parameter.

2.1.7 Distribution Functions

From the Keldysh (upper-right) matrix block of the Usadel equation (2.16) one obtains a kinetic equation of motion for the distribution matrix $\hat{h}$, and since it is a linear equation, we can assume that $\hat{h}$ is diagonal with respect to particle-hole space. Consequently, it can be decomposed according to

$$\hat{h} = \hat{\tau}_3(h + \hat{\alpha}_j\, h_j) + \hat{1}(h_\epsilon + \hat{\alpha}_j\, h_{\epsilon j}), \tag{2.19}$$

where h_ϵ and h are the energy and charge distribution functions, respectively, and $h_{\epsilon j}$ and h_j are the spin-energy and spin distribution functions, respectively. Here, the subscript (j) denotes the spin polarization direction. Relevant physical quantities can now be extracted from the energy resolved distribution matrix $\hat{h}$. For example, the electric charge density is given by

$$Q(\boldsymbol{R}) = -\frac{eN_0}{2}\int \mathrm{d}\epsilon\, N_{\mathrm{S}}(\boldsymbol{R},\epsilon) h(\boldsymbol{R},\epsilon), \tag{2.20}$$

where $e = -|e|$ is the electron charge and

$$N_{\mathrm{S}}(\boldsymbol{R},\epsilon) = \mathrm{Re}\left[g_{\mathrm{s}}^{\mathrm{R}}(\boldsymbol{R},\epsilon)\right] \tag{2.21}$$

is the density of states in the superconducting state normalized by N_0. The charge distribution function can be extracted with a trace operation,

$$h(\boldsymbol{R},\epsilon) = \frac{1}{4}\,\mathrm{Tr}\left[\hat{\tau}_3 \hat{h}(\boldsymbol{R},\epsilon)\right].$$

The expressions for the spin, energy, and spin-energy distribution functions are obtained in a similar fashion.

2.1.8 Currents

Let us now derive current expressions related to the distribution functions of the previous section. To this end, we define the particle current density in terms of the pseudo-spinor of Eq. (2.1) as

$$J_i(1) = \frac{1}{2}\,\mathrm{Tr}\Big[\,\mathrm{Re}\,\big[\langle\hat{\psi}^\dagger(1)\hat{v}_i(\boldsymbol{r}_1)\hat{\psi}(1)\rangle\big]\Big], \tag{2.22a}$$

and the spin current density as

$$J_{ij}(1) = \frac{1}{2}\,\mathrm{Tr}\Big[\,\mathrm{Re}\,\big[\langle\hat{\psi}^\dagger(1)\hat{\alpha}_j\hat{v}_i(\boldsymbol{r}_1)\hat{\psi}(1)\rangle\big]\Big], \tag{2.22b}$$

where the indices i and j denote the flow direction and the spin polarization direction, respectively, and

$$\hat{\boldsymbol{v}}(\boldsymbol{r}) = -\hat{1}\frac{\mathrm{i}}{m}\boldsymbol{\partial}_{\boldsymbol{r}} \tag{2.23}$$

is the velocity operator in spin $\otimes$ particle-hole space. Note that in the presence of magnetic impurities or spin-orbit coupling, the spin current density, as defined by Eq. (2.22b), is not a conserved quantity and does not obey a simple continuity equation (as the charge current density does). Other definitions of spin currents have been proposed, see Refs. [68, 69, 70], for example. It is convenient to define an energy-resolved matrix current in terms of the Keldysh anisotropic Green's function,

$$\hat{\boldsymbol{\jmath}}(\boldsymbol{R},\epsilon) = \frac{\upsilon_\mathrm{F}}{6}\hat{\boldsymbol{g}}^\mathrm{K}(\boldsymbol{R},\epsilon), \tag{2.24}$$

such that the currents of Eqs. (2.22) in the quasiclassical approximation are given by

$$J_i(\boldsymbol{R}) = -\frac{N_0}{4}\int \mathrm{d}\epsilon\ \mathrm{Tr}\left[\hat{\tau}_3\hat{\jmath}_i(\boldsymbol{R},\epsilon)\right] \tag{2.25a}$$

and

$$J_{ij}(\boldsymbol{R}) = -\frac{N_0}{4}\int \mathrm{d}\epsilon\ \mathrm{Tr}\left[\hat{\tau}_3\hat{\alpha}_j\hat{\jmath}_i(\boldsymbol{R},\epsilon)\right]. \tag{2.25b}$$

In addition to the aforementioned corrections to Eqs. (2.15) and (2.16) due to magnetic impurities and spin-orbit coupling, the velocity operator (2.23) acquires anomalous contributions in the presence of spin-orbit coupling. These shall be discussed in Chapters 3 and 4.

2.1.9 Boundary Conditions

The quasiclassical approximation, which assumes that relevant quantities vary on length scales much larger than the Fermi wavelength, naturally breaks down in the vicinity of interfaces. However, the quasiclassical Green's functions describing two distinct regions 1 and 2 can be connected across an intermediate boundary surface with the aid of scattering theory. In the limit of a low-transparency interface perpendicular to the x direction, the boundary condition reads [71, 72]

$$2\sigma \check{g}_{\mathrm{s}}^{(2)} \nabla_x \check{g}_{\mathrm{s}}^{(2)} = G_{\mathrm{T}} \big[\check{g}_{\mathrm{s}}^{(2)}, \check{g}_{\mathrm{s}}^{(1)} \big]_-, \tag{2.26}$$

where $\sigma = 2e^2 N_0 D$ is the conductivity, $G_{\mathrm{T}} = e^2 N_0 v_{\mathrm{F}} \langle e_{p_x} T(e_{p_x}) / R(e_{p_x}) \rangle_{\mathrm{F}}$ is the interface conductance, and T and R are the interface transmission and reflection coefficients, respectively.

2.2 The Normal Limit

A trait of the nonequilibrium Keldysh Green's function formalism introduced in the previous section is that, once established, it also describes nonequilibrium transport in the normal state above the superconducting critical temperature. Naturally, it would be rather pointless to use the theoretical description of a superconducting system as a basis to *only* describe spin transport in the normal state and having to cope with the added layer of complexity that superconducting correlations call for. But for our intended purpose of providing a fundamental footing for the research presented in this thesis, the quasiclassical theory of superconductivity is not only a powerful tool to describe superconducting systems, such as those considered in Papers [1] and [3]. It also facilitates our discussion of the extrinsic spin swapping effect, which we study together with its intrinsic analog in two-dimensional diffusive metals in Paper [2]. The transition to the description of a normal metal is straightforward: By letting the superconducting order parameter approach zero, $\Delta \to 0$, the retarded and the advanced Green's functions become $\hat{g}_{\mathrm{s}}^{\mathrm{R}} = -\hat{g}_{\mathrm{s}}^{\mathrm{A}} = \hat{1}$. The distribution functions and currents are then determined by the diffusion equations and current expressions in a diffusive normal metal. We shall make use of this so-called normal limit in Chapter 5 for illustrative purposes, when we discuss the extrinsic spin swapping effect.

3 Spin Transport Mechanisms

Various spin-dependent scattering mechanisms influence transport in mesoscopic devices and give rise to important, rich, and interesting effects. Of central interest is the spin-orbit coupling, which is the foundation of numerous physical phenomena significant for spin generation and spin manipulation in many spintronic systems. It leads to the decay of spin populations and spin currents through spin relaxation, to the coupling of charge and spin through the spin Hall effect, and to the generation of transverse spin currents from injected longitudinal spin currents through the spin swapping effect. In the present chapter, we discuss the relevant spin-dependent effects and how they influence the transport in diffusive metals and superconductors. The mathematical framework is provided by the quasiclassical theory of superconductivity, which we introduced in the previous chapter. Corresponding expressions for normal metals can readily be obtained in the normal limit, see Section 2.2. Following the convention of Ref. [10], we classify the mechanisms of spin-orbit coupling into two categories: i) *Extrinsic* effects are due to the presence of extrinsic impurities, while ii) *intrinsic* effects are inherent in the band structure and remain finite even in the absence of extrinsic impurities. We first review extrinsic spin-orbit-induced effects, such as spin relaxation, skew scattering, the side-jump mechanism, and the extrinsic spin swapping effect in Section 3.1. We then discuss the influence of magnetic impurities on spin transport and superconductivity in Section 3.2, and, lastly, briefly introduce intrinsic Rashba-type spin-orbit coupling in Section 3.3. The extrinsic spin-dependent effects presented in this Chapter are then incorporated into the quasiclassical theory of superconductivity and further discussed in Chapter 4. The intrinsic spin swapping effect is studied in more detail in Chapter 5 and compared to its extrinsic analog, and in Chapter 6, we elucidate the inverse spin Hall effect in S|N|S Josephson junctions due to intrinsic spin-orbit coupling.

3.1 Extrinsic Spin-Orbit-Induced Effects

The presence of spin-orbit coupling at extrinsic impurities can be understood as originating from intrinsic spin-orbit coupling inside the band structure. This intraband spin-orbit interaction renormalizes the interaction strength γ_0, causing a spin- and velocity-dependent shift in the physical position operator,[1]

$$\boldsymbol{r} \to \hat{\boldsymbol{r}}_{\text{eff}} = \boldsymbol{r} + \hat{\boldsymbol{r}}_{\text{so}}, \quad \hat{\boldsymbol{r}}_{\text{so}} = -\gamma(\hat{\tau}_3\hat{\boldsymbol{\alpha}} \times \boldsymbol{p}), \tag{3.1}$$

such that, to first order in γ,

$$\hat{U}(\hat{\boldsymbol{r}}_{\text{eff}}) = \hat{U}(\boldsymbol{r}) + \hat{U}_{\text{so}}(\boldsymbol{r}),$$

where $\hat{U}$ is the elastic impurity scattering potential of Eq. (2.6) and

$$\hat{U}_{\text{so}}(\boldsymbol{r}) = \sum_i \hat{u}_{\text{so}}(\boldsymbol{r} - \boldsymbol{r}_i) = -\mathrm{i}\gamma \sum_i \left(\hat{\tau}_3\hat{\boldsymbol{\alpha}} \times \boldsymbol{\nabla} u(\boldsymbol{r} - \boldsymbol{r}_i)\right) \cdot \boldsymbol{\partial}_{\boldsymbol{r}} \tag{3.2}$$

describes extrinsic spin-orbit coupling. This shift $\hat{\boldsymbol{r}}_{\text{so}}$ is known as the anomalous coordinate or the Yafet term [73, 10]. Furthermore, we introduced a generalization of the vector of Pauli matrices to spin $\otimes$ particle-hole space:

$$\hat{\boldsymbol{\alpha}} = \begin{pmatrix} \bar{\boldsymbol{\sigma}} & 0 \\ 0 & \bar{\boldsymbol{\sigma}}^* \end{pmatrix}, \tag{3.3}$$

where $\bar{\boldsymbol{\sigma}} = (\bar{\sigma}_x, \bar{\sigma}_y, \bar{\sigma}_z)^{\mathrm{T}}$ is the vector of conventional 2×2 Pauli matrices. The consequences of Eqs. (3.1) and (3.2) to spin-dependent transport are numerous and include spin relaxation, skew scattering, the side-jump mechanism, and spin swapping. Most of these effects can be understood qualitatively by considering the simple schematics in Fig. 3.1, which depicts scattering at a repulsive impurity center. A polarized carrier in the vicinity of the impurity experiences a magnetic field $\boldsymbol{B} \propto \boldsymbol{v} \times \boldsymbol{E}$ in its frame of reference. This magnetic field is perpendicular to the carrier trajectory and has opposite signs for opposite scattering directions. This has important consequences on the transport of spin and charge, which we shall discuss in the following.

[1] Here, we choose the sign of γ such that spin-orbit coupling (3.2) corresponds to its vacuum expression for which $\gamma_{\text{vac}} > 0$.

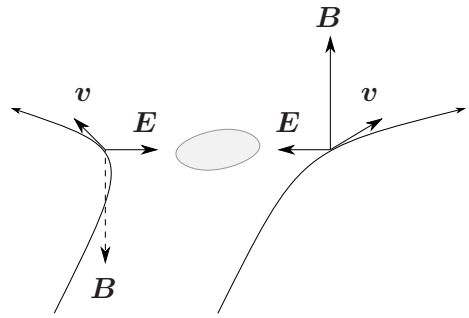

Figure 3.1: Scattering at a repulsive impurity for strongly exaggerated spin-orbit coupling is shown schematically. During the scattering event, a magnetic field $\boldsymbol{B} \propto \boldsymbol{v} \times \boldsymbol{E}$ exists in the carrier's frame of reference. This has several important consequences for spin-dependent transport. Adapted from [74].

3.1.1 Spin Relaxation

If the quasiparticle's spin is not perpendicular to its trajectory, the spin will precess around the magnetic field $\boldsymbol{B}$ during the scattering event. This effectively randomizes the spin polarization. Spin relaxation is only present to second order in the spin-orbit coupling strength γ but fundamentally influences spin transport properties. It causes a nonequilibrium spin population to decay with time and an injected spin current to decay with distance.

3.1.2 The Spin Hall Effect

There are two main contributions to the extrinsic spin Hall effect, see Fig. 3.2: skew scattering, which refers to the spin-dependent angular scattering cross-section the quasiparticle experiences, and the side-jump mechanism, which is a spin-dependent displacement during a scattering event. The transverse current emerging from skew scattering and side-jump constitutes the spin Hall effect. It is calculated from the expectation values of the respective spin-orbit corrections to the current operator, as we shall see in Chapter 4.

Skew Scattering

As can be understood from the schematic in Fig. 3.1, the magnetic field in the carrier's frame of reference $\boldsymbol{B}$ is inhomogeneous in space, because

the velocity $\boldsymbol{v}$ and the electric field $\boldsymbol{E}$ both change during the scattering event. As a consequence, a spin-dependent force proportional to the gradient of the corresponding Zeeman energy $\propto \boldsymbol{B} \cdot \boldsymbol{S}$ changes the carrier's trajectory [74]. This leads to a spin-dependent angular deflection due to spin-orbit coupling [75, 76, 77], see Fig. 3.2. Skew scattering does not appear within the framework of the self-consistent Born approximation and the calculations need to be extended to at least third order in the scattering potential [66, 10], see Fig. 2.1(b). Skew scattering then gives rise to an additional contribution to the anisotropic Green's function of Eq. (2.15) and, consequently, modifies the current expressions.

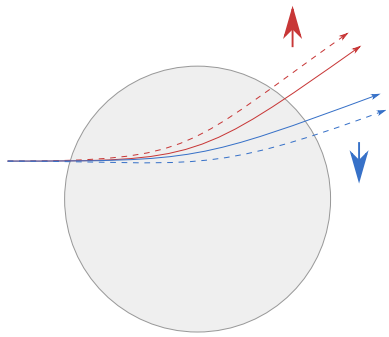

Figure 3.2: Skew scattering and side-jump at a repulsive impurity for strongly exaggerated spin-orbit coupling is shown schematically. Skew scattering is the spin-dependent angular deflection (solid lines) and the side-jump mechanism leads to a lateral displacement during the collision (dashed lines). These two mechanisms give rise to the spin Hall effect. Note that the side-jump does not modify the skew scattering cross-section because it does not change the deflection angle at large distances. Adapted from [10].

The Side-Jump Mechanism

It appears that the side-jump mechanism and its importance to spin-dependent transport are still not fully understood. Particularly in the field of spintronics, the effect is widely discussed and continues to give rise to controversy. The concept of a 'side-jump', a lateral spin-dependent displacement of the electron wave package during a scattering event due to spin-orbit coupling, was introduced by Berger [78] to study the anomalous Hall effect in ferromagnets and further developed by Lyo and Holstein [79]. The overall situation, however, remained unsatisfactory. Several factors contribute to

the effect and to make matters worse, some of the terms cancel while others add up giving rise to factors of 2, rendering the task of determining the side-jump contribution to the spin Hall effect a subtle issue. Nozières and Lewiner [80] studied side-jump in a two-band semiconductor in detail using an elementary theory in terms of the effective Hamiltonian in the conduction band. Numerous more discussions on the subject exist, see for example Refs. [10, 74, 81, 16], but contributions continue to be overlooked. We will here consider the side-jump mechanism in the absence of external magnetic fields for a stationary regime, a situation we consider when studying extrinsic spin-orbit-induced transport in diffusive superconductors in Paper [3]. In this case, there are three distinct contributions to the side-jump:

Self-Energy Contribution to the Side-Jump One contribution arises from the self-energy (2.9) to first order in the spin-orbit coupling. This contribution only appears beyond the lowest order gradient approximation and is therefore often disregarded. However, within the quasiclassical approximation, it is of the same order as the other spin-orbit-induced self-energy contributions and must be included. It gives rise to an additional term in the expression for the anisotropic Green's function of Eq. (2.15) and, consequently, modifies the current expressions.

Anomalous Velocity The normal position operator does not commute with the extrinsic spin-orbit coupling potential (3.2), and as a consequence, the velocity operator acquires an anomalous contribution,

$$\hat{\boldsymbol{v}}_{\mathrm{so}}^{(1)} = -\mathrm{i}\big[\boldsymbol{r}, \hat{U}_{\mathrm{so}}\big]_{-} = \gamma \sum_i \big(\hat{\tau}_3 \hat{\boldsymbol{\alpha}} \times \boldsymbol{\nabla} u(\boldsymbol{r} - \boldsymbol{r}_i)\big). \tag{3.4a}$$

Anomalous Coordinate Additionally, the Yafet shift of the position (3.1) also leads to an anomalous contribution to the velocity operator because it does not commute with the elastic impurity scattering potential,

$$\hat{\boldsymbol{v}}_{\mathrm{so}}^{(2)} = -\mathrm{i}\big[\hat{\boldsymbol{r}}_{\mathrm{so}}, \hat{U}\big]_{-} = \gamma \sum_i \big(\hat{\tau}_3 \hat{\boldsymbol{\alpha}} \times \boldsymbol{\nabla} u(\boldsymbol{r} - \boldsymbol{r}_i)\big). \tag{3.4b}$$

Note that $\hat{\boldsymbol{v}}_{\mathrm{so}}^{(1)}$ and $\hat{\boldsymbol{v}}_{\mathrm{so}}^{(2)}$ are identical, giving rise to an overall factor of 2. This need not be true in general, for example, in the presence of an external magnetic field or when the spin operator is time dependent [80]. Additional terms in the velocity operator then emerge from the side-jump

mechanism. Since these contributions remain finite even in the absence of extrinsic impurities, they should technically be considered as intrinsic effects, however.

3.1.3 Extrinsic Spin Swapping

While the spin Hall effect provides coupling between charge and spin, another spin-orbit-induced transport mechanism has recently been introduced in which only spins couple and which exists even in the absence of charge currents. This effect generates secondary spin currents perpendicular to injected primary spin currents. In its simplest manifestation, spin swapping interchanges the direction of flow and the spin polarization direction. Consequently, the effect was coined 'spin swapping' and first studied by Lifshits and Dyakonov [33] in the presence of extrinsic spin-orbit coupling.[1]

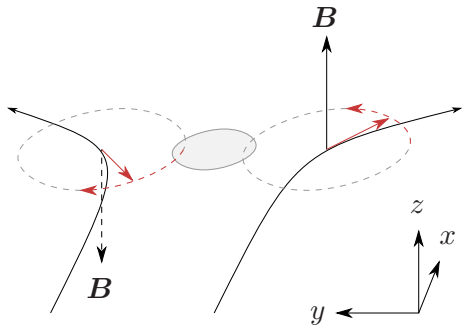

Figure 3.3: Spin swapping for strongly exaggerated spin-orbit coupling is shown schematically. Because the direction in which the spins precess around the magnetic field $\boldsymbol{B}$, which exists in the carrier's frame of reference during a scattering event, depends on the scattering direction, an initial y-polarized spin current flowing along x direction is, in part, transformed into an x-polarized spin current flowing along y direction. This is the simplest manifestation of the extrinsic spin swapping effect. Adapted from [74].

Spin swapping can be understood as emerging from the correlation between the scattering direction and the direction in which the spin rotates around the magnetic field $\boldsymbol{B}$, which exists in the quasiparticle's frame of refer-

[1] The terms responsible for extrinsic spin swapping were already indicated almost 40 years earlier by Dyakonov and Perel in Refs. [11, 12]. However, their physical origin and significance for spin transport was not understood at the time.

ence. Consider, for instance, quasiparticles approaching an extrinsic impurity along the x direction carrying y-polarized spins, see Fig. 3.3. If the spin of a quasiparticle deflected to the left rotates clockwise, the spin of a quasiparticle deflected to the right will rotate counterclockwise. Because of this, quasiparticles traveling left and right acquire a small spin polarization along x direction, but of opposite signs. Consequently, the initial y-polarized spin current flowing along x direction is, in part, transformed into an x-polarized spin current flowing along y direction. The spin currents have been 'swapped'.

3.2 Magnetic Impurities

The interaction of quasiparticle spin with magnetic impurities can be included in the Hamiltonian of Eq. (2.4) via

$$\hat{U}_{\mathrm{m}}(\boldsymbol{r}) = \sum_j \hat{u}_{\mathrm{m}}(\boldsymbol{r} - \boldsymbol{r}_j) = \sum_j \left(\hat{\boldsymbol{\alpha}} \cdot \boldsymbol{S}_j(\boldsymbol{r})\right) u_{\mathrm{m}}(\boldsymbol{r} - \boldsymbol{r}_j), \tag{3.5}$$

where $\boldsymbol{S}_j$ is the spin of the j^{th} magnetic scattering potential $u_{\mathrm{m}}(\boldsymbol{r} - \boldsymbol{r}_j)$ at position $\boldsymbol{r}_j$. While spin-orbit coupling (3.2) is even under time reversal, magnetic impurity scattering is odd. This is reflected in the different structure in particle-hole space (expressed through the presence or the absence of the matrix $\hat{\tau}_3$) and has important consequences on spin transport in superconductors. The way in which spin relaxation processes renormalize below the superconducting critical temperature depends on how they transform under time reversal [82]. The opposite spin electron and hole quasiparticles that form Cooper pairs and give rise to the phenomenon of superconductivity are related by time reversal. Processes that break time-reversal symmetry, such as magnetic impurity scattering, also break up Cooper pairs, and their energy dependence in the superconducting state greatly differs from the energy dependence of processes that are symmetric under time reversal, such as spin-orbit coupling. The presence of magnetic impurities, quantified by the spin-flip scattering rate τ_{m}, thus suppresses superconductivity and reduces the gap in the energy spectrum: For $\tau_{\mathrm{m}}\Delta > 1$, the energy gap is

$$\Delta_{\mathrm{m}} \approx \Delta\left(1 - \frac{1}{(\frac{4\tau_{\mathrm{m}}}{3}\Delta)^{2/3}}\right)^{3/2}, \tag{3.6a}$$

and the critical temperature is reduced to

$$T_{c\mathrm{m}} \approx T_c - \frac{3\pi}{16\tau_{\mathrm{m}}}, \tag{3.6b}$$

for small magnetic impurity concentrations [62]. On the other hand, the fact that the nature of the spin-flip processes determines their energy and temperature dependence in the superconducting state allows for spin-flip spectroscopy [49], in order to determine which mechanism is more efficient.

3.3 Intrinsic Spin-Orbit Coupling

In Paper [1], we study the inverse spin Hall effect in S|N|S Josephson junctions, and in Paper [2], we discuss the intrinsic spin swapping effect. Both are based on the presence of intrinsic Rashba-type spin-orbit coupling, which has gained a lot of attention, at least in part, due to the seminal concept of a spin transistor as proposed by Datta and Das [8]. The Rashba spin-orbit interaction

$$\bar{\mathcal{H}}_{\mathrm{so}}(\boldsymbol{k}) = \bar{\boldsymbol{\sigma}} \cdot \boldsymbol{h}_{\boldsymbol{k}}, \quad \boldsymbol{h}_{\boldsymbol{k}} = \left(\alpha k_y, -\alpha k_x, 0\right)^{\mathrm{T}}, \tag{3.7}$$

where $\boldsymbol{k}$ is the electron wave vector and α is the spin-orbit coupling strength, leads to a momentum-dependent spin splitting in the conduction band, even in the absence of magnetic fields [83, 84]. The Rashba field $\boldsymbol{h}_{\boldsymbol{k}}$ acts as a momentum-dependent effective magnetic field and causes the spin to align perpendicular to the momentum.

3.3.1 Spin Precession and Spin Relaxation

When an electric field is applied and the electrons are accelerated, their spin polarization changes to follow the change in the momentum-dependent Rashba field. As was the case for spin relaxation due to extrinsic spin-orbit coupling, see Section 3.1.1, the spins will precess around the effective magnetic field if they are not aligned with it. In addition, this momentum-dependent spin precession together with frequent momentum-randomizing elastic impurity scattering leads to the D'yakonov-Perel' spin relaxation mechanism [85], effectively causing the spin phase to undergo a random walk as the electron moves along. In analogy to spin relaxation due to extrinsic spin-orbit coupling and magnetic impurities, this causes injected spin currents to decay with distance, and spin populations to decay with time.

Spin precession and spin relaxation also give rise to another interesting phenomenon. When discussing the extrinsic spin swapping effect, it was proposed by Lifshits and Dyakonov [33] that any mechanism producing a

spin Hall effect should also give rise to spin swapping, but it had not been clear how the intrinsic mechanism could induce this effect. In Paper [2], we demonstrate that an intrinsic (Rashba spin-orbit-induced) spin swapping effect exists in two-dimensional diffusive metals and that it is drastically different from its extrinsic analog. An overview of our results is given in Chapter 5.

4 Spin Transport in Superconductors

In Paper [3], we build upon the quasiclassical theory of superconductivity introduced in Chapter 2 and include effects from magnetic impurities and extrinsic spin-orbit coupling. Special attention is given to the two mechanisms which give rise to the spin Hall effect, namely skew scattering and the side-jump mechanism. We have already touched upon some of the difficulties arising from these effects in Chapter 3: Skew scattering is not included within the self-consistent Born approximation, and obtaining the side-jump contribution to the spin Hall effect can be an intricate undertaking. Moreover, it is interesting to see in which form these two mechanisms influence spin transport below the superconducting critical temperature and how they are renormalized due to superconducting correlations. For instance, a different renormalization behavior for side-jump and skew scattering could provide further insight into the nature of these mechanisms. Whether the extrinsic spin swapping effect exists in the superconducting state and how it is influenced by superconductivity is another important problem to tackle. In the present chapter, we present kinetic equations describing the flow of spin, charge, and energy based on the concepts of the previous two chapters, discuss how the various scattering mechanisms influence transport, and how they are renormalized below the superconducting critical temperature.

4.1 Corrections from Scattering Mechanisms

As mentioned in Section 2.1.5, the presence of magnetic impurities and spin-orbit coupling gives rise to additional terms in the Usadel equation (2.16) and the matrix current (2.24) which fundamentally alter spin transport. We already discussed the various transport mechanisms resulting from these corrections in Chapter 3. Let us here lay the groundwork to incorporate them

into the quasiclassical theory of superconductivity. The basic ingredients are the spin-orbit coupling potential of Eq. (3.2) and the magnetic impurity potential of Eq. (3.5). Additionally, the Yafet shift of the position (3.1) also needs to be taken into account.

4.1.1 Spin Relaxation

The self-energy contribution from spin-orbit-induced spin relaxation is calculated within the self-consistent Born approximation in terms of Eq. (2.9) from

$$\check{\Sigma}_{\mathrm{so}}(1,1') = n\int \mathrm{d}\boldsymbol{r}_i\, \hat{u}_{\mathrm{so}}(\boldsymbol{r}_1-\boldsymbol{r}_i)\check{G}_{\mathrm{c}}(1,1')\hat{u}_{\mathrm{so}}(\boldsymbol{r}_{1'}-\boldsymbol{r}_i). \tag{4.1a}$$

In the quasiclassical approximation, the dominating contribution is given by

$$\check{\sigma}_{\mathrm{so}}(\boldsymbol{R},\boldsymbol{p}_{\mathrm{F}},\epsilon) = -\frac{3\mathrm{i}}{16\tau_{\mathrm{so}}}(\hat{\tau}_3\hat{\boldsymbol{\alpha}}\times\boldsymbol{e}_p)\check{g}_{\mathrm{s}}(\boldsymbol{R},\epsilon)(\hat{\tau}_3\hat{\boldsymbol{\alpha}}\times\boldsymbol{e}_p), \tag{4.1b}$$

where

$$\frac{1}{\tau_{\mathrm{so}}} = \frac{8}{3}\pi\gamma^2 p_{\mathrm{F}}^4 n N_0 \Big\langle \big|u(\boldsymbol{e}_p\cdot\boldsymbol{e}_q)\big|^2(\boldsymbol{e}_p\times\boldsymbol{e}_q)^2\Big\rangle_{\mathrm{F}} \tag{4.1c}$$

is the spin-flip scattering rate due to spin-orbit coupling. Similarly, the leading order self-energy contribution from magnetic impurities is

$$\check{\Sigma}_{\mathrm{m}}(1,1') = n_{\mathrm{m}}\int \mathrm{d}\boldsymbol{r}_j\, \hat{u}_{\mathrm{m}}(\boldsymbol{r}_1-\boldsymbol{r}_j)\check{G}_{\mathrm{c}}(1,1')\hat{u}_{\mathrm{m}}(\boldsymbol{r}_{1'}-\boldsymbol{r}_j), \tag{4.2a}$$

where n_{m} is the magnetic impurity concentration. In the quasiclassical approximation, the dominating contribution is given by

$$\check{\sigma}_{\mathrm{m}}(\boldsymbol{R},\epsilon) = -\frac{\mathrm{i}}{8\tau_{\mathrm{m}}}\hat{\boldsymbol{\alpha}}\check{g}_{\mathrm{s}}(\boldsymbol{R},\epsilon)\hat{\boldsymbol{\alpha}}, \tag{4.2b}$$

where

$$\frac{1}{\tau_{\mathrm{m}}} = \frac{8}{3}\pi n_{\mathrm{m}} N_0 S(S+1)\Big\langle \big|u_{\mathrm{m}}(\boldsymbol{e}_p\cdot\boldsymbol{e}_q)\big|^2\Big\rangle_{\mathrm{F}} \tag{4.2c}$$

is the spin-flip scattering rate due to magnetic impurities and S is the impurity spin quantum number. Because these quasiclassical self-energies are even with respect to the momentum $\boldsymbol{e}_p$, they enter the Usadel equation (2.16), which then becomes

$$\begin{aligned} 0 = {} & D\boldsymbol{\nabla}\cdot(\check{g}_{\mathrm{s}}\boldsymbol{\nabla}\check{g}_{\mathrm{s}}) + \mathrm{i}\big[\hat{\tau}_3\epsilon,\check{g}_{\mathrm{s}}\big]_- - \mathrm{i}\big[\hat{\Delta},\check{g}_{\mathrm{s}}\big]_- \\ & - \frac{1}{8\tau_{\mathrm{so}}}\big[\hat{\boldsymbol{\alpha}}\hat{\tau}_3\check{g}_{\mathrm{s}}\hat{\tau}_3\hat{\boldsymbol{\alpha}},\check{g}_{\mathrm{s}}\big]_- - \frac{1}{8\tau_{\mathrm{m}}}\big[\hat{\boldsymbol{\alpha}}\check{g}_{\mathrm{s}}\hat{\boldsymbol{\alpha}},\check{g}_{\mathrm{s}}\big]_-, \end{aligned} \tag{4.3}$$

after carrying out the angular average over the momentum direction.

4.1.2 Corrections to the Anisotropic Green's Function

The remaining contributions to the quasiclassical self-energy are odd with respect to the momentum $\boldsymbol{e}_p$, and give rise to additional terms in the expression for the anisotropic Green's function of Eq. (2.15). They include the spin swapping effect, skew scattering, and one contribution to the side-jump mechanism. Spin swapping and the side-jump contribution arise to first order in the spin-orbit coupling strength,

$$\begin{aligned}\check{\Sigma}^{(1)}_{\mathrm{so}}(1,1') = n\int \mathrm{d}\boldsymbol{r}_i\, \hat{u}_{\mathrm{so}}(\boldsymbol{r}_1-\boldsymbol{r}_i)\check{G}_{\mathrm{c}}(1,1')u(\boldsymbol{r}_{1'}-\boldsymbol{r}_i)\\ + n\int \mathrm{d}\boldsymbol{r}_i\, u(\boldsymbol{r}_1-\boldsymbol{r}_i)\check{G}_{\mathrm{c}}(1,1')\hat{u}_{\mathrm{so}}(\boldsymbol{r}_{1'}-\boldsymbol{r}_i).\end{aligned} \tag{4.4}$$

In the quasiclassical approximation, we obtain the spin swapping self-energy

$$\check{\sigma}_{\mathrm{sw}}(\boldsymbol{R},\boldsymbol{p}_{\mathrm{F}},\epsilon) = -\frac{\eta}{3\tau_{\mathrm{sw}}}\boldsymbol{e}_p\cdot\left[\hat{\tau}_3\hat{\boldsymbol{\alpha}}\stackrel{\times}{,}\check{\boldsymbol{g}}(\boldsymbol{R},\epsilon)\right]_+, \tag{4.5a}$$

where $[\boldsymbol{a}\stackrel{\times}{,}\boldsymbol{b}]_\pm = \boldsymbol{a}\times\boldsymbol{b}\pm\boldsymbol{b}\times\boldsymbol{a}$ and

$$\frac{1}{\tau_{\mathrm{sw}}} = 3\pi n N_0\Big\langle\big|u(\boldsymbol{e}_p\cdot\boldsymbol{e}_q)\big|^2(\boldsymbol{e}_p\times\boldsymbol{e}_q)^2\Big\rangle_{\mathrm{F}} \tag{4.5b}$$

is the spin swapping scattering rate. The dimensionless quantity $\eta = \gamma p_{\mathrm{F}}^2/2$ is governed by the spin-orbit coupling strength. To next-to-leading order in the gradient approximation, we also find the side-jump contribution

$$\check{\sigma}_{\mathrm{sj}}(\boldsymbol{R},\boldsymbol{p}_{\mathrm{F}},\epsilon) = \frac{\mathrm{i}\gamma p_{\mathrm{F}}}{4\tau_{\mathrm{tr}}}\boldsymbol{e}_p\cdot\left[\hat{\tau}_3\hat{\boldsymbol{\alpha}}\stackrel{\times}{,}\boldsymbol{\nabla}\check{g}_{\mathrm{s}}(\boldsymbol{R},\epsilon)\right]_- \tag{4.6}$$

from Eq. (4.4). The skew scattering contribution needs to be calculated beyond the self-consistent Born approximation, see Fig. 2.1(b),

$$\begin{aligned}&\check{\Sigma}_{\mathrm{sk}}(1,1')\\ &= n\int \mathrm{d}\boldsymbol{r}_i\int \mathrm{d}2\,\hat{u}_{\mathrm{so}}(\boldsymbol{r}_1-\boldsymbol{r}_i)\check{G}_{\mathrm{c}}(1,2)u(\boldsymbol{r}_2-\boldsymbol{r}_i)\check{G}_{\mathrm{c}}(2,1')u(\boldsymbol{r}_{1'}-\boldsymbol{r}_i)\\ &+ n\int \mathrm{d}\boldsymbol{r}_i\int \mathrm{d}2\,u(\boldsymbol{r}_1-\boldsymbol{r}_i)\check{G}_{\mathrm{c}}(1,2)\hat{u}_{\mathrm{so}}(\boldsymbol{r}_2-\boldsymbol{r}_i)\check{G}_{\mathrm{c}}(2,1')u(\boldsymbol{r}_{1'}-\boldsymbol{r}_i)\\ &+ n\int \mathrm{d}\boldsymbol{r}_i\int \mathrm{d}2\,u(\boldsymbol{r}_1-\boldsymbol{r}_i)\check{G}_{\mathrm{c}}(1,2)u(\boldsymbol{r}_2-\boldsymbol{r}_i)\check{G}_{\mathrm{c}}(2,1')\hat{u}_{\mathrm{so}}(\boldsymbol{r}_{1'}-\boldsymbol{r}_i).\end{aligned} \tag{4.7a}$$

In the quasiclassical approximation, the contribution is given by

$$\check{\sigma}_{\mathrm{sk}}(\boldsymbol{R},\boldsymbol{p}_{\mathrm{F}},\epsilon) = -\frac{\mathrm{i}\eta}{3\tau_{\mathrm{sk}}}\boldsymbol{e}_p\cdot\left[\hat{\tau}_3\hat{\boldsymbol{\alpha}}\stackrel{\times}{,}\check{g}_{\mathrm{s}}(\boldsymbol{R},\epsilon)\check{\boldsymbol{g}}(\boldsymbol{R},\epsilon)\right]_-, \tag{4.7b}$$

where

$$\frac{1}{\tau_{\mathrm{sk}}} = 2\pi^2 n N_0^2 u_0^3 \tag{4.7c}$$

is the skew scattering rate and $u_0 = u(\boldsymbol{q} = 0)$ is the Fourier transformed scattering potential at $\boldsymbol{q} = 0$. Note that Eq. (4.7b) is valid only to lowest order in the anisotropy of the scattering potentials in order to keep the result compact and simple. However, the first order contribution in an expansion in spherical harmonics vanishes, which indicates that the anisotropy of the scattering potential is less relevant for skew scattering.

Let us now find the corrections to the anisotropic Green's function. To first order in the spin-orbit coupling, they are simply additive,

$$\check{\boldsymbol{g}} \to \check{\boldsymbol{g}} + \delta\check{\boldsymbol{g}}^{(\mathrm{sw})} + \delta\check{\boldsymbol{g}}^{(\mathrm{sj})} + \delta\check{\boldsymbol{g}}^{(\mathrm{sk})}, \tag{4.8a}$$

and are readily obtained with the aid of the normalization condition (2.13b): The correction from the skew scattering self-energy (4.7) reads as

$$\delta\check{\boldsymbol{g}}^{(\mathrm{sk})} = -\frac{\eta l_{\mathrm{tr}}}{3}\frac{\tau_{\mathrm{tr}}}{\tau_{\mathrm{sk}}}\Big[\check{g}_{\mathrm{s}}\big[\hat{\tau}_3\hat{\boldsymbol{\alpha}}, \check{g}_{\mathrm{s}}\big]_+ \overset{\times}{,} \boldsymbol{\nabla}\check{g}_{\mathrm{s}}\Big]_-, \tag{4.8b}$$

and the correction from the side-jump contribution (4.6) is

$$\delta\check{\boldsymbol{g}}^{(\mathrm{sj})} = -\frac{\gamma p_{\mathrm{F}}}{4}\Big[\check{g}_{\mathrm{s}}\big[\hat{\tau}_3\hat{\boldsymbol{\alpha}}, \check{g}_{\mathrm{s}}\big]_+ \overset{\times}{,} \boldsymbol{\nabla}\check{g}_{\mathrm{s}}\Big]_-. \tag{4.8c}$$

Lastly, the spin swapping self-energy (4.5) contributes with

$$\delta\check{\boldsymbol{g}}^{(\mathrm{sw})} = \frac{\mathrm{i}\eta l_{\mathrm{tr}}}{3}\frac{\tau_{\mathrm{tr}}}{\tau_{\mathrm{sw}}}\Big[\big[\hat{\tau}_3\hat{\boldsymbol{\alpha}}, \check{g}_{\mathrm{s}}\big]_+ \overset{\times}{,} \boldsymbol{\nabla}\check{g}_{\mathrm{s}}\Big]_-. \tag{4.8d}$$

These corrections successively alter the current expressions through the matrix current of Eq. (2.24). By comparing the skew scattering (4.8b) and side-jump (4.8c) contributions, it already becomes evident that they both contribute to the same mechanism. This result also confirms our decision to not disregard the side-jump self-energy contribution (4.6), which technically only appears to next-to-leading order in the gradient approximation.

4.1.3 Anomalous Current

In addition to the corrections discussed in the previous section, which enter the current expressions by giving rise to additional terms in the anisotropic

Green's function, the side-jump contributions stemming from the anomalous velocity and the Yafet term discussed in Section 3.1.2 directly alter the velocity operator and, consequently, the current operator. In total, the anomalous corrections to the velocity operator are given in terms of Eqs. (3.4):

$$\hat{\boldsymbol{v}}(\boldsymbol{r}) \to \hat{\boldsymbol{v}}(\boldsymbol{r}) + \hat{\boldsymbol{v}}_{\mathrm{so}}(\boldsymbol{r}), \quad \hat{\boldsymbol{v}}_{\mathrm{so}}(\boldsymbol{r}) = 2\gamma \sum_i \left(\hat{\tau}_3 \hat{\boldsymbol{\alpha}} \times \boldsymbol{\nabla} u(\boldsymbol{r} - \boldsymbol{r}_i)\right). \tag{4.9}$$

In light of our definitions of the current densities in Eqs. (2.22), the anomalous contribution to the matrix current of Eq. (2.24) reads

$$\hat{\boldsymbol{\jmath}}_{\mathrm{so}}(1) = \frac{\mathrm{i}}{2N_0} \lim_{1' \to 1} \left(\hat{\boldsymbol{v}}_{\mathrm{so}}(\boldsymbol{r}_1)\hat{G}^{\mathrm{K}}(1,1') + \hat{G}^{\mathrm{K}}(1,1')\hat{\boldsymbol{v}}_{\mathrm{so}}(\boldsymbol{r}_{1'})\right). \tag{4.10}$$

The challenge here lies in calculating the impurity average. While the conventional velocity operator is independent of the impurity configuration, the anomalous contribution explicitly depends on the impurities. The impurity average of Eq. (4.10) can be obtained by following the procedure which was employed by Shchelushkin and Brataas [86] in order to calculate the side-jump contribution to the spin Hall effect in a diffusive metal. To first order in the spin-orbit coupling strength we find, see Appendix B,

$$\begin{aligned}
\left\langle \hat{\boldsymbol{v}}_{\mathrm{so}}(\boldsymbol{r}_1)\hat{G}^{\mathrm{K}}(1,1') \right\rangle_{\mathrm{c}} &= \int \mathrm{d}2 \left(\check{\boldsymbol{\Sigma}}^{(\mathrm{l})}_{\mathrm{sj}}(1,2)\check{G}_{\mathrm{c}}(2,1')\right)^{\mathrm{K}}, \\
\left\langle \hat{G}^{\mathrm{K}}(1,1')\hat{\boldsymbol{v}}_{\mathrm{so}}(\boldsymbol{r}_{1'}) \right\rangle_{\mathrm{c}} &= \int \mathrm{d}2 \left(\check{G}_{\mathrm{c}}(1,2)\check{\boldsymbol{\Sigma}}^{(\mathrm{r})}_{\mathrm{sj}}(2,1')\right)^{\mathrm{K}},
\end{aligned}$$

where, within the self-consistent Born approximation,

$$\check{\boldsymbol{\Sigma}}^{(\mathrm{l})}_{\mathrm{sj}}(1,1') = 2\gamma n \int \mathrm{d}\boldsymbol{r}_i \left(\hat{\tau}_3 \hat{\boldsymbol{\alpha}} \times \boldsymbol{\nabla} u(\boldsymbol{r}_1 - \boldsymbol{r}_i)\right)\check{G}_{\mathrm{c}}(1,1')u(\boldsymbol{r}_{1'} - \boldsymbol{r}_i)$$

and

$$\check{\boldsymbol{\Sigma}}^{(\mathrm{r})}_{\mathrm{sj}}(1,1') = 2\gamma n \int \mathrm{d}\boldsymbol{r}_i\, u(\boldsymbol{r}_1 - \boldsymbol{r}_i)\check{G}_{\mathrm{c}}(1,1')\left(\hat{\tau}_3 \hat{\boldsymbol{\alpha}} \times \boldsymbol{\nabla} u(\boldsymbol{r}_{1'} - \boldsymbol{r}_i)\right)$$

are 'vector self-energies' and proportional to the spin-orbit coupling. Using this, we obtain the impurity-averaged anomalous correction to the matrix current (2.24)

$$\hat{\boldsymbol{\jmath}}(\boldsymbol{R},\epsilon) \to \hat{\boldsymbol{\jmath}}(\boldsymbol{R},\epsilon) + \hat{\boldsymbol{\jmath}}_{\mathrm{so}}(\boldsymbol{R},\epsilon), \quad \hat{\boldsymbol{\jmath}}_{\mathrm{so}}(\boldsymbol{R},\epsilon) = -\frac{\gamma p_{\mathrm{F}} l_{\mathrm{tr}}}{6\tau_{\mathrm{tr}}} \left[\hat{\tau}_3 \hat{\boldsymbol{\alpha}} \circledast \boldsymbol{\nabla} \hat{g}^{\mathrm{K}}_{\mathrm{s}}(\boldsymbol{R},\epsilon)\right]_-, \tag{4.11}$$

in the quasiclassical approximation.

4.2 Diffusion Equations

We now have all the ingredients to derive kinetic equations describing the transport of spin, charge, and energy in a diffusive superconductor in terms of the distribution functions and currents introduced in Chapter 2. In this section, we first present and discuss the diffusion equations. The next section is devoted to the current expressions.

Using the expression for the anisotropic Green's function (4.8), the Keldysh matrix block of the Usadel equation (4.3) can now be expressed in terms of the divergence of the matrix current (4.11). By multiplying with suitable matrices and taking the trace, we then obtain the following diffusion equations:

$$\nabla_i j_i = -2\alpha\Delta h, \tag{4.12a}$$

$$\nabla_i j_{ij} = -\Big(\frac{\alpha_{\rm so}}{\tau_{\rm so}} + \frac{\alpha_{\rm m}}{\tau_{\rm m}}\Big) h_j, \tag{4.12b}$$

$$\nabla_i j_{\epsilon i} = 0, \tag{4.12c}$$

$$\nabla_i j_{\epsilon ij} = -2\alpha\Delta h_{\epsilon j} - \Big(\frac{\alpha_{\epsilon\rm so}}{\tau_{\rm so}} + \frac{\alpha_{\epsilon\rm m}}{\tau_{\rm m}}\Big) h_{\epsilon j}. \tag{4.12d}$$

Here, j_i and j_{ij} are the charge and the spin currents introduced in Section 2.1, $j_{\epsilon i}$ is the energy current and $j_{\epsilon ij}$ is the spin-energy current. Eq. (4.12c) expresses energy conservation at each energy in the elastic transport regime that we study. The terms proportional to the superconducting order parameter Δ in Eqs. (4.12a) and (4.12d) convert quasiparticle currents into supercurrents [87]. The terms proportional to the spin relaxation scattering times $\tau_{\rm so}$ and $\tau_{\rm m}$ are due to spin-orbit coupling and magnetic impurities, respectively. Superconducting correlations introduce renormalization factors, which are energy dependent and governed by the superconducting state. They are given in terms of the elements of the retarded Green's function (2.18b),

$$\alpha = \mathrm{Im}[f_{\rm s}^{\rm R}], \tag{4.13a}$$

$$\alpha_{\rm so} = \mathrm{Re}[g_{\rm s}^{\rm R}]^2 - \mathrm{Re}[f_{\rm s}^{\rm R}]^2, \tag{4.13b}$$

$$\alpha_{\rm m} = \mathrm{Re}[g_{\rm s}^{\rm R}]^2 + \mathrm{Re}[f_{\rm s}^{\rm R}]^2, \tag{4.13c}$$

$$\alpha_{\epsilon\rm so} = \mathrm{Re}[g_{\rm s}^{\rm R}]^2 + \mathrm{Im}[f_{\rm s}^{\rm R}]^2, \tag{4.13d}$$

$$\alpha_{\epsilon\rm m} = \mathrm{Re}[g_{\rm s}^{\rm R}]^2 - \mathrm{Im}[f_{\rm s}^{\rm R}]^2. \tag{4.13e}$$

As indicated in Chapter 3, the spin relaxation rates induced by spin-orbit

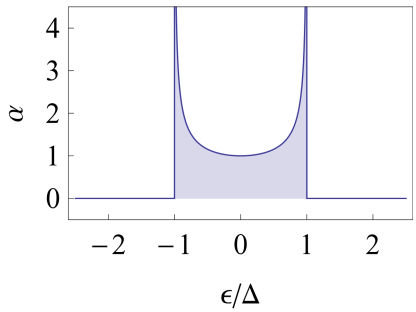

(a) Renormalization of gap scattering.

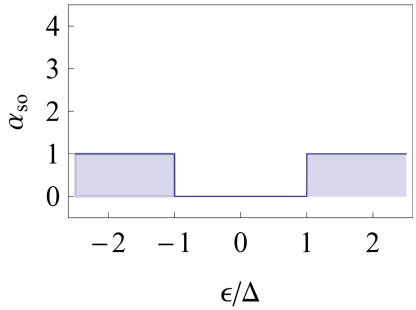

(b) Renormalization of spin relaxation due to spin-orbit coupling.

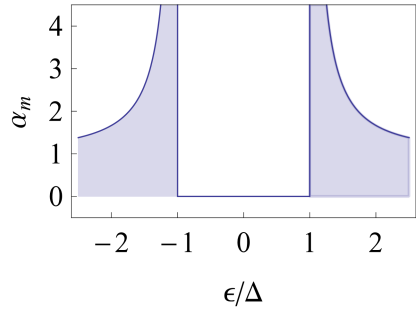

(c) Renormalization of spin relaxation due to magnetic impurities.

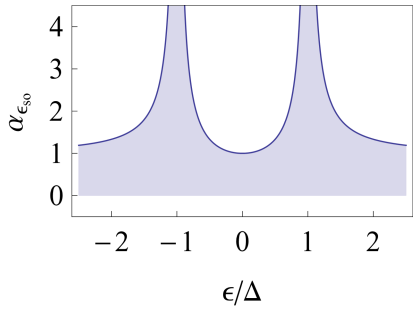

(d) Renormalization of spin-energy relaxation due to spin-orbit coupling.

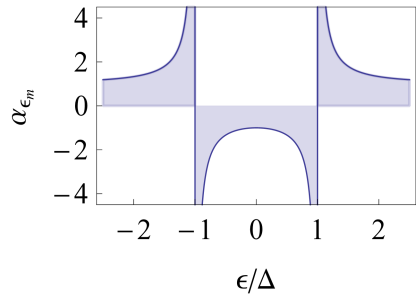

(e) Renormalization of spin-energy relaxation due to magnetic impurities.

Figure 4.1: Renormalization factors for gap scattering and spin relaxation in the BCS limit.

coupling and magnetic impurities are renormalized differently. This makes them easily distinguishable in the superconducting state and allows for a spin-flip spectroscopy [49] in order to determine which scattering mechanism is more efficient. To gain inside into how these renormalization factors

influence diffusion, let us consider the case of a bulk BCS superconductor (BCS limit). This is, for instance, realized in large superconductors coupled weakly to reservoirs that inject spin and charge currents. The renormalization factors in this limit are given by, see Fig. 4.1,

$$\alpha = \frac{\Delta}{\sqrt{\Delta^2 - \epsilon^2}}\Theta(\Delta^2 - \epsilon^2), \tag{4.14a}$$

$$\alpha_{\mathrm{so}} = \Theta(\Delta^2 - \epsilon^2), \tag{4.14b}$$

$$\alpha_{\mathrm{m}} = \frac{\epsilon^2 + \Delta^2}{\epsilon^2 - \Delta^2}\Theta(\epsilon^2 - \Delta^2), \tag{4.14c}$$

$$\alpha_{\epsilon\mathrm{so}} = \frac{\epsilon^2}{\epsilon^2 - \Delta^2}\Theta(\epsilon^2 - \Delta^2) + \frac{\Delta^2}{\Delta^2 - \epsilon^2}\Theta(\Delta^2 - \epsilon^2), \tag{4.14d}$$

$$\alpha_{\epsilon\mathrm{m}} = \frac{\epsilon^2}{\epsilon^2 - \Delta^2}\Theta(\epsilon^2 - \Delta^2) - \frac{\Delta^2}{\Delta^2 - \epsilon^2}\Theta(\Delta^2 - \epsilon^2). \tag{4.14e}$$

Quasiparticles can propagate for energies above the gap, $|\epsilon| > |\Delta|$, when there is no conversion of quasiparticle currents into supercurrents and $\alpha = 0$. The spin-orbit-induced spin relaxation rate is identical in the superconducting and normal states whereas the spin-energy relaxation rate is enhanced in the superconducting state. In contrast, the spin relaxation and spin-energy relaxation rates are both enhanced for quasiparticles with energies close to the superconducting gap for scattering at magnetic impurities. Note that $\alpha_{\epsilon\mathrm{m}}$ is negative for energies below the gap, $|\Delta| > |\epsilon|$, and acts as a source for spin-energy in Eq. (4.12d).

4.3 Current Expressions

The diffusion equations (4.12) are complemented with expressions for the currents in terms of the distribution functions. To first order in the spin-orbit coupling, there are three contributions to the current: the conventional diffusion terms $j^{(0)}$, the spin Hall effect $j^{(\mathrm{sH})}$, and the spin swapping effect $j^{(\mathrm{sw})}$:

$$j = j^{(0)} + j^{(\mathrm{sH})} + j^{(\mathrm{sw})}. \tag{4.15}$$

Let us now discuss these contributions. Note that the following currents satisfy Onsager's reciprocal relations.

4.3.1 Diffusion Currents

Using Eqs. (2.15) and (2.24), we obtain, to zeroth order in the spin-orbit interaction strength,

$$j_i^{(0)} = -D_\mathrm{p}\nabla_i h, \tag{4.16a}$$
$$j_{ij}^{(0)} = -D_\epsilon\nabla_i h_j, \tag{4.16b}$$
$$j_{\epsilon i}^{(0)} = -D_\epsilon\nabla_i h_\epsilon, \tag{4.16c}$$
$$j_{\epsilon ij}^{(0)} = -D_\mathrm{p}\nabla_i h_{\epsilon j}. \tag{4.16d}$$

The generalized diffusion constants

$$D_\mathrm{p} = D(\mathrm{Re}[g_\mathrm{s}^\mathrm{R}]^2 + \mathrm{Im}[f_\mathrm{s}^\mathrm{R}]^2), \tag{4.17a}$$
$$D_\epsilon = D(\mathrm{Re}[g_\mathrm{s}^\mathrm{R}]^2 - \mathrm{Re}[f_\mathrm{s}^\mathrm{R}]^2), \tag{4.17b}$$

are energy-dependent and governed by the superconducting correlations. In the BCS limit, they are given by

$$D_\mathrm{p}/D = \frac{\epsilon^2}{\epsilon^2-\Delta^2}\Theta(\epsilon^2-\Delta^2) + \frac{\Delta^2}{\Delta^2-\epsilon^2}\Theta(\Delta^2-\epsilon^2), \tag{4.18a}$$
$$D_\epsilon/D = \Theta(\epsilon^2-\Delta^2). \tag{4.18b}$$

While the diffusion of spin and energy is governed by the normal state diffusion constant D and only exists for energies above the gap, $|\epsilon| > |\Delta|$, the diffusion of charge and spin-energy is enhanced close to the superconducting gap, see Fig. 4.2.

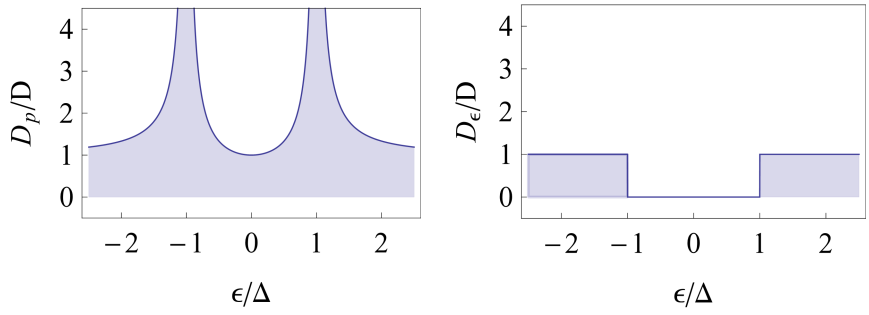

(a) Generalized diffusion constant for charge and spin-energy.

(b) Generalized diffusion constant for energy and spin.

Figure 4.2: Generalized diffusion constants in the BCS limit.

4.3.2 Spin Hall Effect

To first order in the spin-orbit coupling, the direct and inverse spin Hall contributions to the currents are

$$j_i^{(\mathrm{sH})} = N_\mathrm{S}\chi_\mathrm{sH}\varepsilon_{ijk}D\nabla_j h_k, \tag{4.19a}$$
$$j_{ij}^{(\mathrm{sH})} = -N_\mathrm{S}\chi_\mathrm{sH}\varepsilon_{ijk}D\nabla_k h, \tag{4.19b}$$
$$j_{\epsilon i}^{(\mathrm{sH})} = N_\mathrm{S}\chi_\mathrm{sH}\varepsilon_{ijk}D\nabla_j h_{\epsilon k}, \tag{4.19c}$$
$$j_{\epsilon ij}^{(\mathrm{sH})} = -N_\mathrm{S}\chi_\mathrm{sH}\varepsilon_{ijk}D\nabla_k h_\epsilon, \tag{4.19d}$$

where the normal state spin Hall angle $\chi_\mathrm{sH} = \chi_\mathrm{sH}^{(\mathrm{sk})} + \chi_\mathrm{sH}^{(\mathrm{sj})}$ is given in terms of the skew scattering constant,

$$\chi_\mathrm{sH}^{(\mathrm{sk})} = \frac{4\eta}{3}\frac{\tau_\mathrm{tr}}{\tau_\mathrm{sk}}, \tag{4.20a}$$

and the side-jump constant,

$$\chi_\mathrm{sH}^{(\mathrm{sj})} = \frac{3\gamma m}{\tau_\mathrm{tr}}. \tag{4.20b}$$

The spin Hall angles arising from skew scattering and side-jump are all renormalized by equal amounts below the superconducting critical temperature by the renormalized density of states N_S introduced in Eq. (2.21). In the BCS limit, the renormalized density of states N_S is given by

$$N_\mathrm{S} = \frac{|\epsilon|}{\sqrt{\epsilon^2 - \Delta^2}}\Theta(\epsilon^2 - \Delta^2). \tag{4.21}$$

In the normal state, $N_\mathrm{S} = 1$, while in the BCS limit the spin Hall angle is greatly enhanced by N_S around the gap for $|\epsilon| > |\Delta|$, see Fig. 4.3.

4.3.3 Spin Swapping

The spin swapping effect is most clearly represented in terms of the zeroth order diffusion currents of Eqs. (4.16):

$$j_{ij}^{(\mathrm{sw})} = -\chi_\mathrm{sw}\Big(j_{ji}^{(0)} - \delta_{ij}j_{kk}^{(0)}\Big), \tag{4.22a}$$
$$j_{\epsilon ij}^{(\mathrm{sw})} = -\chi_\mathrm{sw}\Big(j_{\epsilon ji}^{(0)} - \delta_{ij}j_{\epsilon kk}^{(0)}\Big), \tag{4.22b}$$

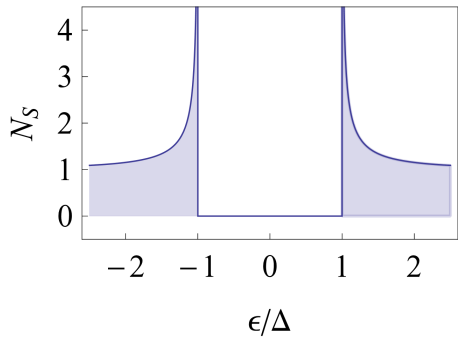

Figure 4.3: Normalized density of states in the superconducting state.

where the normal state spin swapping constant is

$$\chi_{\mathrm{sw}} = \frac{4\eta}{3}\frac{\tau_{\mathrm{tr}}}{\tau_{\mathrm{sw}}}. \tag{4.23}$$

Spin swapping is dependent on the superconducting state only through the generalized diffusion constants contained in the diffusion currents in Eqs. (4.22),

$$j_{ij}^{(\mathrm{sw})} = \chi_{\mathrm{sw}} D_\epsilon \Big(\nabla_j h_i - \delta_{ij} \nabla_k h_k \Big), \tag{4.24a}$$

$$j_{\epsilon ij}^{(\mathrm{sw})} = \chi_{\mathrm{sw}} D_{\mathrm{p}} \Big(\nabla_j h_{\epsilon i} - \delta_{ij} \nabla_k h_{\epsilon k} \Big), \tag{4.24b}$$

but otherwise is of the same form as in the normal state. We shall discuss spin swapping in the normal state in more detail in Chapter 5.

4.4 Conclusion and Outlook

We obtain our results in the elastic transport regime, in which the energy relaxation time τ_ϵ is much larger than the spin-flip length τ_{sf}, and find that the skew scattering and side-jump contributions to the spin Hall effect are renormalized alike by the superconducting density of states. In contrast, Takahashi and Maekawa [57, 47, 50] consider the spin Hall effect in the inelastic regime, in which $\tau_{\mathrm{sf}} \gg \tau_\epsilon$ and the occupation of quasiparticle states is determined by Fermi-Dirac distributions. They report that the magnitudes of the skew scattering and side-jump contributions have different temperature dependences in the superconducting state. In principle, this could prove a valuable tool to study the spin-dependent transport caused by the

interplay of the spin and charge degrees of freedom, and help determine which of the two mechanisms is more efficient. However, Tserkovnyak and Brataas [45] conclude that the elastic transport regime can be realized in a variety of conventional s-wave superconducting materials for relatively clean systems, in which electron-phonon scattering processes dominate energy relaxation. In very dirty systems, in which the impurity mean free path $l_{\mathrm{tr}} \lesssim 1\,\mathrm{nm}$, electron-electron interactions can be significant and both transport regimes can be relevant, depending on the used contacts. Experimental observations of the spin Hall effect in superconductors could provide further clarification, but are difficult to conduct due to the high susceptibility of superconductors to magnetic fields and electric currents.

As mentioned earlier in Section 3.1.2, the origins of the side-jump mechanism are three-fold for our model: i) When evaluating the self-energy to first order in the spin-orbit coupling, an additional term appears to next-to-leading order in the gradient approximation. This term contributes to the side-jump constant $\chi_{\mathrm{sH}}^{(\mathrm{sj})}$ with $\gamma m/\tau_{\mathrm{tr}}$. In addition, the velocity operator acquires two spin-dependent corrections due to spin-orbit coupling: ii) the anomalous velocity and iii) the Yafet term. Both contribute to the side-jump constant with $\gamma m/\tau_{\mathrm{tr}}$ each. In total, the side-jump contribution to the spin Hall effect is expressed by the overall side-jump constant $\chi_{\mathrm{sH}}^{(\mathrm{sj})} = 3\gamma m/\tau_{\mathrm{tr}}$.

The extrinsic spin swapping effect is also present in the superconducting state, but shows no explicit renormalization below the superconducting critical temperature. Instead, it is influenced by superconducting correlations through the generalized diffusion constants.

At the time of writing, Paper [3] is still unpublished, and we plan to discuss experimental consequences in the future. First calculations seem to indicate a great enhancement of the extrinsic spin Hall and spin swapping signals in nonlocal geometries. We also intend to study the transport of energy and spin-energy in such devices.

5 Spin Swapping in Diffusive Metals

In this chapter, we further discuss the spin swapping effect arising from intrinsic (Rashba-type) spin-orbit coupling in two-dimensional diffusive metals, which we study in detail in Paper [2]. This effect is interesting because it is drastically different from its extrinsic counterpart. Because it is proportional to the spin-orbit coupling strength, extrinsic spin swapping is a small effect, irrespective of the system size. In contrast, the secondary spin currents and spin accumulations generated by the intrinsic spin swapping effect are of the same order of magnitude as the primary spin currents for system dimensions exceeding the spin-orbit precession length. On the other hand, a long-range intrinsic spin swapping effect takes place in narrow strips, where the system width is small compared to the spin-orbit precession length. Intrinsic spin swapping is also more complex and richer than its extrinsic counterpart, resulting in a nontrivial relation between the injected spin flow and the spin polarization. We shall first discuss the extrinsic spin swapping effect in more detail in Section 5.1, before we dwell on the nature of the intrinsic effect in Sections 5.2 and 5.3.

5.1 Extrinsic Spin Swapping

For illustrative purposes, let us demonstrate how to readily obtain the spin diffusion equation and the spin current in the presence of extrinsic spin-orbit coupling from the kinetic equations we obtained in the previous chapter by taking the normal limit as discussed in Section 2.2: Using the spin diffusion equation (4.12b) and the diffusion current expression for spin (4.16b) and setting $\Delta = 0$, directly recovers the spin diffusion equation for a two-

dimensional diffusive metal,

$$\nabla^2 h_j - \frac{1}{l_{\rm sf}^2} h_j = 0. \tag{5.1a}$$

Additionally, using the spin swapping current (4.22a) yields the corresponding spin current,

$$j_{ij} = j_{ij}^{(0)} - \chi_{\rm sw}\Big(j_{ji}^{(0)} - \delta_{ij} j_{kk}^{(0)}\Big), \tag{5.1b}$$

where $j_{ij}^{(0)} = -D\nabla_i h_j$ is the spin diffusion current and $l_{\rm sf} = \sqrt{D/(\tau_{\rm so}^{-1} + \tau_{\rm m}^{-1})}$ is the spin diffusion length. Note that extrinsic spin swapping only affects the spin current expression (5.1b). It therefore alters the boundary conditions for a conventional spin diffusion differential equation (5.1a). In general, the inverse spin Hall effect gives an additional contribution to the spin current, but because our focus lies on pure spin transport, we disregard it here. As we indicated in Chapter 3, the term proportional to the swapping constant $\chi_{\rm sw}$ relates the spin polarization to the direction of flow and results in the induction of secondary spin currents [33]. For example, a primary spin current directed along x will induce transverse spin currents that arise as follows,

$$\begin{aligned} j_{xi}^{(0)} &\Rightarrow j_{ix}, && \text{if } i \neq x, \\ j_{xx}^{(0)} &\Rightarrow -j_{yy} - j_{zz}, && \text{if } i = x, \end{aligned}$$

as can be understood from the schematic in Fig. 3.3. Here, we shall restrict ourselves to a discussion of the second of these transformations, and consider the case where an x-polarized spin current $j_{xx}^{(0)}$ is injected into a diffusive metal along the x direction. The first transformation swaps the current's flow direction and its polarization, and we consider it in detail in Paper [2] for the extrinsic and intrinsic effects.

In general, the spin currents generated by spin swapping cause spin accumulations at the lateral edges of a sample. Let us illustrate this by considering a semi-infinite two-dimensional diffusive metal of width L into which we inject a spin current $j_{xx}^{(0)}$ that is assumed to be homogeneous along y at the injection edge $x = 0$. In addition, we assume impenetrable lateral boundaries, such that $j_{yj}(y = \pm L/2) = 0$. As can be understood from Eqs. (5.1), the injected spin current decays exponentially away from the injection edge on the scale of the spin diffusion length $l_{\rm sf}$. In addition, a transverse spin current polarized along y direction is generated through spin swapping. This secondary spin current in turn gives rise to a spin accumulation at lateral

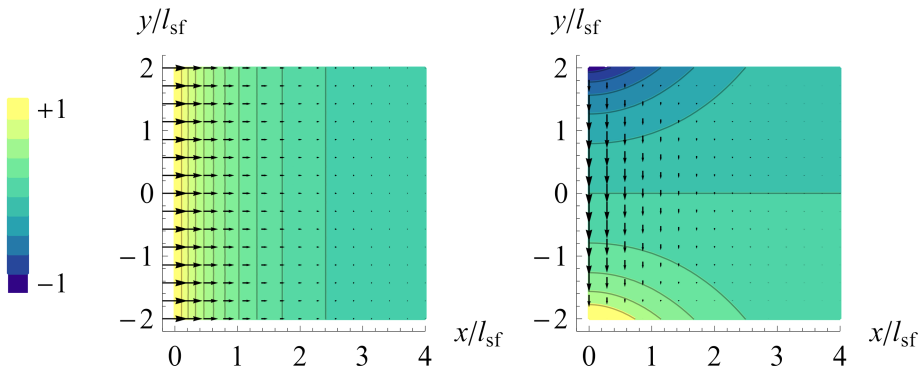

(a) Spin density and spin current polarized along x direction.

(b) Spin density and spin current polarized along y direction.

Figure 5.1: Extrinsic spin swapping in a semi-infinite two-dimensional diffusive metal of width $L = 4l_{\mathrm{sf}}$. Shown are the scaled spin densities (contours) and the scaled spin currents (arrows) according to Eqs. (5.1). A primary spin current $j_{xx}^{(0)}$ injected at $x = 0$ in (a) induces a transverse spin current j_{yy} through the spin swapping effect in (b). Note that the secondary spin accumulation and spin currents in (b) are proportional to the small swapping constant χ_{sw}.

boundaries which is antisymmetric in y. The spin currents and spin accumulations are shown in Fig. 5.1 for $L = 4l_{\mathrm{sf}}$. Note that the spin currents and spin accumulations generated through extrinsic spin swapping are proportional to the spin swapping constant χ_{sw}, and thus small compared to the injected current. This is an essential feature of the extrinsic spin swapping effect when compared to its intrinsic counterpart. In addition, there is no generation of z spin polarizations in a two-dimensional system. To further illustrate the effect, we solve the Eqs. (5.1) for the spin swapping induced spin accumulation at the lateral edges, and find

$$h_y(x, y = \pm L/2) = \begin{cases} \pm\,\chi_{\mathrm{sw}} \dfrac{2}{\pi} \dfrac{j_{xx}^{(0)}}{D} x K_1(x/l_{\mathrm{sf}}), & \text{for} \quad L \gg l_{\mathrm{sf}}, \\ \pm\,\chi_{\mathrm{sw}} \dfrac{L}{2} \dfrac{j_{xx}^{(0)}}{D} \mathrm{e}^{-x/l_{\mathrm{sf}}}, & \text{for} \quad L \ll l_{\mathrm{sf}}, \end{cases}$$

where K_1 is the modified Bessel function of the second kind and first order. This coincides with the numerical result illustrated in Fig. 5.1(b).

5.2 Intrinsic Spin Swapping

Let us now elucidate the nature of the intrinsic spin swapping effect that takes place in two-dimensional diffusive metals with Rashba spin-orbit coupling (3.7). If we assume that the spin-orbit coupling strength α is sufficiently small, such that the spin-orbit precession length $l_\mathrm{s} = (\alpha m)^{-1}$ is much larger than the elastic mean free path, the spin diffusion equations are [88]

$$\nabla^2 h_x - \frac{4}{l_\mathrm{s}^2} h_x = \frac{4}{l_\mathrm{s}} \nabla_x h_z, \tag{5.2a}$$

$$\nabla^2 h_y - \frac{4}{l_\mathrm{s}^2} h_y = \frac{4}{l_\mathrm{s}} \nabla_y h_z, \tag{5.2b}$$

$$\nabla^2 h_z - \frac{8}{l_\mathrm{s}^2} h_z = -\frac{4}{l_\mathrm{s}} (\nabla_x h_x + \nabla_y h_y), \tag{5.2c}$$

and the spin current is given by [88, 89]

$$j_{ij} = -D \nabla_i h_j + \frac{2}{l_\mathrm{s}} D (\delta_{ij} h_z - \delta_{jz} h_i). \tag{5.2d}$$

These equations are more difficult so solve than those for the extrinsic case (5.1), because they couple x, y, and z polarizations in the presence of mixed boundary conditions (determined by the spin current expression).

To demonstrate the intrinsic spin swapping effect, we first solve the Eqs. (5.2) for the spin currents and spin accumulations far away from the lateral edges of the system. For the case that we considered for extrinsic spin swapping, in which a spin current $j_{xx}^{(0)}$ is injected, we find that the primary spin current is decaying exponentially away from the injection edge at $x = 0$,

$$\frac{j_{xx}(x)}{j_{xx}^{(0)}} = \Big(\cos\left(k_i x / l_\mathrm{s}\right) + \frac{k_r^2}{\sqrt{7}} \sin\left(k_i x / l_\mathrm{s}\right) \Big) \, \mathrm{e}^{-k_r x / l_\mathrm{s}} \tag{5.3a}$$

where $k_{r/i} = \sqrt{2\sqrt{2} \mp 1}$. As was the case for extrinsic spin swapping, a transverse swapped spin current is generated,

$$\frac{j_{yy}(x)}{j_{xx}^{(0)}} = \Big((\sqrt{2} - 1) \cos\left(k_i x / l_\mathrm{s}\right) - \frac{3 + \sqrt{2}}{\sqrt{7}} \sin\left(k_i x / l_\mathrm{s}\right) \Big) \, \mathrm{e}^{-k_r x / l_\mathrm{s}}, \tag{5.3b}$$

flowing along y direction carrying y-polarized spins. But there are several important features that differ from the extrinsic effect: i) The exponential

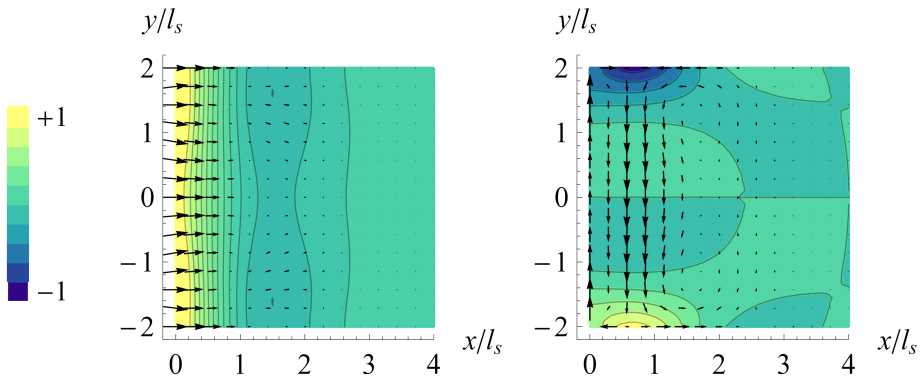

(a) Spin density and spin current polarized along x direction.

(b) Spin density and spin current polarized along y direction.

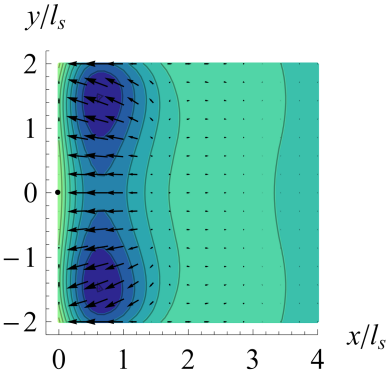

(c) Spin density and spin current polarized along z direction.

Figure 5.2: Intrinsic spin swapping in a two-dimensional diffusive metal of width $L = 4l_s$ and length $L_x = 16l_s$. A primary spin current $j_{xx}^{(0)}$ injected at $x = 0$ in (a) induces an oscillating transverse spin current j_{yy} in (b) through coupling with the z components of the spins in (c). The resulting accumulation of y components of the spins at the sample edges in (b) is a signature of the intrinsic spin swapping effect. Shown are the spin densities (contours) and spin currents (arrows) according to Eqs. (5.2) on a relative scale for each plot. Note that all quantities are of the same order of magnitude.

decay is determined by $l_s/k_r \approx 0.74 l_s$. ii) The spin currents oscillate as a function of the distance x on a scale set by $l_s/k_i \approx 0.51 l_s$. iii) The secondary spin current (5.3b) is of the same order of magnitude as the injected spin current, reaching its maximum $|\max(j_{yy}/j_{xx}^{(0)})| \approx 61\%$ within one spin-

orbit precession length from the injection edge. iv) Additional spin currents and accumulations are generated for z-polarized spins. Fig. 5.2 further illustrates the situation for a two-dimensional system of width $L = 4l_\mathrm{s}$ and length $L_x = 16l_\mathrm{s}$. The injected x-polarized spin current in Fig. 5.2(b) is coupled to the z spin components in Fig. 5.2(d) through Eqs. (5.2). In turn, this induces a transverse y-polarized spin current in Fig. 5.2(b), which is approximately given by Eq. (5.3b) for $y = 0$. This swapped spin current causes an oscillating accumulation of y-polarized spin components at the lateral edges. This is a signature of the intrinsic spin swapping effect that may be probed experimentally, for instance, by optical means or by measuring the interface voltage at weak contacts between the lateral boundaries and ferromagnets, see Paper [2].

5.3 Intrinsic Spin Swapping in a Narrow Strip

In Paper [2], we also study the spin accumulations arising from intrinsic spin swapping in a narrow strip where $L \ll l_\mathrm{s}$. This case is interesting because a long-range spin swapping effect can then be realized, for which the swapped spin accumulations can extend far along the strip on length scales much greater than the spin-orbit precession length. Due to the small parameter L/l_s, the Eqs. (5.2) can be solved analytically. Again, we shall consider the case where an x-polarized spin current is injected along x direction. The resulting population of y-polarized spins then reads, to first order in y/l_s,

$$h_y(x,y) = -2\frac{j_{xx}^{(0)} l_\mathrm{s}}{\sqrt{\Gamma} D}\frac{y}{l_\mathrm{s}}\sin\left(2x/l_\mathrm{s}\right)\mathrm{e}^{-\sqrt{\Gamma}x/l_\mathrm{s}}, \tag{5.4}$$

where the spin-orbit precession length is renormalized by the parameter $\Gamma = 2L^2/3l_\mathrm{s}^2$. Since $\sqrt{\Gamma} \ll 1$, the spin accumulation oscillates and slowly decreases along the x direction. This long-range behavior is closely related to the increase of the D'yakonov-Perel spin relaxation time in narrow strips [90]. Fig. 5.3 exemplifies the drastic increase in the spin-orbit precession length for a system of width $L = 0.3l_\mathrm{s}$ compared to the previous system illustrated in Fig. 5.2.

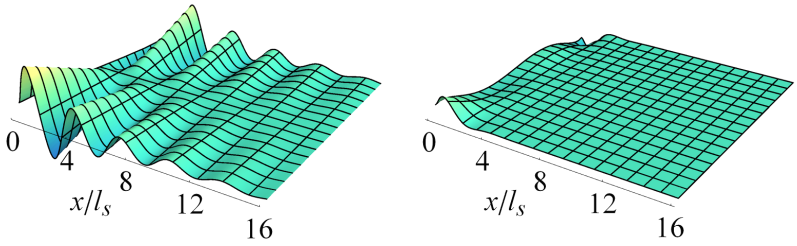

(a) System width $L = 0.3l_\mathrm{s}$. (b) System width $L = 4l_\mathrm{s}$.

Figure 5.3: Density of y-polarized spins generated via the intrinsic spin swapping effect by an x-polarized spin current injected at $x = 0$ for various system widths. (a) The swapped y-polarized spin density exhibits a long-range propagation along the x direction in a system with width $L = 0.3l_\mathrm{s}$ and length $L_x = 24l_\mathrm{s}$. In this particular case, $l_\mathrm{s}/\sqrt{\Gamma} \approx 4l_\mathrm{s}$. (b) Swapped spin density in the system shown in Fig. 5.2 with a width $L = 4l_\mathrm{s}$ and a length $L_x = 16l_\mathrm{s}$, scaled to the maximum amplitude of the spin density in (a).

5.4 Conclusion and Outlook

The spin swapping effect, especially the strong intrinsic effect, might prove a capable tool for spin manipulation in spintronic devices. In addition, the long-range spin propagation in narrow strips could help increase the effective range of spin transport in mesoscopic systems, one of the central concerns in the field of spintronics. On the other hand, the fact that secondary transverse spin currents are generated in the presence of an injected primary spin current via the spin-orbit coupling should be kept in mind when designing spintronic devices.

6 Inverse Spin Hall Effect in S|N|S Josephson Junctions

In Chapter 3, we discussed the extrinsic spin Hall effect, and in Chapter 4, we studied how it influences transport in a diffusive superconductor. Some superconductivity-induced features of the direct spin Hall effect originating from intrinsic spin-orbit coupling were analyzed in s-wave bulk superconductors by Kontani *et al.* [55], and in S|N|S Josephson junctions by Mal'shukov and Chu [56]. The latter work reveals an equilibrium spin accumulation at lateral sample edges induced by a supercurrent, similar to a nonequilibrium spin accumulation induced by the direct spin Hall effect in normal conductors. There is, however, no spin current present due to the time-reversal symmetry of the considered stationary Josephson effect. Another manifestation of the spin-orbit interaction and a demonstration of the coupling between spin and charge that the spin Hall effect provides, is the equilibrium inverse spin Hall effect in S|N|S Josephson junctions, which we study in Paper [1]. Unlike the conventional inverse spin Hall effect, which requires a nonequilibrium distribution of spins, the interplay between intrinsic spin-orbit coupling and a transverse spin distribution created by a Zeeman field inside the normal part of an S|N|S Josephson junction is sufficient to induce a supercurrent between the superconducting terminals of the junction in thermal equilibrium. The spin distribution can either be created by i) a perpendicular Zeeman field which is inhomogeneous along the transverse coordinate y, see Fig. 6.1, or ii) a homogeneous in-plane Zeeman field parallel to y. Moreover, spin-orbit coupling diminishes the depairing effects of strong Zeeman fields in such a system and leads to a long-range propagation of ± 1 triplet components on the scale of the spin-orbit precession length, providing a link between the two superconducting terminals.

The starting point for our considerations is the anomalous retarded Green's

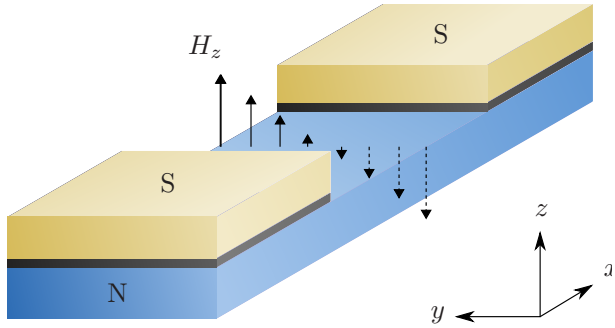

Figure 6.1: S|N|S Josephson junction. The interplay between Rashba-type spin-orbit interaction and Zeeman fields in a two-dimensional diffusive metal (N) induces a phase difference between the order parameters of the two superconducting terminals of the junction (S) in thermal equilibrium and gives rise to a supercurrent. This inverse spin Hall effect can be observed with i) a perpendicular Zeeman field which is inhomogeneous along the transverse coordinate y, or ii) a homogeneous in-plane Zeeman field parallel to y (not shown).

function $\bar{F}^{\mathrm{R}}$, i.e. the upper-right matrix block of the retarded Green's function $\hat{G}^R$ of Eq. (2.2a), which gives rise to superconducting correlations and determines the supercurrent in the junction. For convenience, we choose a decomposition in the singlet-triplet basis,

$$\bar{F}^{\mathrm{R}} = \bar{1}\frac{F_0}{\sqrt{2}} + \bar{\sigma}_z\frac{F_{\mathrm{s}}}{\sqrt{2}} + \bar{\sigma}_+\frac{F_{+1}}{2} + \bar{\sigma}_-\frac{F_{-1}}{2}, \tag{6.1}$$

where F_{s} denotes the singlet component, F_0 and $F_{\pm1}$ are the triplet components corresponding to the 0 and ±1 projections of the Cooper pair's total spin onto the z axis, and $\bar{\sigma}_\pm = \bar{\sigma}_x \pm \mathrm{i}\bar{\sigma}_y$. We assume Rashba-type spin-orbit coupling (3.7), $\bar{\mathcal{H}}_{\mathrm{so}} = \bar{\boldsymbol{\sigma}} \cdot \boldsymbol{h}_{\boldsymbol{k}}$, and the Zeeman interaction is included via

$$\bar{\mathcal{H}}_{\mathrm{Z}}(\boldsymbol{r}) = \bar{\sigma}_z H_z(\boldsymbol{r}) + \bar{\sigma}_y H_y(\boldsymbol{r}), \tag{6.2}$$

where H_z and H_y are the perpendicular and the in-plane components of the Zeeman field, respectively, which produce the equilibrium spin distribution. The Zeeman field may be created externally by a current wire or magnets or by the internal exchange field of, for example, a magnetic semiconductor. In the diffusion approximation, the transport properties are described by a generalized Usadel equation, which is obtained with the equation of motion for the Green's function (2.8) as a starting point, and by using a standard quasiclassical method [91, 54] in the limit of low S|N barrier transparency.

To fourth order in the elastic scattering time τ, it can be written as

$$\Big(2\mathrm{i}\omega_n - \tau\Big\langle\big(-\mathrm{i}\boldsymbol{v}\cdot\boldsymbol{\nabla}+2\boldsymbol{J}\cdot\boldsymbol{h_k}\big)^2\Big\rangle_{\mathrm{F}} + M\Big)\boldsymbol{\Psi} = 0, \tag{6.3}$$

where $\boldsymbol{\Psi}$ is a vector containing the energy-integrated singlet and triplet components of the anomalous retarded Green's function of Eq. (6.1), $\boldsymbol{J}$ is the vector of 3×3 matrix spin 1 operators, and $\langle\ldots\rangle_{\mathrm{F}}$ denotes the usual averaging over the Fermi surface. The discrete energies $\epsilon = \mathrm{i}\omega_n$ of the system in thermal equilibrium are expressed in terms of the Matsubara frequencies $\omega_n = (2n+1)\pi T$ for the finite temperature T. This generalized Usadel equation is similar to the one derived by Mal'shukov and Chu in Ref. [56], but includes important nontrivial new terms beyond the diffusion approximation, which emerge from the interplay between the spin-orbit coupling and the Zeeman field and give rise to the inverse spin Hall effect. These terms are contained in the rather convoluted matrix M and provide a coupling between singlet and triplet components, see Paper [1].

6.1 'Local' Approximation

In order to give a qualitative insight into the underlying physics at work, we shall now assume that spin-orbit coupling is strong, or the system sufficiently long. Derivatives in the triplet components of $\boldsymbol{\Psi}$ can then be neglected (except within one spin diffusion length near the boundaries), and a greatly simplified kinetic equation for the singlet components is obtained:

$$2\mathrm{i}\omega_n\Psi_{\mathrm{s}} = -D\nabla_x^2\Psi_{\mathrm{s}} + 2\mathrm{i}A\nabla_x\Psi_{\mathrm{s}}, \tag{6.4a}$$

where the real coefficient A is obtained from

$$2\mathrm{i}A\nabla_x = M_{\mathrm{ss}} + \frac{1}{\Gamma_{\mathrm{so}}}\sum_{m=\pm1} M_{\mathrm{s}m}M_{m\mathrm{s}}, \tag{6.4b}$$

and $\Gamma_{\mathrm{so}} = 2\tau\langle h_{\boldsymbol{k}}^2\rangle_{\mathrm{F}}$ is the spin relaxation rate. To second order in A, the solution to Eq. (6.4) is given by

$$\Psi_{\mathrm{s}}(x) = \Psi_{\mathrm{s}}^{(0)}(x)\,\mathrm{e}^{\mathrm{i}Ax/D}, \tag{6.4c}$$

where $\Psi_{\mathrm{s}}^{(0)}$ is the solution for $A = 0$. This means that an additional phase difference $\theta = LA/D$ is acquired between the superconducting terminals which are separated by a length L. Consequently, A acts as a weak electromagnetic vector potential and, similar to the Meissner effect, induces a

supercurrent $j_c \sin(\phi+\theta)$, where ϕ is the initial phase difference between the terminals and j_c is the critical current determined by the function $\Psi_s^{(0)}$. For a parallel Zeeman field, we find $A = 4\alpha\tau H_y$, which corroborates the numerical analysis by Reynoso *et al.* [92], in which an in-plane external magnetic field causes a supercurrent between the superconducting terminals, even in the absence of a phase difference. If the Zeeman field is perpendicular, however, the two terms on the r.h.s. of Eq. (6.4b) produce contributions $\propto \alpha^2\tau^3\nabla_y H_z$, which precisely cancel each other in the 'local' approximation. This is expected because this case is similar to the behavior of the spin Hall conductance, which vanishes for Rashba spin-orbit coupling [93, 94, 95]. Consequently, we should expect that $A \neq 0$ for the cubic Dresselhaus [96] spin-orbit coupling, for which the spin Hall conductance is finite [97].

6.2 Perturbative Treatment

In order to find a finite inverse spin Hall effect for Rashba spin-orbit coupling and a perpendicular Zeeman field, we need to abandon the 'local' approximation. We consider the case that the two superconducting terminals are described in terms of equal real order parameters $\Delta \gg \omega_n$ and are connected to the normal metal via tunnel barriers of low transparency. We can then express the supercurrent as a sum over the Matsubara frequencies [71] and treat M in Eq. (6.3) perturbatively. The parameter of interest is the effective phase difference θ_{eff} between the superconducting terminals, and assuming that it is small, we can express the resulting supercurrent as

$$j_c \sin(\theta_{\text{eff}}), \tag{6.5a}$$

where

$$\theta_{\text{eff}} = \frac{2l_{\text{tr}}\tau}{k_F L}\overline{\nabla_y H_z}\rho, \tag{6.5b}$$

l_{tr} is the impurity mean free path, and k_F is the Fermi wave vector. The effective phase difference thus depends on the average gradient of the perpendicular Zeeman field $\overline{\nabla_y H_z}$ within the contact region and the quantity ρ, which is shown in Fig. 6.2 as a function of the ratio of the spin relaxation rate Γ_{so} and the Thouless energy $E_T = D/L^2$, a convenient measure for the spin-orbit coupling strength. It is terms arising from the perturbation of M, which increase slower than the terms $\propto \alpha^2$ (which cancel in the 'local' approximation) and contribute to the effective phase difference.

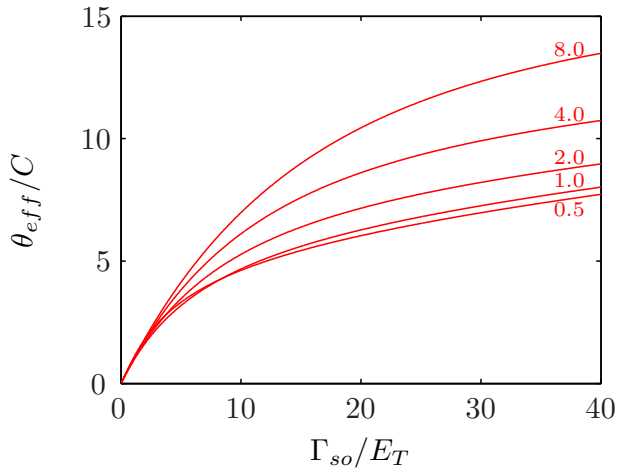

Figure 6.2: Effective phase difference $\theta_{\rm eff}$ between the superconducting terminals as a function of the ratio of the spin relaxation rate and the Thouless energy, for $0.5 < k_{\rm B}T/E_{\rm T} < 8$. The parameter $C = 2l_{\rm tr}\tau\overline{\nabla_y H_z}/k_{\rm F}L$ is a function of the average gradient of the perpendicular Zeeman field.

6.3 Long-Range Propagation in Strong Fields

The perturbative approach breaks down in the presence of strong Zeeman fields. For the case of a perpendicular field, the singlet and 0 triplet components decay exponentially close to the S|N contacts, and the latter become effectively disconnected. At the same time, ±1 triplet components are not subject to the depairing effect, as follows from Eq. (6.3), and are able to propagate on relatively large length scales set by the spin diffusion length. Such long-range triplet propagation, immune to even strong exchange fields, was studied in S|F|S junctions, where the mixing between triplet and singlet components was provided by an inhomogeneous rotating magnetization (see Ref. [54] and references therein). In our case, a coupling between $\Psi_{\pm1}$ components and $\Psi_{\rm s}$ and Ψ_0 components is achieved by the spin-orbit coupling and expressed through the matrix elements $M_{\pm1{\rm s}}$ and the spin precession operator

$$R_{0,\pm1} = -4{\rm i}\tau\Big\langle (\boldsymbol{J}_{0,\pm1}\cdot\boldsymbol{h_k})(\boldsymbol{v}\cdot\nabla)\Big\rangle_{\rm F}, \tag{6.6}$$

emerging from the second term on the l.h.s. of Eq. (6.3). Assuming that $H_z \gg \Gamma_{\rm so}, E_{\rm T}$, the relevant contribution to the supercurrent (6.5a) has the general form

$$f^{(0)}_{\rm s0}(x_{\rm L},x)R_{0m}f^{(0)}_{mm}(x,x')M_{m{\rm s}}f^{(0)}_{\rm ss}(x',x_{\rm R}), \tag{6.7}$$

where x_L and x_R define the range for free electron motion inside the normal part of the junction, and x and x' are integration variables. The unperturbed functions $f_{\mathrm{s}0}^{(0)}$ and $f_{\mathrm{ss}}^{(0)}$ are obtained from the singlet and 0 triplet projections of Eq. (6.3), where the precession term and all matrix elements of M, except $M_{\mathrm{s}0}$ and $M_{0\mathrm{s}}$, are ignored. This provides an insight into the physical processes behind the long-range propagation of $\Psi_{\pm1}$ components: the Zeeman field mixes Ψ_s and Ψ_0 components within a short range close to the left contact region (x_L). Next, the spin precession in the spin-orbit field transforms Ψ_0 triplet components into $\Psi_{\pm1}$ triplet components, which then, uninhibited by the strong exchange field, propagate towards the right contact region (x_R), where they are converted back into Ψ_s components by the matrix M. In contrast to the case with a perpendicular Zeeman field, in a parallel field alignment, ±1 triplets decay exponentially near the contacts, and thus fail to provide a long-range link between the superconducting terminals.

6.4 Conclusion and Outlook

As we have seen, the interplay of spin-orbit coupling and Zeeman fields can give rise to rich and interesting phenomena. It should be noted, that the equilibrium inverse spin Hall effect discussed here is expected to be strong in the ballistic transport regime in a metallic normal layer with strong Rashba spin-orbit coupling. Candidates for such materials are, for instance, Bi/Ag surface alloys [98] or the polar layered semiconductor BiTeI, which exhibits a giant bulk Rashba spin splitting [99, 100]. Certain niobium alloys are able to withstand high magnetic fields and maintain high critical currents [101], and could thus be a suitable choice for the superconducting terminals.

A Notation and Conventions

A.1 Fourier Transform

We define the Fourier transforms as

$$x(\boldsymbol{r},t) = \int \frac{\mathrm{d}\boldsymbol{q}}{(2\pi)^3}\, e^{i\boldsymbol{q}\boldsymbol{r}} \int \frac{\mathrm{d}\epsilon}{2\pi}\, e^{-i\epsilon t} x(\boldsymbol{q},\epsilon), \tag{A.1a}$$

$$x(\boldsymbol{q},\epsilon) = \int \mathrm{d}\boldsymbol{r}\, e^{-i\boldsymbol{q}\boldsymbol{r}} \int \mathrm{d}t\, e^{i\epsilon t} x(\boldsymbol{r},t), \tag{A.1b}$$

and we use these definitions throughout this thesis unless otherwise stated.

A.2 Einstein Notation

We use the Einstein notation throughout this thesis unless otherwise stated, i.e. repeated indices are implicitly summed over: $a_i b_i = \sum_i a_i b_i$.

A.3 Natural Units

We use natural units throughout this thesis unless otherwise stated,

$$\hbar = k_\mathrm{B} = 1. \tag{A.2}$$

A.4 Matrices

We use a 'bar' superscript to denote 2×2 matrices $\bar{A}$ in spin space, a 'hat' superscript to denote 4×4 matrices $\hat{A}$ in spin $\otimes$ particle-hole space,

and a 'check' superscript to denote 8×8 matrices $\check{A}$ in spin $\otimes$ particle-hole $\otimes$ Keldysh space.

A.4.1 Pauli Matrices

The conventional 2×2 Pauli matrices are

$$\bar{\sigma}_x = \begin{pmatrix} 0 & 1 \\ 1 & 0 \end{pmatrix}, \quad \bar{\sigma}_y = \begin{pmatrix} 0 & -\mathrm{i} \\ \mathrm{i} & 0 \end{pmatrix}, \quad \bar{\sigma}_z = \begin{pmatrix} 1 & 0 \\ 0 & -1 \end{pmatrix}, \tag{A.3}$$

and the vector of Pauli matrices is denoted by $\bar{\boldsymbol{\sigma}} = (\bar{\sigma}_x, \bar{\sigma}_y, \bar{\sigma}_z)^{\mathrm{T}}$. When dealing with superconductivity and matrices in spin $\otimes$ particle-hole space, we also make use of generalized Pauli matrices. Specifically,

$$\hat{\tau}_3 = \hat{1} \otimes \bar{\sigma}_z = \begin{pmatrix} 1 & 0 & 0 & 0 \\ 0 & 1 & 0 & 0 \\ 0 & 0 & -1 & 0 \\ 0 & 0 & 0 & -1 \end{pmatrix} \tag{A.4}$$

is a generalization of the third Pauli matrix, and

$$\hat{\boldsymbol{\alpha}} = \begin{pmatrix} \bar{\boldsymbol{\sigma}} & 0 \\ 0 & \bar{\boldsymbol{\sigma}}^* \end{pmatrix} \tag{A.5}$$

is a generalization of the vector of Pauli matrices to spin $\otimes$ particle-hole space.

B Anomalous Current Impurity Average

We shall here compute the impurity average of the anomalous current contribution following the procedure employed by Shchelushkin and Brataas in Ref. [86], exemplified by the first term on the r.h.s. of Eq. (4.10),

$$\langle \hat{\boldsymbol{v}}_{\mathrm{so}}(\boldsymbol{r}_1)\hat{G}^{\mathrm{K}}(1,1')\rangle_{\mathrm{c}} = 2\gamma\,\hat{\tau}_3\hat{\boldsymbol{\alpha}} \times \Big(\langle(\boldsymbol{\nabla}\hat{U}(\boldsymbol{r}_1))\check{G}(1,1')\rangle_{\mathrm{c}}\Big)^{\mathrm{K}}.$$

To this end, we need to calculate

$$2\gamma\,\hat{\tau}_3\hat{\boldsymbol{\alpha}} \times \langle(\boldsymbol{\nabla}\hat{U}(\boldsymbol{r}_1))\check{G}(1,1')\rangle_{\mathrm{c}}. \tag{B.1}$$

In the dirty limit, elastic impurity scattering $\hat{U}$ is the dominating perturbative term in the Hamiltonian of Eq. (2.4), and because we restrict ourselves to first order in the spin-orbit coupling, it is sufficient to use

$$\hat{\mathcal{H}}(1) = -\hat{1}\tfrac{1}{2m}\partial^2_{\boldsymbol{r}_1} - \hat{1}\mu + \hat{U}(\boldsymbol{r}_1) \tag{B.2}$$

in the following arguments. In addition, we shall further employ the self-consistent Born approximation in which only irreducible diagrams to second order in the scattering potential are considered in the self-energy and diagrams which contain crossing scattering lines are disregarded.

From the equation of motion for the Keldysh Green's function (2.8), it follows that

$$\Big(\hat{\tau}_3\mathrm{i}\partial_{t_1} - (\hat{\mathcal{H}}(1) - \hat{U}(\boldsymbol{r}_1))\Big)\check{G}_0(1,1') = \check{1}\delta(1-1'), \tag{B.3}$$

where $\check{G}_0$ is the Green's function of the unperturbed Hamiltonian $(\hat{\mathcal{H}} - \hat{U})$. Using Eq. (B.3) in Eq. (2.8) yields

$$\begin{aligned}(\hat{\tau}_3\mathrm{i}\partial_{t_1} - \hat{\mathcal{H}}(1))\check{G}(1,1') &= (\hat{\tau}_3\mathrm{i}\partial_{t_1} - \hat{\mathcal{H}}(1))\check{G}_0(1,1') + \hat{U}(\boldsymbol{r}_1)\check{G}_0(1,1') \\ &= (\hat{\tau}_3\mathrm{i}\partial_{t_1} - \hat{\mathcal{H}}(1))\check{G}_0(1,1') \\ &\quad + \int \mathrm{d}2\,\delta(1-2)\hat{U}(2)\check{G}_0(2,1').\end{aligned}$$

Letting $\left(\hat{\tau}_3 \mathrm{i}\partial_{t_1} - \hat{\mathcal{H}}(1)\right)^{-1}$ act from the left gives an integral equation,

$$\check{G}(1,1') = \check{G}_0(1,1') + \int \mathrm{d}\, 2\, \check{G}(1,2)\hat{U}(2)\check{G}_0(2,1'), \tag{B.4a}$$

where we again used Eq. (2.8). This is the so-called Dyson equation. By successively inserting the full propagator $\check{G}$ into the integrand, we obtain the infinite perturbation series

$$\check{G} = \check{G}_0 + \check{G}_0\hat{U}\check{G}_0 + \check{G}_0\hat{U}\check{G}_0\hat{U}\check{G}_0 + \check{G}_0\hat{U}\check{G}_0\hat{U}\check{G}_0\hat{U}\check{G}_0 + \ldots, \tag{B.4b}$$

where we omitted the arguments and the integrals over the inner variables for brevity. The interpretation of the Dyson equation (B.4) is straightforward: The full propagator $\check{G}$ is the sum of all possible processes in which the path of the free propagator $\check{G}_0$ is intersected by any number of scattering events at external impurities described by $\hat{U}$. Multiplying the Dyson equation (B.4) by $(\boldsymbol{\nabla}\hat{U})$ from the left and carrying out the impurity average yields

$$\left\langle (\boldsymbol{\nabla}\hat{U})\check{G}\right\rangle_{\mathrm{c}} = \left\langle (\boldsymbol{\nabla}\hat{U})\check{G}_0\hat{U}\check{G}_0\right\rangle_{\mathrm{c}} + \left\langle (\boldsymbol{\nabla}\hat{U})\check{G}_0\hat{U}\check{G}_0\hat{U}\check{G}_0\right\rangle_{\mathrm{c}} + \ldots,$$

where we used that $\langle\hat{U}\rangle_{\mathrm{c}} = 0$. In terms of a diagrammatic expansion within the self-consistent Born approximation, we obtain

$2\gamma\,\hat{\tau}_3\hat{\boldsymbol{\alpha}} \times \left\langle (\boldsymbol{\nabla}\hat{U})\check{G}\right\rangle_{\mathrm{c}}$

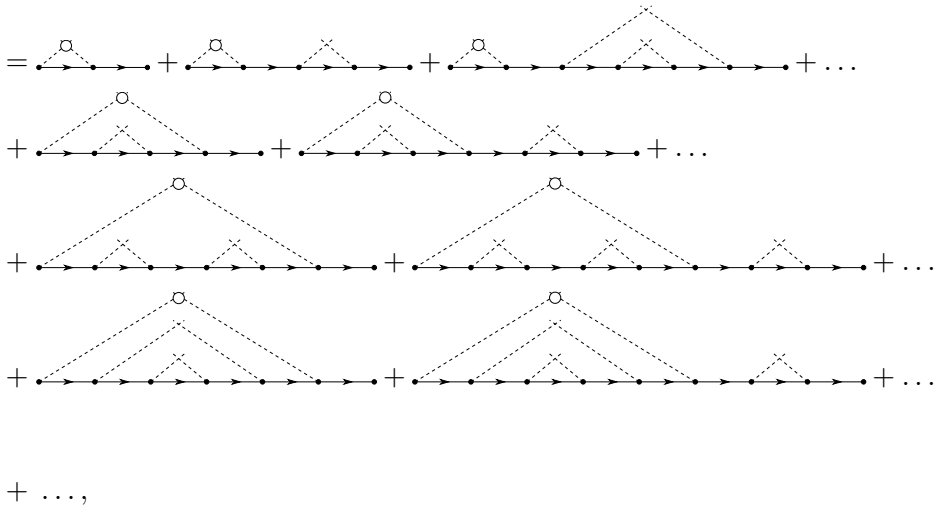

$+ \ldots,$

(B.5)

where the spin-coupled gradient of the elastic impurity scattering potential

$$2\gamma\,\hat{\tau}_3\hat{\boldsymbol{\alpha}} \times (\boldsymbol{\nabla}\hat{U}) = \text{○} \tag{B.6}$$

exclusively appears on the very left of every single contribution. By rearranging the terms in the diagrammatic expansion, we observe that

$2\gamma\,\hat{\tau}_3\hat{\boldsymbol{\alpha}} \times \langle(\boldsymbol{\nabla}\hat{U})\check{G}\rangle_{\mathrm{c}}$

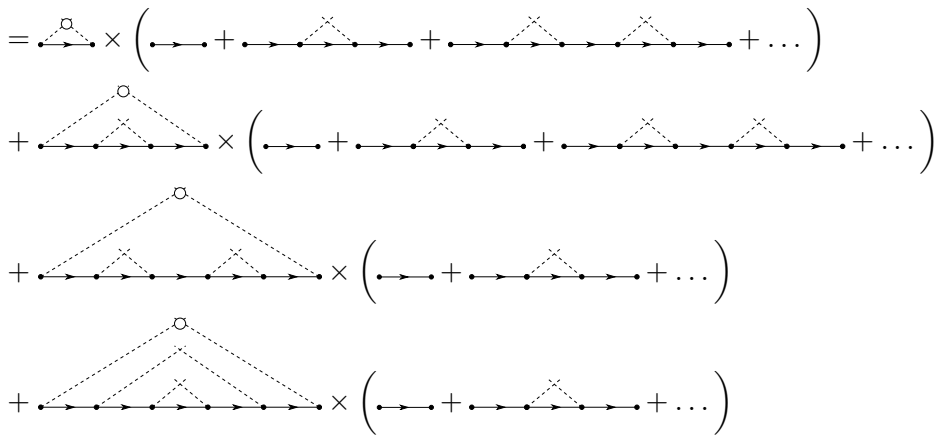

$+\ \ldots,$ (B.7)

and thus

$2\gamma\,\hat{\tau}_3\hat{\boldsymbol{\alpha}} \times \langle(\boldsymbol{\nabla}\hat{U})\check{G}\rangle_{\mathrm{c}}$

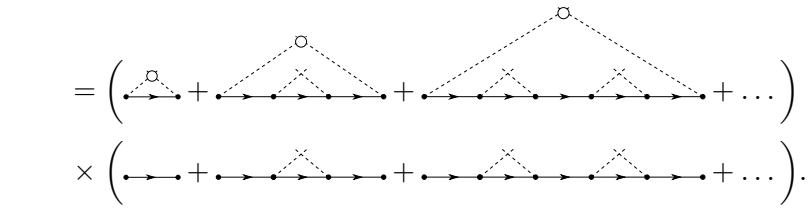

(B.8)

We now define a 'vector self-energy' within the self-consistent Born approximation,

$$\check{\boldsymbol{\Sigma}}^{(\mathrm{l})}_{\mathrm{sj}}(1,1') = 2\gamma\,\hat{\tau}_3\hat{\boldsymbol{\alpha}} \times \big\langle(\boldsymbol{\nabla}\hat{U}(\boldsymbol{r}_1))\check{G}_{\mathrm{c}}(1,1')\hat{U}(\boldsymbol{r}_{1'})\big\rangle_{\mathrm{c}} =$$ 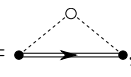 (B.9)

which is proportional to the spin-orbit coupling strength γ. The impurity-averaged full propagator $\check{G}_{\mathrm{c}} = \langle\check{G}\rangle_{\mathrm{c}}$ has the diagrammatic expansion

$$\check{G}_{\mathrm{c}}(1,1') = \check{G}_0(1,1') + \int \mathrm{d}\,2 \int \mathrm{d}\,3\, \check{G}_0(1,2)\check{\Sigma}(2,3)\check{G}_{\mathrm{c}}(3,1'),$$ (B.10)

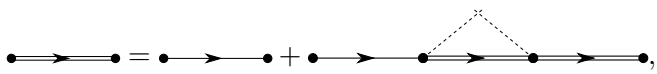

where

$$\check{\Sigma}(1,1') = \langle \hat{U}_{\rm tot}(\boldsymbol{r}_1)\check{G}_{\rm c}(1,1')\hat{U}_{\rm tot}(\boldsymbol{r}_{1'})\rangle_{\rm c} = \tag{B.11}$$

is the self-energy in the self-consistent Born approximation as defined in Eq. (2.9). Using Eqs. (B.9) and (B.10), we conclude that, to first order in the spin-orbit coupling strength,

$$\langle \hat{\boldsymbol{v}}_{\rm so}(\boldsymbol{r}_1)\hat{G}^{\rm K}(1,1')\rangle_{\rm c} = \int {\rm d}\,2\,\left(\check{\boldsymbol{\Sigma}}^{(\rm l)}_{\rm sj}(1,2)\check{G}_{\rm c}(2,1')\right)^{\rm K}. \tag{B.12}$$

Following the same arguments, we also find

$$\langle \hat{G}^{\rm K}(1,1')\hat{\boldsymbol{v}}_{\rm so}(\boldsymbol{r}_{1'})\rangle_{\rm c} = \int {\rm d}\,2\,\left(\check{G}_{\rm c}(1,2)\check{\boldsymbol{\Sigma}}^{(\rm r)}_{\rm sj}(2,1')\right)^{\rm K}, \tag{B.13}$$

where

$$\check{\boldsymbol{\Sigma}}^{(\rm r)}_{\rm sj}(1,1') = 2\gamma\langle \hat{U}(\boldsymbol{r}_1)\check{G}_{\rm c}(1,1')(\hat{\tau}_3\hat{\boldsymbol{\alpha}}\times\boldsymbol{\nabla}\hat{U}(\boldsymbol{r}_{1'}))\rangle_{\rm c}, \tag{B.14}$$

again, is a vector and proportional to the spin-orbit coupling strength γ.

Bibliography

[1] A. G. Mal'shukov, S. Sadjina, and A. Brataas. Inverse spin hall effect in superconductor/normal-metal/superconductor josephson junctions. *Phys. Rev. B*, 81:060502, 2010.

[2] S. Sadjina, A. Brataas, and A. G. Mal'shukov. Intrinsic spin swapping. *Phys. Rev. B*, 85:115306, 2012.

[3] S. Sadjina, A. Brataas, and A. G. Mal'shukov. Extrinsic spin-orbit induced spin, charge, and energy transport in diffusive superconductors, 2013. Preprint.

[4] G. E. Moore. Cramming more components onto integrated circuits. *Electronics*, 38(8):114–117, 1965.

[5] W. P. McCray. How spintronics went from the lab to the ipod. *Nat. Nano.*, 4:2–4, 2009.

[6] P. A. M. Dirac. The quantum theory of the electron. *Proc. R. Soc. Lond. A*, 117(778):610–624, 1928.

[7] S. S. P. Parkin, N. More, and K. P. Roche. Oscillations in exchange coupling and magnetoresistance in metallic superlattice structures: Co/Ru, Co/Cr, and Fe/Cr. *Phys. Rev. Lett.*, 64:2304–2307, May 1990.

[8] S. Datta and B. Das. Electronic analog of the electro-optic modulator. *Appl. Phys. Lett.*, 56(7):665–667, 1990.

[9] M. P. Walser, C. Reichl, W. Wegscheider, and G. Salis. Direct mapping of the formation of a persistent spin helix. *Nat. Phys.*, 8:757–762, 2012.

[10] H.-A. Engel, E. I. Rashba, and B. I. Halperin. Theory of spin hall effects in semiconductors. In H. Kronmüller and S. Parkin, editors,

Handbook of Magnetism and Advanced Magnetic Materials, volume 5, pages 2858–2877. Wiley, Chichester, 2007.

[11] M. I. Dyakonov and V. I. Perel. Possibility of orienting electron spins with current. *JETP Lett.*, 13:467–469, 1971.

[12] M. I. Dyakonov and V. I. Perel. Current-induced spin orientation of electrons in semiconductors. *Phys. Lett. A*, 35(6):459–460, 1971.

[13] S. Murakami, N. Nagaosa, and S.-C. Zhang. Dissipationless quantum spin current at room temperature. *Science*, 301(5638):1348–1351, 2003.

[14] J. Sinova, D. Culcer, Q. Niu, N. A. Sinitsyn, T. Jungwirth, and A. H. MacDonald. Universal intrinsic spin hall effect. *Phys. Rev. Lett.*, 92:126603, 2004.

[15] J. Sinova and A. H. MacDonald. Theory of spin–orbit effects in semiconductors. volume 82 of *Semiconductors and Semimetals*, chapter 2, pages 45–87. Elsevier, 2008.

[16] R. Raimondi, P. Schwab, C. Gorini, and G. Vignale. Spin-orbit interaction in a two-dimensional electron gas: A SU(2) formulation. *Ann. Phys.*, 524(3–4):153–162, 2012.

[17] T. Jungwirth, J. Wunderlich, and K. Olejnik. Spin hall effect devices. *Nat. Mater.*, 11:382–390, 2012.

[18] S. O. Valenzuela and M. Tinkham. Direct electronic measurement of the spin hall effect. *Nature*, 442(7099):176–179, 2006.

[19] E. Saitoh, M. Ueda, H. Miyajima, and G. Tatara. Conversion of spin current into charge current at room temperature: Inverse spin-hall effect. *Appl. Phys. Lett.*, 88(18):182509–1–182509–3, 2006.

[20] T. Kimura, Y. Otani, T. Sato, S. Takahashi, and S. Maekawa. Room-temperature reversible spin hall effect. *Phys. Rev. Lett.*, 98:156601, 2007.

[21] Y. K. Kato, R. C. Myers, A. C. Gossard, and D. D. Awschalom. Observation of the spin hall effect in semiconductors. *Science*, 306(5703):1910–1913, 2004.

[22] V. Sih, R. C. Myers, Y. K. Kato, W. H. Lau, A. C. Gossard, and D. D. Awschalom. Spatial imaging of the spin hall effect and current-

induced polarization in two-dimensional electron gases. *Nat. Phys.*, 1:31–35, 2005.

[23] J. Wunderlich, B. Kaestner, J. Sinova, and T. Jungwirth. Experimental observation of the spin-hall effect in a two-dimensional spin-orbit coupled semiconductor system. *Phys. Rev. Lett.*, 94:047204, 2005.

[24] J. Wunderlich, A. C. Irvine, J. Sinova, B. G. Park, L. P. Zarbo, X. L. Xu, B. Kaestner, V. Novak, and T. Jungwirth. Spin-injection hall effect in a planar photovoltaic cell. *Nat. Phys.*, 5:675–681, 2009.

[25] K. Ando, M. Morikawa, T. Trypiniotis, Y. Fujikawa, C. H. W. Barnes, and E. Saitoh. Photoinduced inverse spin-hall effect: Conversion of light-polarization information into electric voltage. *Appl. Phys. Lett.*, 96(8):082502, 2010.

[26] C. Brüne, A. Roth, E. G. Novik, M. Konig, H. Buhmann, E. M. Hankiewicz, W. Hanke, J. Sinova, and L. W. Molenkamp. Evidence for the ballistic intrinsic spin hall effect in hgte nanostructures. *Nat. Phys.*, 6:448–454, 2010.

[27] J. Wunderlich, B.-G. Park, A. C. Irvine, L. P. Zârbo, E. Rozkotová, P. Nemec, V. Novák, J. Sinova, and T. Jungwirth. Spin hall effect transistor. *Science*, 330(6012):1801–1804, 2010.

[28] D. Pesin and A. H. MacDonald. Spintronics and pseudospintronics in graphene and topological insulators. *Nat. Mater.*, 11:409–416, 2012.

[29] D. Culcer. Transport in three-dimensional topological insulators: Theory and experiment. *Physica E*, 44(5):860 – 884, 2012. ¡ce:title¿SI:Topological Insulators¡/ce:title¿.

[30] W. Han and R. K. Kawakami. Spin relaxation in single-layer and bilayer graphene. *Phys. Rev. Lett.*, 107:047207, Jul 2011.

[31] T.-Y. Yang, J. Balakrishnan, F. Volmer, A. Avsar, M. Jaiswal, J. Samm, S. R. Ali, A. Pachoud, M. Zeng, M. Popinciuc, G. Güntherodt, B. Beschoten, and B. Özyilmaz. Observation of long spin-relaxation times in bilayer graphene at room temperature. *Phys. Rev. Lett.*, 107:047206, Jul 2011.

[32] J.-H. Gao, J. Yuan, W.-Q. Chen, Y. Zhou, and F.-C. Zhang. Giant mesoscopic spin hall effect on the surface of topological insulator. *Phys. Rev. Lett.*, 106:057205, Feb 2011.

[33] M. B. Lifshits and M. I. Dyakonov. Swapping spin currents: Interchanging spin and flow directions. *Phys. Rev. Lett.*, 103(18):186601, 2009.

[34] H. K. Onnes. The resistance of pure mercury at helium temperatures. *Commun. Phys. Lab. Univ. Leiden*, 12:120, 1911.

[35] K. Fossheim and A. Sudbø. *Superconductivity: Physics and Applications*. Wiley, Chichester, 2004.

[36] M. Tinkham. *Introduction to Superconductivity: Second Edition*, volume 1 of *Dover Books on Physics*. Dover Publications, 2 edition, 2004.

[37] W. Meissner and R. Ochsenfeld. Ein neuer Effekt bei Eintritt der Supraleitfähigkeit. *Naturwissenschaften*, 21:787–788, 1933.

[38] F. London and H. London. The electromagnetic equations of the supraconductor. *Proceedings of the Royal Society of London. Series A - Mathematical and Physical Sciences*, 149(866):71–88, 1935.

[39] E. Maxwell. Isotope effect in the superconductivity of mercury. *Phys. Rev.*, 78:477–477, May 1950.

[40] C. A. Reynolds, B. Serin, W. H. Wright, and L. B. Nesbitt. Superconductivity of isotopes of mercury. *Phys. Rev.*, 78:487–487, May 1950.

[41] J. Bardeen, L. N. Cooper, and J. R. Schrieffer. Theory of superconductivity. *Phys. Rev.*, 108:1175–1204, Dec 1957.

[42] L. P. Gor'kov. Microscopic derivation of the ginzburg-landau in the theory of superconductivity. *Soviet Phys. JETP*, 9:1364, 1959.

[43] G. Eilenberger. Transformation of gorkov's equation for type ii superconductors into transport-like equations. *Zeitschrift für Physik*, 214:195–213, 1968.

[44] B. D. Josephson. Possible new effects in superconductive tunnelling. *Physics Letters*, 1(7):251–253, 1962.

[45] Y. Tserkovnyak and A. Brataas. Current and spin torque in double tunnel barrier ferromagnet-superconductor- ferromagnet systems. *Phys. Rev. B*, 65:094517, Feb 2002.

[46] J. P. Morten, A. Brataas, and W. Belzig. Spin transport in diffusive superconductors. *Phys. Rev. B*, 70:212508, Dec 2004.

[47] S. Takahashi and S. Maekawa. Spin current in metals and superconductors. *J. Phys. Soc. Jpn.*, 77:031009, 2008.

[48] H. Yang, S.-H. Yang, S. Takahashi, S. Maekawa, and S. S. P. Parkin. Extremely long quasiparticle spin lifetimes in superconducting aluminium using mgo tunnel spin injectors. *Nat. Mater.*, 9:586–593, 2010.

[49] N. Poli, J. P. Morten, M. Urech, A. Brataas, D. B. Haviland, and V. Korenivski. Spin injection and relaxation in a mesoscopic superconductor. *Phys. Rev. Lett.*, 100:136601, 2008.

[50] S. Takahashi and S. Maekawa. Spin hall effect in superconductors. *Jpn. J. Appl. Phys.*, 51:010110, 2012.

[51] H. L. Zhao and S. Hershfield. Tunneling, relaxation of spin-polarized quasiparticles, and spin-charge separation in superconductors. *Phys. Rev. B*, 52:3632–3638, Aug 1995.

[52] J. Y. Gu, C.-Y. You, J. S. Jiang, J. Pearson, Ya. B. Bazaliy, and S. D. Bader. Magnetization-orientation dependence of the superconducting transition temperature in the ferromagnet-superconductor-ferromagnet system: CuNi/Nb/CuNi. *Phys. Rev. Lett.*, 89:267001, Dec 2002.

[53] J. P. Morten, A. Brataas, and W. Belzig. Spin transport and magnetoresistance in ferromagnet/superconductor/ferromagnet spin valves. *Phys. Rev. B*, 72:014510, Jul 2005.

[54] F. S. Bergeret, A. F. Volkov, and K. B. Efetov. Odd triplet superconductivity and related phenomena in superconductor-ferromagnet structures. *Rev. Mod. Phys.*, 77:1321–1373, Nov 2005.

[55] H. Kontani, J. Goryo, and D. S. Hirashima. Intrinsic spin hall effect in the *s*-wave superconducting state: Analysis of the rashba model. *Phys. Rev. Lett.*, 102:086602, Feb 2009.

[56] A. G. Mal'shukov and C. S. Chu. Spin hall effect in a josephson contact. *Phys. Rev. B*, 78:104503, Sep 2008.

[57] S. Takahashi and S. Maekawa. Hall effect induced by a spin-polarized current in superconductors. *Phys. Rev. Lett.*, 88:116601, 2002.

[58] J. W. Serene and D. Rainer. The quasiclassical approach to superfluid 3he. *Physics Reports*, 101(4):221–311, 1983.

[59] J. Rammer and H. Smith. Quantum field-theoretical methods in transport theory of metals. *Rev. Mod. Phys.*, 58:323–359, 1986.

[60] W. Belzig, F. K. Wilhelm, C. Bruder, G. Schön, and A. D. Zaikin. Quasiclassical green's function approach to mesoscopic superconductivity. *Superlattices and microstructures*, 25(5–6):1251–1288, 1999.

[61] V. Chandrasekhar. An introduction to the quasiclassical theory of superconductivity for diffusive proximity-coupled systems. volume 2 of *The Physics of Superconductors*, pages 55–108. Springer Verlag, 2004.

[62] N. B. Kopnin. *Theory of Nonequilibrium Superconductivity.* The International Series of Monographs on Physics Series. Oxford University Press, Oxford, 2009.

[63] L. P. Gor'kov and G. M. Eliashberg. Generalization of ginzburg-landau equations for non-stationary problems in the case of alloys with paramagnetic impurities. *Soviet Phys. JETP*, 27:328–334, 1968.

[64] G. M. Eliashberg. Inelastic electron collisions and nonequilibrium stationary states in superconductors. *Soviet Phys. JETP*, 34:668–676, 1972.

[65] L. V. Keldysh. Diagram technique for nonequilibrium processes. *Soviet Phys. JETP*, 20:1018–26, 1965.

[66] W. Kohn and J. M. Luttinger. Quantum theory of electrical transport phenomena. *Phys. Rev.*, 108:590–611, Nov 1957.

[67] J. Rammer. *Quantum Field Theory of Non-Equilibrium States.* Cambridge University Press, Cambridge, 2007.

[68] S. Zhang and Z. Yang. Intrinsic spin and orbital angular momentum hall effect. *Phys. Rev. Lett.*, 94:066602, Feb 2005.

[69] J. Shi, P. Zhang, D. Xiao, and Q. Niu. Proper definition of spin current in spin-orbit coupled systems. *Phys. Rev. Lett.*, 96:076604, Feb 2006.

[70] V. V. Bryksin and P. Kleinert. Theory of electric-field-induced spin accumulation and spin current in the two-dimensional rashba model. *Phys. Rev. B*, 73:165313, Apr 2006.

[71] M. Yu. Kuprianov and V. F. Lukichev. Influence of boundary transparency on the critical current of dirty SS'S structures. *Soviet Phys. JETP*, 67:1163–1168, 1988.

[72] C. J. Lambert and R. Raimondi. Phase-coherent transport in hybrid superconducting nanostructures. *J. Phys.: Condens. Matter*, 10(5):901, 1998.

[73] Y. Yafet. g factors and spin-lattice relaxation of conduction electrons. volume 14 of *Solid State Physics*, pages 1 – 98. Academic Press, 1963.

[74] M. I. Dyakonov and A. V. Khaetskii. *Spin Hall effect*. Springer Series in Solid-State Sciences. Springer, 2008.

[75] N. F. Mott. The scattering of fast electrons by atomic nuclei. *Proc. R. Soc. Lond. A*, 124(794):425–442, 1929.

[76] J. Smit. The spontaneous hall effect in ferromagnetics ii. *Physica*, 24(1–5):39–51, 1958.

[77] N. F. Mott and H. S. W. Massey. *The theory of atomic collisions*. International series of monographs on physics. Oxford : Clarendon Press, 3rd edn. edition, 1965.

[78] L. Berger. Side-jump mechanism for the hall effect of ferromagnets. *Phys. Rev. B*, 2:4559–4566, 1970.

[79] S. K. Lyo and T. Holstein. Side-jump mechanism for ferromagnetic hall effect. *Phys. Rev. Lett.*, 29:423–425, 1972.

[80] P. Nozières and C. Lewiner. A simple theory of the anomalous hall effect in semiconductors. *J. Phys.*, 34(10):901–915, 1973.

[81] S.-Y. Lee and H.-W. Lee. Anomalous velocity operator in a multiparticle dirac system with electron-electron interactions. *J. Korean Phys. Soc.*, 53(6):3584–3587, 2008.

[82] Y. Yafet. Conduction electron spin relaxation in the superconducting state. *Phys. Lett. A*, 98(5–6):287–290, 1983.

[83] Yu. A. Bychkov and E. I. Rashba. Oscillatory effects and the magnetic susceptibility of carriers in inversion layers. *J. Phys. C: Solid State Phys.*, 17(33):6039–6045, 1984.

[84] G. Lommer, F. Malcher, and U. Rossler. Spin splitting in semiconductor heterostructures for $B \to 0$. *Phys. Rev. Lett.*, 60:728–731, Feb 1988.

[85] M. I. Dyakonov and V. I. Perel. Spin relaxation of conduction electrons in noncentrosymetric semiconductors. *Sov. Phys. Solid State*, 13:3023–3026, 1971.

[86] R. V. Shchelushkin and A. Brataas. Spin hall effects in diffusive normal metals. *Phys. Rev. B*, 71:045123, Jan 2005.

[87] A. Schmid and G. Schön. Linearized kinetic equations and relaxation processes of a superconductor near T_c. *Journal of Low Temperature Physics*, 20:207–227, 1975.

[88] C. S. Tang, A. G. Mal'shukov, and K. A. Chao. Generation of spin current and polarization under dynamic gate control of spin-orbit interaction in low-dimensional semiconductor systems. *Phys. Rev. B: Condens. Matter*, 71(19):195314, 2005.

[89] A. Brataas, A. G. Mal'shukov, and Y. Tserkovnyak. Spin injection in quantum wells with spatially dependent rashba interaction. *New J. Phys.*, 9(9):345, 2007.

[90] A. G. Mal'shukov and K. A. Chao. Waveguide diffusion modes and slowdown of d'yakonov-perel' spin relaxation in narrow two-dimensional semiconductor channels. *Phys. Rev. B: Condens. Matter*, 61:R2413–R2416, 2000.

[91] A. I. Buzdin. Proximity effects in superconductor-ferromagnet heterostructures. *Rev. Mod. Phys.*, 77:935–976, Sep 2005.

[92] A. A. Reynoso, G. Usaj, C. A. Balseiro, D. Feinberg, and M. Avignon. Anomalous josephson current in junctions with spin polarizing quantum point contacts. *Phys. Rev. Lett.*, 101:107001, Sep 2008.

[93] J.-I. Inoue, G. E. W. Bauer, and L. W. Molenkamp. Suppression of the persistent spin hall current by defect scattering. *Phys. Rev. B*, 70:041303, Jul 2004.

[94] R. Raimondi and P. Schwab. Spin-hall effect in a disordered two-dimensional electron system. *Phys. Rev. B*, 71:033311, Jan 2005.

[95] D. N. Sheng, L. Sheng, Z. Y. Weng, and F. D. M. Haldane. Spin hall effect and spin transfer in a disordered rashba model. *Phys. Rev. B*, 72:153307, Oct 2005.

[96] G. Dresselhaus. Spin-orbit coupling effects in zinc blende structures. *Phys. Rev.*, 100:580–586, Oct 1955.

[97] A. G. Mal'shukov and K. A. Chao. Spin hall conductivity of a disordered two-dimensional electron gas with dresselhaus spin-orbit interaction. *Phys. Rev. B*, 71:121308, Mar 2005.

[98] Ch. R. Ast, J. Henk, A. Ernst, L. Moreschini, M. C. Falub, D. Pacilé, P. Bruno, K. Kern, and M. Grioni. Giant spin splitting through surface alloying. *Phys. Rev. Lett.*, 98:186807, May 2007.

[99] K. Ishizaka, M. S. Bahramy, H. Murakawa, M. Sakano, T. Shimojima, T. Sonobe, K. Koizumi, S. Shin, H. Miyahara, A. Kimura, K. Miyamoto, T. Okuda, H. Namatame, M. Taniguchi, R. Arita, N. Nagaosa, K. Kobayashi, Y. Murakami, R. Kumai, Y. Kaneko, Y. Onose, and Y. Tokura. Giant rashba-type spin splitting in bulk bitei. *Nat. Mater.*, 10:521–526, 2011.

[100] M. S. Bahramy, R. Arita, and N. Nagaosa. Origin of giant bulk rashba splitting: Application to bitei. *Phys. Rev. B*, 84:041202, Jul 2011.

[101] B. A. Glowacki, X.-Y. Yan, D. Fray, G. Chen, M. Majoros, and Y. Shi. Niobium based intermetallics as a source of high-current/high magnetic field superconductors. *Physica C: Superconductivity*, 372–376, Part 3(0):1315–1320, 2002.

[102] H. Bruus and K. Flensberg. *Many-Body Quantum Theory in Condensed Matter Physics: An Introduction.* Oxford graduate texts in mathematics. Oxford University Press, Oxford, 2004.

[103] R. Karplus and J. M. Luttinger. Hall effect in ferromagnetics. *Phys. Rev.*, 95:1154–1160, 1954.

[104] J. E. Hirsch. Spin hall effect. *Phys. Rev. Lett.*, 83(9):1834–1837, 1999.

[105] S. Zhang. Spin hall effect in the presence of spin diffusion. *Phys. Rev. Lett.*, 85(2):393–396, 2000.

[106] L. G. Aslamazov, A. I. Larkin, and Yu. N. Ovchinnikov. Josephson effect in superconductors separated by a normal metal. *Soviet Phys. JETP*, 55:171–176, 1969.

[107] A. L. Shelankov. On the derivation of quasiclassical equations for superconductors. *Journal of Low Temperature Physics*, 60:29–44, 1985.

[108] A. A. Burkov, A. S. Núñez, and A. H. MacDonald. Theory of spin-charge-coupled transport in a two-dimensional electron gas with rashba spin-orbit interactions. *Phys. Rev. B*, 70:155308, Oct 2004.

[109] I. Žutić, J. Fabian, and S. Das Sarma. Spintronics: Fundamentals and applications. *Rev. Mod. Phys.*, 76:323–410, Apr 2004.

[110] J. J. Binney, N. J. Dowrick, A. J. Fisher, and M. E. J. Newman. *The theory of critical phenomena: an introduction to the renormalization group; Corrigendum.* Clarendon Press, Oxford, 1993.

[111] S.-Q. Shen. Spintronics and spin current. *AAPPS Bulletin*, 18:29–36, 2008.

[112] S. A. Wolf, D. D. Awschalom, R. A. Buhrman, J. M. Daughton, S. von Molnár, M. L. Roukes, A. Y. Chtchelkanova, and D. M. Treger. Spintronics: A spin-based electronics vision for the future. *Science*, 294(5546):1488–1495, 2001.

Paper 1

Inverse spin hall effect in
superconductor/normal-metal/superconductor josephson junctions.
Phys. Rev. B, 81:060502, 2010.

PHYSICAL REVIEW B **81**, 060502(R) (2010)

Inverse spin Hall effect in superconductor/normal-metal/superconductor Josephson junctions

A. G. Mal'shukov,[1] Severin Sadjina,[2] and Arne Brataas[2]
[1]*Institute of Spectroscopy, Russian Academy of Sciences, Troitsk, Moscow oblast 142190, Russia*
[2]*Department of Physics, Norwegian University of Science and Technology, NO-7491 Trondheim, Norway*
(Received 9 December 2009; published 11 February 2010)

We consider dc supercurrents in SNS junctions. Spin-orbit coupling in combination with Zeeman fields can induce an effective vector potential in the normal conductor. As a consequence, an out-of-plane spin density varying along the transverse direction causes a longitudinal phase difference between the superconducting terminals. The resulting equilibrium phase-coherent supercurrent is analog to the nonequilibrium inverse spin Hall effect in normal conductors. We explicitly compute the effect for the Rashba spin-orbit coupling in a disordered two-dimensional electron gas with an inhomogeneous perpendicular Zeeman field.

DOI: 10.1103/PhysRevB.81.060502 PACS number(s): 72.25.Dc, 71.70.Ej, 73.40.Lq, 74.50.+r

The spin Hall effect (SHE) and inverse SHE (ISHE) are remarkable demonstrations of the influence of the spin-orbit coupling on electron transport. Via this coupling, a longitudinal electric current can induce a perpendicular spin current and vice versa. These effects take place in metals and semiconductors, where the spin-orbit interaction (SOI) arises from impurity scattering[1] or band-structure effects.[2] Utilizing spin injection, SHE, and ISHE, electron spins can be controlled, as recently demonstrated experimentally.[3]

We discuss the intrinsic SHE and ISHE, where the dominant spin-orbit coupling is from the electron band structure. The study of SHE has been focused on normal conductors, e.g., normal metals and semiconductors. Interesting, and rich physics occurs in superconductors where electron transport is dissipationless and the ground state exhibits macroscopic coherence. Some superconductivity induced features of the intrinsic SHE have recently been analyzed in bulk superconductors[4] and superconductor-normal-superconductor (SNS) Josephson junctions.[5] The latter work reveals an equilibrium spin accumulation at lateral sample edges, similar to nonequilibrium spin accumulation in normal conductors, but the spin Hall current vanishes due to time-reversal symmetry in the dc Josephson effect.

We focus on ISHE in Josephson junctions. There are two scenarios depending on how the spin current (density) is created in the normal metal. In a dissipative setup, additional normal/ferromagnetic terminals in the transverse direction inject a nonequilibrium spin current. Subsequently, the ISHE induces an electric potential difference V_{SH} between superconducting terminals, causing Josephson oscillations at frequency $2eV_{SH}/\hbar$. Transport is dissipative due to the spin flow between transverse normal/ferromagnetic terminals. This phenomenon is interesting from an experimental point of view and we will study it quantitatively elsewhere, but we consider here a dissipationless effect.

We present a inverse dissipationless SHE: an out-of-plane equilibrium spin density spatially varying in the transverse direction induces a longitudinal electric supercurrent. Equivalently, it induces a phase shift between two superconducting terminals. In general, since the equilibrium spin density controls ISHE, Zeeman interaction from magnetic or exchange fields manipulates the resulting Josephson supercurrent. As an explicit illustration, we consider the interplay of spin-orbit coupling and Zeeman fields in a disordered two-dimensional electron gas (2DEG), and compute the magnitude of the equilibrium Josephson ISHE.

The interplay of Zeeman field and SOI leading to an effective phase difference between superconducting terminals has recently also been studied in two quite different systems, but neither exhibits the ISHE we discuss: a supercurrent in response to a *spatially homogenous* magnetic field occurs in Josephson tunneling through a one-dimensional (1D) wire[6] and appears in numerical simulations of the superconducting transport through a ballistic point contact[7] in a *spatially homogenous* parallel magnetic field. Note that a normal system analog of the latter phenomenon is the spin-galvanic effect[8] that is different from ISHE. In addition to our main finding of an inverse SHE, we provide an improved understanding of these phenomena by showing how the interplay of Zeeman field and SOI can result in the appearance of an effective electromagnetic vector potential. Such a vector potential, in direct analogy with the Meissner effect, gives rise to a supercurrent.

Let us outline our model. The spin-orbit interaction arises from the band structure, $H_{so}=\boldsymbol{\sigma}\cdot\mathbf{h}_{\boldsymbol{k}}$, where $\boldsymbol{\sigma}=(\sigma_x,\sigma_y,\sigma_z)$ is a vector of Pauli matrices. We assume that the spin-orbit field $\mathbf{h}_{\boldsymbol{k}}$ is given by Rashba SOI where $h_x=\alpha k_y$ and $h_y=-\alpha k_x$ (Ref. 9). Two examples of spin-density manipulations in 2DEG will be considered: (i) a perpendicular to 2DEG Zeeman field spatially varying in the transverse direction y, as shown in Fig. 1 and (ii) a homogeneous Zeeman field directed along the y axis. We will show that setup (i) exhibits an equilibrium inverse SHE. Setup ii) also changes the current-phase relation in SNS contacts. All relevant length scales are assumed larger than the mean-free path $l=v_F\tau$, and we are in the metallic regime $k_Fl\gg 1$, where k_F and v_F are the Fermi wave vector and velocity, respectively. These conditions allow a diffusion approximation in the description of electron transport. In this regime, the transport properties are described by a generalized Usadel equation, which we will now derive. The resulting Usadel equation is similar to the one in Ref. 5, but important nontrivial new terms essential for the effects we discuss are added due to the Zeeman interaction $H_Z(\mathbf{r})=\sigma_zH_z(\mathbf{r})+\sigma_yH_y(\mathbf{r})$, where H_z (H_y) are the perpendicular (in-plane) components of the Zeeman field. We start from the anomalous retarded thermal equilibrium Green function $F_{\alpha\beta}(\mathbf{r},\mathbf{k},\omega)$, which is the Fourier transform of

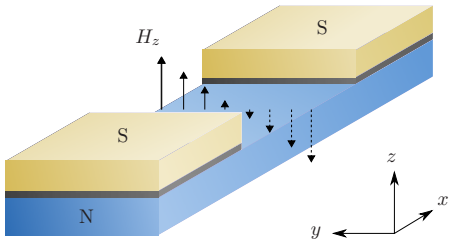

FIG. 1. (Color online) An SNS Josephson junction. Interplay between Rashba spin-orbit interaction and Zeeman splitting in a normal 2D film (n) induces a phase difference between order parameters of two superconducting terminals (s). An inhomogenous Zeeman interaction can be created by, e.g., a ferromagnetic layer on top of the film or magnetic impurities. Another possible configuration (not shown) is a uniform field parallel to the y axis

$$F_{\alpha\beta} = -i\left\langle \left[\psi_\alpha\left(\mathbf{r}+\frac{\boldsymbol{\rho}}{2},t\right), \psi_\beta\left(\mathbf{r}-\frac{\boldsymbol{\rho}}{2},t'\right)\right]_+ \right\rangle \theta(t-t') \quad (1)$$

with respect to the relative coordinate $\boldsymbol{\rho}$ and relative time $t-t'$. It is convenient to use a singlet-triplet basis representing the Green's function,

$$F_{\alpha\bar{\beta}} = \frac{1}{\sqrt{2}}(\delta_{\alpha\beta}F_0 + \sigma^z_{\alpha\beta}F_s) + \frac{\sigma^+_{\alpha\beta}}{2}F_{+1} + \frac{\sigma^-_{\alpha\beta}}{2}F_{-1}, \quad (2)$$

where $\bar{\beta}$ denotes a spin projection opposite to β, $\sigma^\pm_{\alpha\beta} = \sigma^x_{\alpha\beta} \pm i\sigma^y_{\alpha\beta}$. F_s denotes the singlet component. F_0 and $F_{\pm 1}$ are triplet components corresponding to 0 and ± 1 projections of the Cooper pair's total spin on the z axis. Using a standard method starting from Gor'kov equations[10,11] and assuming low SN barrier transmittance, we derive the linearized diffusion equation

$$\sum_m (\delta_{nm} - i\tau K_{nm})F_m = \frac{i}{2\pi N_F}[G^0_{11}\Psi + \Psi G^0_{22}]_n, \quad (3)$$

where subscripts n and m attain the values 0, ± 1, or s, τ is the elastic scattering time and

$$K = 2\omega - \mathbf{v}\hat{\mathbf{q}} - 2\mathbf{J}\mathbf{h}_\mathbf{k} - S - B. \quad (4)$$

Here $\hat{\mathbf{q}} = -i\nabla$, $\mathbf{J}$ is the 3×3 matrix spin 1 operator in the triplet subspace, and operators S and B provide mixing of triplet and singlet components,

$$S_{\pm 1,s} = -S_{s,\mp 1} = \mp\frac{\hat{\mathbf{q}}}{\sqrt{2}}\frac{\partial h^\mp_\mathbf{k}}{\partial \mathbf{k}}; \; B_{0,s} = B_{s,0} = 2H_z$$

$$B_{\pm 1,s} = -B_{s,\pm 1} = i\sqrt{2}H_y, \quad (5)$$

where $h^\pm = h^x \pm ih^y$. In the right-hand side of Eq. (3) $\Psi = \Sigma_\mathbf{k} F$ and the unperturbed retarded Green's functions are

$$G^0_{11/22} = (\omega \mp E_k - \boldsymbol{\sigma}\cdot\mathbf{h}_\mathbf{k} - \sigma_z H_z \mp \sigma_y H_y + i\Gamma)^{-1}. \quad (6)$$

The diffusion equation can be derived from Eq. (3) by expanding the operator $(1 - i\tau K)^{-1}$ for small τK and averaging over $\mathbf{k}$. The resulting Usadel equation is

$$2i\omega\Psi = \tau\langle(-i\boldsymbol{v}\cdot\nabla + 2\mathbf{J}\cdot\mathbf{h}_k)^2\rangle_F\Psi - M\Psi, \quad (7)$$

where the angular brackets denote averaging over the Fermi surface. The matrix M originates from the SOI and the Zeeman interaction expressed via the operators S and B. Its off-diagonal terms describe singlet-triplet transitions. The relevant matrix elements for our further analysis are

$$M_{ss} = 2\tau^3 \sum_{\nu=\pm} \nu\langle b^{-\nu}_\mathbf{q} H_z a^\nu_\mathbf{q} + a^{-\nu}_\mathbf{q} H_z b^\nu_\mathbf{q}\rangle_F,$$

$$M_{s\pm 1} = \frac{4i\tau^2}{\sqrt{2}}\left\langle 2H_z b^\pm_\mathbf{q} + b^\pm_\mathbf{q} H_z \mp \frac{1}{2}h^2_\mathbf{k} a^\pm_\mathbf{q}\right\rangle_F - \sqrt{2}H_y,$$

$$M_{\pm 1s} = \frac{4i\tau^2}{\sqrt{2}}\left\langle H_z b^\mp_\mathbf{q} + 2b^\mp_\mathbf{q} H_z \mp \frac{1}{2}h^2_\mathbf{k} a^\mp_\mathbf{q}\right\rangle_F + \sqrt{2}H_y,$$

$$M_{s0} = M_{0s} = -2iH_z, \quad (8)$$

where $a^\pm_\mathbf{q} = \hat{q}^i \partial h^\pm_\mathbf{k}/\partial \hat{k}^i$ and $b^\pm_\mathbf{q} = h^\pm_\mathbf{k}(\mathbf{v}\cdot\hat{\mathbf{q}})$ so that, e.g., the singlet-singlet diagonal element is proportional to ∇_x.

In order to understand some of the underlying physics described by Eq. (7), we will demonstrate that SOI in combination with the Zeeman field gives rise to an effective Meissner effect. Let us first discuss this in the most transparent "local" approximation when the SOI is strong enough/the system long enough, so that the spin-diffusion length $L_{so} = \sqrt{D/\Gamma_{so}} \ll L$, $\sqrt{D/T}$, where L is the length of the junction, $\Gamma_{so} = 2\tau\langle h^2\rangle_F$ is the spin-relaxation rate and $D = v_F^2\tau/2$ is the diffusion constant. In this approximation derivatives in triplet parts of Eq. (7) can be disregarded, except in a narrow range $\sim L_{so}$ near the boundaries. H_z is assumed to vary slowly on the L_{so} scale. Expressing the triplet components of Ψ via the singlet Ψ_s and substituting them into the singlet projection of Eq. (7), the latter takes the form

$$2i\omega\Psi_s = -D\nabla_x^2\Psi_s + 2iA\nabla_x\Psi_s, \quad (9)$$

where A is a real coefficient obtained from the equation

$$2iA\nabla_x = M_{ss} + \frac{1}{\Gamma_{so}}\sum_{m=\pm 1} M_{sm}M_{ms}. \quad (10)$$

Here we have only included dominant terms proportional to $\alpha^2\partial H_z/\partial y$ and αH_y. Higher order contributions to Eq. (9) proportional to H^2 and α^4 have been disregarded.

The diffusion Eq. (9) demonstrates that cA/e is an effective weak-electromagnetic vector potential. Therefore, similar to the Meissner effect, it will induce a supercurrent. To order A^2 the solution of Eq. (9) is $\Psi_s = \Psi_s^0 \exp(ixA/D)$, where Ψ_s^0 satisfies Eq. (9) with $A=0$. The exponential factor gives rise to an additional phase difference $\theta = LA/D$ between the superconducting terminals, the Josephson current is $j_c \sin(\phi+\theta)$, where ϕ is the initial phase difference between the terminals and j_c is the critical current determined by the function Ψ_s^0. The coefficient A is simple for Rashba SOI. For a parallel Zeeman field $A = 4\alpha\tau H_y$. For a perpendicular field it vanishes, which is expected since it is similar

to the behavior of the spin Hall conductance. Continuing such an analogy, one can expect that $A \neq 0$ for the cubic Dresselhaus[13] SOI.[12]

In order to find a finite ISHE even for the Rashba SOI, we must go beyond the local approximation. In this case, the diffusion Eq. (7) cannot be reduced to simple form (9). We consider superconducting leads with equal real order parameters Δ connected via two SN interfaces with a low transparency t. The barriers are assumed to extend into the 2DEG under the superconducting leads, so that the range of a free-electron motion is between x_L and x_R at the left and right leads, respectively. Depending on contact fabrication, other models can be similarly studied. For example, the electrons in the 2DEG could move freely underneath the contacts, with the barriers present only in z direction, as shown in Fig. 1. The choice of the model is not important for the main qualitative results obtained below.

To the lowest order in the tunneling transparency t, the superconducting current can be expressed[14] as a sum over Matsubara frequencies $\omega = \pi(2n+1)T$,

$$j = \frac{\pi e T}{2R_b^2 N_F} \sum_{\omega} \frac{\Delta^2}{\Delta^2 + \omega^2} \mathrm{Im}\left[\int dy dy' f_{\mathrm{ss}}(\mathbf{r}_L, \mathbf{r}'_R) \right], \quad (11)$$

where R_b is the boundary resistance,[15] $\mathbf{r}_{L/R} = (x_{L/R}, y)$ and $f_{ab}(\mathbf{r}_L, \mathbf{r}'_R)$, with $a, b = 0, \pm 1$, s, is the Green's function of Eq. (7), i.e., a solution of Eq. (7) with a delta source in its right-hand side. The equations for retarded and advanced functions must be properly continued to the upper and lower complex semiplanes of ω, respectively. Treating M in Eq. (7) perturbatively one can express the correction to $f_{\mathrm{ss}}^{(0)}(\mathbf{r}_L, \mathbf{r}'_R)$ as

$$\delta f_{\mathrm{ss}}(\mathbf{r}_L, \mathbf{r}'_R) = -\int d\mathbf{r} f_{\mathrm{ss}}^{(0)}(\mathbf{r}_L, \mathbf{r}) M_{\mathrm{ss}} f_{\mathrm{ss}}^{(0)}(\mathbf{r}, \mathbf{r}_R) + \sum_{mm'} \int d\mathbf{r}_1 d\mathbf{r}_2 f_{\mathrm{ss}}^{(0)} \times (\mathbf{r}_L, \mathbf{r}_1) M_{sm} f_{mm'}^{(0)}(\mathbf{r}_1, \mathbf{r}_2) M_{m's} f_{\mathrm{ss}}^{(0)}(\mathbf{r}_2, \mathbf{r}'_R), \quad (12)$$

where the unperturbed diffusion propagators $f_{\mathrm{ss}}^{(0)}(\mathbf{r}, \mathbf{r}')$ and $f_{mm'}^{(0)}(\mathbf{r}, \mathbf{r}')$, with $m, m' = 0$ or ± 1, are obtained from Eq. (7) with hard-wall boundary conditions, $\nabla_x f_{\mathrm{ss}}^{(0)} \to 0$ at $x = x_L$ and $x = x_R$, while the triplet components in the case of Rashba SOI satisfy the boundary condition $(iL_{so}\nabla_x + 2J_y) f = 0$.[16]

To illustrate the ISHE, we consider the case of Rashba SOI with finite H_z, $H_y = 0$, and $\Delta \gg \omega$. The parameter of interest is the effective phase difference between superconducting terminals,

$$\theta_{\mathrm{eff}} = \frac{\sum_{\omega} \frac{\Delta^2}{\Delta^2 + \omega^2} \mathrm{Im}\left[\int dy dy' f_{\mathrm{ss}}(\mathbf{r}_L, \mathbf{r}'_R) \right]}{\sum_{\omega} \frac{\Delta^2}{\Delta^2 + \omega^2} \mathrm{Re}\left[\int dy dy' f_{\mathrm{ss}}^{0}(\mathbf{r}_L, \mathbf{r}'_R) \right]}. \quad (13)$$

At $\theta_{\mathrm{eff}} \ll 1$ this parameter allows to express Eq. (11) in the form $j = j_c \sin \theta_{\mathrm{eff}}$. From Eq. (7), $\theta_{\mathrm{eff}} = C\rho$, where $C = 2l\overline{\nabla_y H_z}\tau / k_F L$ and $\overline{\nabla_y H_z}$ denotes the average value of the magnetic field gradient in the contact range. ρ is shown in Fig. 2 as a function of ratio of the spin-relaxation rate $\Gamma_{so} = 2\tau\alpha^2 k_F^2$ versus the Thouless energy $E_T = D/L^2$. For large SOI the "local" approximation is obtained by using the approximate form of $f_{\pm 1 \pm 1} = 2f_{00} = -\delta(\mathbf{r}_1 - \mathbf{r}_2)/\Gamma_{so}$ in the second term of Eq. (12). In this case both terms in Eq. (12) are proportional to α^2 and precisely cancel each other, as in the r.h.s. of Eq. (10). Beyond this leading "local" approximation there are terms increasing slower than α^2. They contribute to Fig. 2.

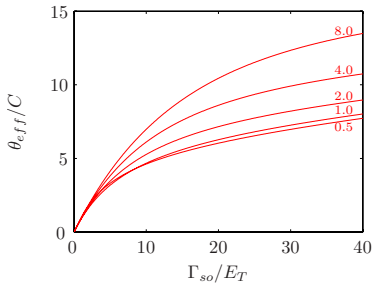

FIG. 2. (Color online) The phase difference versus a ratio of the spin-relaxation rate and the Thouless energy, at $0.5 < k_B T/E_T < 8$. The parameter C is described in the text.

Larger Zeeman fields cannot be treated perturbatively. A strong depairing effect takes place when the characteristic length $L_Z = \sqrt{D/2H}$ is small, $L_Z \ll \min(L, L_{so})$. Then, for $H = H_z$, both Ψ_s and Ψ_0 decay exponentially near contacts with superconducting terminals and the latter become effectively disconnected. On the other hand, as it follows from Eq. (7), $\Psi_{\pm 1}$ components are not subject to the depairing effect and can propagate at the relatively large distance $\sim L_{so}$. Such a long-range triplet effect has been studied in SFS junctions, where a link between triplet and singlet Cooper pairs has been induced by an inhomogeneous (rotating) magnetization (see Ref. 11 and references therein). In our case, a coupling of $\Psi_{\pm 1}$ to Ψ_0 and Ψ_s can be provided by SOI through the matrix elements $M_{\pm 1 s}$ and the spin precession operator $R_{\pm 1,0} = -i4\tau\langle(\mathbf{J}_{\pm 1,0} \cdot \mathbf{h}_k)(\boldsymbol{v} \cdot \nabla)\rangle_F$ originating from the first term in the right-hand side of Eq. (7). Indeed, assuming that $H_z \gg \Gamma_{so}$ and E_T, it is easy to show that modified Eq. (12) is represented by its second term, where the integrand has the form

$$f_{s0}^{(0)}(x_L, x) R_{0m} f_{mm}^{(0)}(x, x') M_{ms} f_{\mathrm{ss}}^{(0)}(x', x_R). \quad (14)$$

The unperturbed functions $f_{s0}^{(0)}$ and $f_{\mathrm{ss}}^{(0)}$ are obtained from s and 0 projections of Eq. (7), where the precession term and all M_{ij}, except M_{s0} and M_{0s} are ignored. The physics of the process described by Eq. (14) is clear: the magnetic field mixes 0-triplet and singlet components of the pairing function within the short range near the left boundary. Further, due to the spin precession in the SOI field the 0-triplet transforms to ± 1 triplet components. The latter propagate to the right contact where they convert to the singlet through $M_{\pm 1 s}$. Integrating Eq. (14) over x and x' gives a power-law dependence of $\mathrm{Im}[\delta f_{\mathrm{ss}}(x_L, x_R)]$ on the magnetic field,

$$\mathrm{Im}[\delta f_{\mathrm{ss}}(x_L, x_R)] \propto (|H_z(y_1)|^{-3/2} - |H_z(y_2)|^{-3/2}), \quad (15)$$

where y_1 and y_2 are y coordinates of the junction edges. Accordingly, at $L_{so} \ll L$ and $|y_1 - y_2| \sim L$ an order-of-magnitude evaluation of θ_{eff} can be written as

$$\theta_{\text{eff}} \simeq \frac{l^3}{2L_{so}^2 L}\frac{\rho}{k_F l}\left(\left|\frac{H_c}{H_z(y_1)}\right|^{3/2} - \left|\frac{H_c}{H_z(y_2)}\right|^{3/2}\right), \quad (16)$$

where $2H_c = D/L_{so}^2 = \Gamma_{so}$ and ρ is shown at Fig. 2.

In contrast to a perpendicular Zeeman field, in a parallel field ± 1 triplets exponentially decay near boundaries, as can be seen from Eqs. (7) and (8). So they cannot provide a long-range link between superconducting terminals.

In conclusion, an analog to the ISHE exists in dc Josephson SNS junctions. Unlike the normal ISHE, the supercurrent through the SNS contact can be induced by a static Zeeman interaction by magnetic or exchange fields oriented normal to the 2DEG and varying in the direction transverse to the electric current. A destructive depairing effect of the strong Zeeman field is diminished by Rashba SOI leading to a power-low dependence on this field. We show that a supercurrent through the junction can also be induced by a uniform parallel Zeeman field, corroborating thus the numerical analysis of Ref. 7. On the other hand, the depairing effect of such a field was found to be strong (exponential). In both cases an appearance of the supercurrent can be explained in terms of the Meissner effect produced by an effective vector potential, which is a combined effect of the Zeeman field and Rashba spin-orbit interaction.

We considered the diffusive transport regime which is relevant in low mobility metals and (magnetic) semiconductors. Furthermore, the diffusive regime, allows an elucidation of the main physics and parameters governing this phenomena. We expect a strong Josephson ISHE in ballistic junctions containing a metallic normal layer with a strong Rashba interaction, for example in Bi films on some substrates.[17] Ballistic quantum wells of narrow gap semiconductors are also expected to exhibit an increased Josephson ISHE.

A.G.M. gratefully acknowledges hospitality of NTNU.

[1] M. I. Dyakonov and V. I. Perel, Phys. Lett. A **35**, 459 (1971); J. E. Hirsch, Phys. Rev. Lett. **83**, 1834 (1999); S. Zhang, *ibid.* **85**, 393 (2000).

[2] S. Murakami, N. Nagaosa, and S. C. Zhang, Science **301**, 1348 (2003); J. Sinova, D. Culcer, Q. Niu, N. A. Sinitsyn, T. Jungwirth, and A. H. MacDonald, Phys. Rev. Lett. **92**, 126603 (2004).

[3] Y. K. Kato, R. C. Myers, A. C. Gossard, and D. D. Awschalom, Science **306**, 1910 (2004); J. Wunderlich, B. Kaestner, J. Sinova, and T. Jungwirth, Phys. Rev. Lett. **94**, 047204 (2005); S. O. Valenzuela and M. Tinkham, Nature (London) **442**, 176 (2006); E. Saitoh, M. Ueda, H. Miyajima, and G. Tatara, Appl. Phys. Lett. **88**, 182509 (2006); Takeshi Seki, Yu Hasegawa, Seiji Mitani, Saburo Takahashi, Hiroshi Imamura, Sadamichi Maekawa, Junsaku Nitta, and Koki Takanashi, Nature Mater. **7**, 125 (2008); T. Kimura, Y. Otani, T. Sato, S. Takahashi, and S. Maekawa, Phys. Rev. Lett. **98**, 156601 (2007).

[4] H. Kontani, J. Goryo, and D. S. Hirashima, Phys. Rev. Lett. **102**, 086602 (2009).

[5] A. G. Mal'shukov and C. S. Chu, Phys. Rev. B **78**, 104503 (2008).

[6] I. V. Krive, S. I. Kulinich, R. I. Shekhter, and M. Jonson, Low Temp. Phys. **30**, 554 (2004); I. V. Krive, A. M. Kadigrobov, R. I. Shekhter, and M. Jonson, Phys. Rev. B **71**, 214516 (2005).

[7] A. A. Reynoso, G. Usaj, C. A. Balseiro, D. Feinberg, and M. Avignon, Phys. Rev. Lett. **101**, 107001 (2008).

[8] S. D. Ganichev, E. L. Ivchenko, V. V. Bel'kov, S. A. Tarasenko, M. Sollinger, D. Weiss, W. Wegscheider, and W. Prettl, Nature (London) **417**, 153 (2002).

[9] Yu. A. Bychkov and E. I. Rashba, J. Phys. C **17**, 6039 (1984).

[10] A. I. Buzdin, Rev. Mod. Phys. **77**, 935 (2005).

[11] F. S. Bergeret, A. F. Volkov, and K. B. Efetov, Rev. Mod. Phys. **77**, 1321 (2005).

[12] A. G. Mal'shukov and K. A. Chao, Phys. Rev. B **71**, 121308(R) (2005).

[13] G. Dresselhaus, Phys. Rev. **100**, 580 (1955).

[14] L. G. Aslamazov, A. I. Larkin, and Yu. N. Ovchinnikov, Zh. Eksp. Teor. Fiz. **55**, 323 (1968) [Sov. Phys. JETP **28**, 171 (1968)].

[15] M. Yu. Kupriyanov and V. F. Lukichev, Zh. Eksp. Teor. Fiz. **94**, 139 (1988)] [Sov. Phys. JETP **67**, 1163 (1988)].

[16] A. G. Mal'shukov, L. Y. Wang, C. S. Chu, and K. A. Chao, Phys. Rev. Lett. **95**, 146601 (2005); O. Bleibaum, Phys. Rev. B **74**, 113309 (2006).

[17] C. R. Ast, J. Henk, A. Ernst, L. Moreschini, M. C. Falub, D. Pacile, P. Bruno, K. Kern, and M. Grioni, Phys. Rev. Lett. **98**, 186807 (2007); I. Gierz, T. Suzuki, E. Frantzeskakis, S. Pons, S. Ostanin, A. Ernst, J. Henk, M. Grioni, K. Kern, and C. Ast, *ibid.* **103**, 046803 (2009).

Paper 2

Intrinsic spin swapping.
Phys. Rev. B, 85:115306, 2012.

PHYSICAL REVIEW B **85**, 115306 (2012)

Intrinsic spin swapping

Severin Sadjina and Arne Brataas
Department of Physics, Norwegian University of Science and Technology, NO-7491 Trondheim, Norway

A. G. Mal'shukov
Institute of Spectroscopy, Russian Academy of Sciences, 142190, Troitsk, Moscow oblast, Russia
(Received 17 November 2011; published 12 March 2012)

Here, we study diffusive spin transport in two dimensions and demonstrate that an intrinsic analog to a previously predicted extrinsic spin swapping effect, where the spin polarization and the direction of flow are interchanged due to spin-orbit coupling at extrinsic impurities, can be induced by intrinsic (Rashba) spin-orbit coupling. The resulting accumulation of intrinsically spin-swapped polarizations is shown to be much larger than for the extrinsic effect. Intrinsic spin swapping is particularly strong when the system dimensions exceed the spin-orbit precession length and the generated transverse spin currents are of the order of the injected primary spin currents. In contrast, spin accumulations and spin currents caused by extrinsic spin swapping are proportional to the spin-orbit coupling. We present numerical and analytical results for the secondary spin currents and accumulations generated by intrinsic spin swapping, and we derive analytic expressions for the induced spin accumulation at the edges of a narrow strip, where a long-range propagation of spin polarizations takes place.

DOI: 10.1103/PhysRevB.85.115306 PACS number(s): 72.25.−b, 71.70.Ej, 72.20.Dp

I. INTRODUCTION

Understanding the spin-orbit interaction is essential to the development of spintronics and gives rise to various spin transport mechanisms. Effects of the spin-orbit interaction can be intrinsic or extrinsic. Intrinsic effects are caused by the spin-orbit interaction in the band structure. Extrinsic contributions arise from spin-orbit coupling at impurities. The spin Hall effect, where a transverse spin current is generated via a longitudinal charge current, is one of the effects resulting from the spin-orbit coupling and has attracted much attention, both theoretically[1–8] and experimentally.[9–15] In a sample, this transverse spin current generates opposite spin accumulations at the lateral boundaries.

While the spin Hall effect provides coupling between charge and spin, another spin-orbit-induced transport mechanism has recently been introduced in which only spins couple and which emerges even in the absence of charge currents. Primary longitudinal spin currents give rise to secondary transverse spin currents due to spin-orbit coupling at extrinsic impurities.[16] The generated secondary spin currents are proportional to the extrinsic spin-orbit coupling strength. The effect has been coined "spin swapping" because, in its simplest manifestation, it interchanges the spin polarization direction and the spin flow.[17] It has been suggested that any mechanism inducing a spin Hall effect should also give rise to spin swapping. However, it has not yet been clear how the intrinsic mechanism could produce this effect.

In this paper, we demonstrate that an intrinsic (Rashba spin-orbit-induced) spin swapping effect exists in two-dimensional diffusive metals and that it is drastically different from its extrinsic analog. The main distinction between these two effects is that the extrinsic effect is of the same order as the spin-orbit coupling strength and is thus small, irrespective of the system size. In contrast, the intrinsic spin swapping effect is large for system dimensions exceeding the spin-orbit precession length, and the secondary spin currents generated by this effect are then of the same order as the primary spin currents. If, however, the system width is small compared to the spin-orbit precession length, the effect is small but leads to a long-range propagation of spin polarizations closely related to the increase of the D'yakonov-Perel spin relaxation time in narrow strips.[18] Furthermore, the symmetry of intrinsic spin swapping is more complex and richer than that of the extrinsic spin swapping effect resulting in a nontrivial dependence on the relative orientation of the injected spin flow and the spin polarization. We present numerical and analytical results for the transverse secondary spin currents and accumulations induced by primary spin currents in two-dimensional diffusive metals, and we compare the intrinsic and extrinsic spin swapping effects.

This paper is organized as follows. We first provide a review of the previously discussed extrinsic spin swapping effect in Sec. II, and we compute the spin accumulations and spin currents induced by an injected primary spin current in a two-dimensional diffusive metal. In Sec. III, we discuss the intrinsic spin swapping effect, numerically evaluate the spin densities and spin currents generated through intrinsic spin swapping, and derive analytical results for the resulting spin currents far away from the lateral edges of a sample. Next, in Sec. IV, we treat the case of a narrow strip whose width is small compared to the spin-orbit precession length and find analytical expressions for the spin accumulations at the lateral edges of a sample stemming from the intrinsic spin swapping effect. In Sec. V, we briefly discuss how the spin swapping effects could be observed in experiment. Finally, we give our conclusions in Sec. VI.

II. EXTRINSIC SPIN SWAPPING

First, we review the extrinsic spin swapping effect introduced in Ref. 16 and present its features in two-dimensional diffusive metals in order to compare it to the intrinsic spin swapping effect to be discussed later. The Hamiltonian of the

system under consideration reads

$$\mathcal{H}(\boldsymbol{\rho}) = -\frac{1}{2m}\partial_{\boldsymbol{\rho}}^2 + V_{\mathrm{imp}}(\boldsymbol{\rho}) + V_{\mathrm{so}}(\boldsymbol{\rho}), \tag{1}$$

where $\boldsymbol{\rho} = (x,y)$ is a two-dimensional coordinate,

$$V_{\mathrm{imp}}(\boldsymbol{\rho}) = \frac{1}{A}\sum_{\boldsymbol{\rho}_i}\sum_{\boldsymbol{k}} v(\boldsymbol{k})\, e^{i\,\boldsymbol{k}\cdot(\boldsymbol{\rho}-\boldsymbol{\rho}_i)}, \tag{2a}$$

is the elastic impurity scattering potential, and

$$V_{\mathrm{so}}(\boldsymbol{\rho}) = -i\,\gamma[\boldsymbol{\sigma}\times\boldsymbol{\nabla}V_{\mathrm{imp}}(\boldsymbol{\rho})]\cdot\boldsymbol{\partial}_{\boldsymbol{\rho}} \tag{2b}$$

is the spin-orbit coupling. $\boldsymbol{\rho}_i$ is the position of the i^{th} impurity, A is the area, $v(\boldsymbol{k})$ is the Fourier transformed scattering potential, $\boldsymbol{\sigma} = (\sigma_x,\sigma_y,\sigma_z)^{\mathrm{T}}$ is a vector of Pauli matrices, and γ is the dimensionless spin-orbit coupling strength.

Considering transport in the diffusive limit, the spin diffusion equation reads

$$\partial_{\boldsymbol{\rho}}^2 f_b - \frac{1}{l_{\mathrm{sf}}^2} f_b = 0, \tag{3}$$

where f_b is the b component of the spin density, $b \in \{x,y,z\}$, and l_{sf} is the spin-flip length. In order to study spin transport, one also needs to define the spin current. In the leading approximation, while neglecting spin-orbit effects, the spin current is given by the spin diffusion current $j_{ab}^{(0)} = -D\partial_a f_b$ flowing along a and polarized along b, where D is the diffusion constant. The spin-orbit interaction gives rise to additional terms in the spin current. To first order in the spin-orbit coupling strength γ, when there is no charge current giving rise to the spin Hall effect, the spin current is[16]

$$j_{ab} = j_{ab}^{(0)} + \chi\left(j_{ba}^{(0)} - \delta_{ab} j_{cc}^{(0)}\right). \tag{4}$$

The term proportional to the swapping constant χ relates the spin polarization to the direction of flow and results in the induction of secondary spin currents (i.e., a "spin swapping" effect).[16] For example, a primary spin current directed along x will induce transverse spin currents that arise as follows,

$$j_{xb}^{(0)} \Rightarrow j_{bx},$$

if $b \neq x$, and

$$j_{xx}^{(0)} \Rightarrow -j_{yy} - j_{zz}.$$

The first of these transformations swaps the current's flow direction and its polarization. In general, this causes spin accumulations at the lateral edges of a sample, as we shall see shortly. The swapping constant is linear in the spin-orbit coupling strength and can be calculated explicitly,[16]

$$\chi = 2\gamma p_{\mathrm{F}}^2, \tag{5}$$

where p_{F} is the momentum at the Fermi level and short-ranged scattering potentials are assumed.

Extrinsic spin swapping arises from the additional terms in the spin current (4) that are proportional to χ, whereas the spin diffusion Eq. (3) is unaltered. Extrinsic spin swapping therefore affects the boundary conditions for an unaltered, conventional spin diffusion differential equation. We will see later that the spin diffusion equation for the intrinsic spin swapping effect is altered as well, giving rise to a richer class of phenomena.

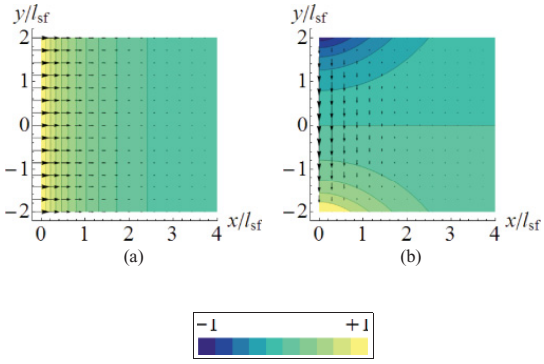

FIG. 1. (Color online) The extrinsic spin swapping effect in a semi-infinite two-dimensional diffusive metal of width $L = 4l_{\mathrm{sf}}$. Shown are the scaled spin densities and the scaled spin currents according to Eqs. (3) and (4). (a) Spin density and spin current polarized along x. (b) Spin density and spin current polarized along y. A primary spin current $j_{xx}^{(0)}$ injected at $x = 0$ in 1(a) induces a transverse spin current j_{yy} through the spin swapping effect in 1(b). Note that the secondary spin accumulation and spin currents in 1(b) are linear with respect to the small swapping constant χ. If, instead, a primary spin current $j_{xy}^{(0)}$ polarized along y is injected, f_y and j_{xy} are illustrated by 1(a) and the resulting secondary spin density and spin current (f_x and j_{yx}, respectively) only differ from 1(b) by a sign.

In order to compare the extrinsic spin swapping effect with its intrinsic analog to be discussed in the next section, we first study the spin polarizations generated via the extrinsic spin swapping effect beyond the discussion given in Ref. 16. We consider a semi-infinite two-dimensional diffusive metal of width L into which a spin current $j_{xx}^{(0)}$ directed along x and carrying spins polarized along x is injected at $x = 0$. We assume that the injected current is homogeneous along y at the injection edge. Furthermore, we assume impenetrable lateral sample edges such that no spin current flows through, with $j_{yb}(y = \pm L/2) = 0$ for any spin polarization b. The spin-orbit coupling at extrinsic impurities generates a transverse spin current j_{yy} on length scales larger than the mean free path according to Eq. (4). In turn, this gives rise to an accumulation of spins at the lateral edges of the sample polarized along y that is antisymmetric in the transverse coordinate y. The spin accumulation and spin current are plotted in Fig. 1: Fig. 1(a) shows the polarization along x, and Fig. 1(b) shows the polarization along y. In the two-dimensional case considered here, no transformation into spins polarized along z takes place. Note that the extrinsic spin swapping effect and, therefore, the resulting secondary spin accumulations and spin currents are of the order of the small swapping constant χ. Solving the spin diffusion equation with the above-mentioned boundary conditions, the accumulation of spins at the lateral edges of a sample can be obtained analytically and may be probed experimentally,

$$f_y(y = \pm L/2) = \begin{cases} \pm\frac{2}{\pi}\frac{j_{xx}^{(0)}\chi}{D}\, x\, K_1(x/l_{\mathrm{sf}}), & \text{for} \quad L \gg l_{\mathrm{sf}}, \\ \pm\frac{L}{2}\frac{j_{xx}^{(0)}\chi}{D}\, e^{-x/l_{\mathrm{sf}}}, & \text{for} \quad L \ll l_{\mathrm{sf}}, \end{cases}$$

where K_1 is the modified Bessel function of the second kind and first order. This coincides with the numerical result illustrated in Fig. 1. If, instead, a primary spin current $j_{xy}^{(0)}$ polarized along y is injected, the resulting secondary spin densities and spin currents (f_x and j_{yx}, respectively) differ only by a sign according to Eq. (4) and can also be illustrated as shown in Fig. 1.

III. INTRINSIC SPIN SWAPPING

We now elucidate the nature of the intrinsic spin swapping effect. The Hamiltonian of a two-dimensional metal with intrinsic spin-orbit coupling reads as

$$\mathcal{H}(\boldsymbol{k}) = \frac{\hbar^2 k^2}{2m^*} + \boldsymbol{\sigma}\cdot\boldsymbol{h_k} + v(\boldsymbol{k}), \tag{6}$$

where m^* is the effective electron mass, $\boldsymbol{k}$ is the electron wave vector, and $v(\boldsymbol{k})$ is the Fourier transformed scattering potential. We assume Rashba spin-orbit coupling,[19]

$$\boldsymbol{h_k} = (\alpha k_y, -\alpha k_x, 0)^{\mathrm{T}}, \tag{7}$$

where α defines the spin-orbit coupling strength. When α is sufficiently small, such that the spin-orbit precession length $l_s = (\alpha m^*)^{-1}$ is much larger than the elastic mean free path, the spin diffusion equation reads[20]

$$\boldsymbol{\partial}_\rho^2 f_x - \frac{4}{l_s^2} f_x = \frac{4}{l_s}\partial_x f_z, \tag{8a}$$

$$\boldsymbol{\partial}_\rho^2 f_y - \frac{4}{l_s^2} f_y = \frac{4}{l_s}\partial_y f_z, \tag{8b}$$

$$\boldsymbol{\partial}_\rho^2 f_z - \frac{8}{l_s^2} f_z = -\frac{4}{l_s}(\partial_x f_x + \partial_y f_y). \tag{8c}$$

The spin current is given by[20,21]

$$j_{ab} = -D\partial_a f_b + \frac{2}{l_s} D(\delta_{ab} f_z - \delta_{bz} f_a). \tag{9}$$

The diffusion equations (8) for the case of intrinsic spin-orbit coupling are more difficult to solve analytically than for the extrinsic case because the x, y, and z spin components are coupled. Therefore, we numerically study the spin currents and the accumulations of spins resulting from intrinsic spin swapping in a two-dimensional system. Before presenting the numerical results, we discuss the simple analytical expressions that can be derived for the spin accumulations and spin currents induced by intrinsic spin swapping far away from the lateral edges of a sample. The problem can also be treated analytically for a narrow strip system whose width is small compared to the spin-orbit precession length (see Sec. IV).

We first consider a case analogous to that given for extrinsic spin swapping. A spin current $j_{xx}^{(0)} = j_{xx}(x=0)$ carrying spins polarized along the x direction and directed along x is injected at $x = 0$. Again, we assume that the injected current is homogeneous along y at the injection edge and that the lateral edges of the sample are impenetrable [i.e., $j_{yb}(y = \pm L/2) = 0$ for any spin polarization b]. The situation is, to some extent, similar to the extrinsic case depicted in Fig. 1. However, while the swapping effect in this scenario is straightforward for the extrinsic case, it is much more complex and rich for intrinsic spin swapping. As mentioned before, analytical expressions can be found for the spin currents and accumulations far away from the lateral boundaries, at distances much larger than l_s. In this region, the influence of the boundaries is weak, and the expressions approach the limit of a system that is infinite in the y direction. We thus find that a transverse spin current j_{yy} flowing along the y direction carrying spins polarized along y is induced,

$$\frac{j_{yy}(x)}{j_{xx}^{(0)}} = e^{-k_r x/l_s}\left[(\sqrt{2}-1)\cos(k_i x/l_s) - \frac{3+\sqrt{2}}{\sqrt{7}}\sin(k_i x/l_s)\right], \tag{10}$$

where $k_{r/i} = \sqrt{2\sqrt{2}\mp 1}$. This is the intrinsic spin swapping effect. The induced spin current reaches its maximum, $|j_{yy}(x_{\max})|/j_{xx}^{(0)} \approx 61\%$, within one spin-orbit precession length from the injection edge at $x = 0$. The injected spin current itself decays away from the spin current source at $x = 0$,

$$\frac{j_{xx}(x)}{j_{xx}^{(0)}} = e^{-k_r x/l_s}\left[\cos(k_i x/l_s) + \frac{k_r^2}{\sqrt{7}}\sin(k_i x/l_s)\right]. \tag{11}$$

While extrinsic spin swapping in general directly couples x-polarized and y-polarized spins, in intrinsic spin swapping the conversion between x-polarized and y-polarized spin currents occurs via spins polarized along z as can be seen from Eqs. (8) and (9). In addition, spin currents and spin accumulations oscillate as a function of the distance from the injection edge. The situation is depicted in Fig. 2 for a system with width $L = 4l_s$ and length $L_x = 16l_s$. In Fig. 2(a), we see that the spin current carrying spins polarized along x, which is given by Eq. (11) in the bulk, as well as the spin accumulation decay away from the spin current source at $x = 0$. The x components of the spins are converted to z components, as shown in Fig. 2(c), which in turn gives rise to a swapped transverse spin current j_{yy}, shown in Fig. 2(b), that is polarized along y. In the bulk, this current is given by Eq. (10). We also see that this swapped spin current causes an oscillating spin accumulation at the lateral edges, which is a signature of the intrinsic spin swapping effect that may be probed experimentally (see Sec. IV for an explicit expression of this spin swapping induced spin accumulation in a narrow strip system).

Next, we turn to the case in which a homogeneous spin current $j_{xy}^{(0)} = j_{xy}(x=0)$ carrying spins polarized along y is injected at $x = 0$. To analyze this situation, we first find an analytic expression for the transverse spin current induced through spin swapping far from the lateral edges of the system. We find that the primary spin current j_{xy} is directly transformed into a transverse spin current,

$$\frac{j_{yz}(x)}{j_{xy}^{(0)}} = -e^{-2x/l_s} = -\frac{j_{xy}(x)}{j_{xy}^{(0)}}, \tag{12}$$

that gives rise to an accumulation of z spins at the lateral edges of the sample (again, refer to Sec. IV for an explicit expression for the induced spin accumulation in a narrow strip system). In contrast to the case of extrinsic spin swapping, Eqs. (8) and (9) provide a direct coupling between the y and z spins, with

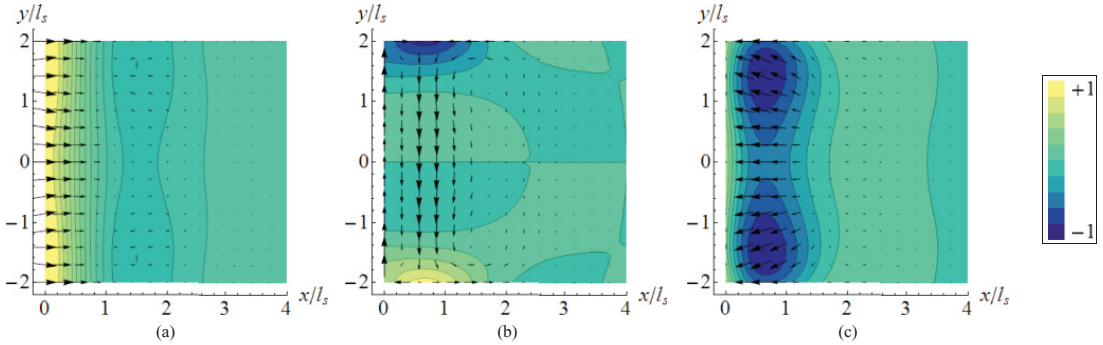

FIG. 2. (Color online) The intrinsic spin swapping effect in a two-dimensional diffusive metal of width $L = 4l_s$ and length $L_x = 16l_s$. (a) Spin density and spin current polarized along x. (b) Spin density and spin current polarized along y. (c) Spin density and spin current polarized along z. A primary spin current $j_{xx}^{(0)}$ injected at $x = 0$ in (a) induces an oscillating transverse spin current j_{yy} in (b) through coupling with the z components of the spins in (c). The resulting accumulation of y components of the spins at the sample edges in (b) is a signature of the intrinsic spin swapping effect. Shown are the spin densities and spin current densities according to Eqs. (8) and (9) on a relative scale for each plot. Note that all quantities are of the same order of magnitude.

the resulting spin current having polarization along z (rather than x): Again, the resulting current is of the same order as the primary spin current. It is only near the lateral boundaries that spin currents polarized along x are generated as well. This spin current leads to an oscillating spin accumulation at the sample edges. This situation is depicted in Fig. 3.

In both scenarios of injected spin currents discussed above, intrinsic spin swapping is a much stronger effect than extrinsic spin swapping.

IV. INTRINSIC SPIN SWAPPING IN A NARROW STRIP

In this section, we will consider the special case of a strip whose width L is much less than l_s. This case is interesting because, in such a system, a long-range spin swapping effect can be realized, such that the spin-swapped accumulation can extend far along the strip, over a length much greater than l_s. This long-range behavior is closely related to the increase of the D'yakonov-Perel spin relaxation time in narrow strips.[18]

Due to the small parameter L/l_s, the spin-swapping problem can be treated analytically. Following Ref. 18, we introduce new spin density variables,

$$\psi_{\pm 1} = \frac{1}{\sqrt{2}}(\pm f_x - i\, f_y), \quad \psi_0 = f_z. \tag{13}$$

In terms of these variables, Eq. (8) can be transformed into

$$\left(i\,\partial_x + \frac{2}{l_s}J_y\right)^2 \boldsymbol{\psi} + \left(i\,\partial_y - \frac{2}{l_s}J_x\right)^2 \boldsymbol{\psi} = 0, \tag{14}$$

where $\boldsymbol{\psi}$ is a 3-vector $(\psi_1, \psi_0, \psi_{-1})^{\mathrm{T}}$ and J_i, $i \in \{x, y, z\}$, are the corresponding 3×3 angular momentum operators for

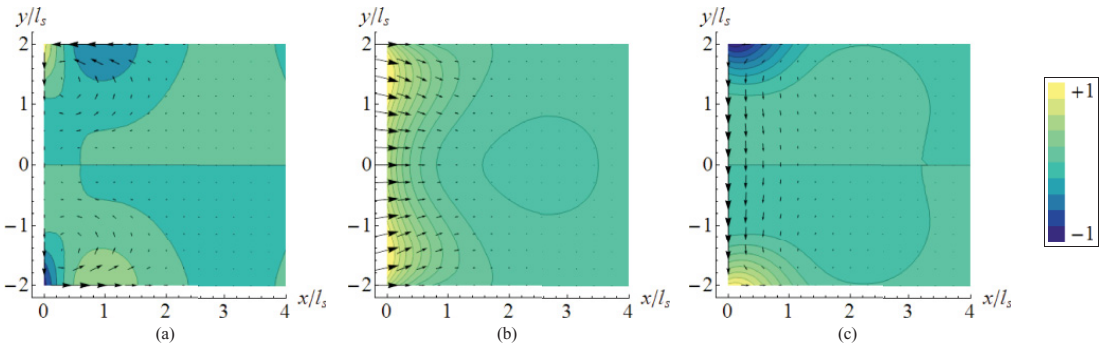

FIG. 3. (Color online) The intrinsic spin swapping effect in a two-dimensional diffusive metal of width $L = 4l_s$ and length $L_x = 16l_s$. (a) Spin density and spin current polarized along x. (b) Spin density and spin current polarized along y. (c) Spin density and spin current polarized along z. A primary spin current $j_{xy}^{(0)}$ injected at $x = 0$ in (b) induces a transverse spin current j_{yz} in (c). In turn, this leads to an accumulation of z spins at the sample edges, which is a signature of the intrinsic spin swapping effect. In (a), an oscillating spin current polarized along x is only generated close to the lateral edges of the system. Shown are the spin densities and spin current densities according to Eqs. (8) and (9) on a relative scale for each plot. Note that all quantities are of the same order of magnitude.

spin 1. Using Eq. (9), the boundary conditions can be expressed as

$$\left(i\,\partial_x + \frac{2}{l_s}J_y\right)\boldsymbol{\psi}|_{x=0} = \boldsymbol{I}, \tag{15a}$$

$$\left(i\,\partial_y - \frac{2}{l_s}J_x\right)\boldsymbol{\psi}|_{y=\pm L/2} = 0, \tag{15b}$$

where $\boldsymbol{I}$ is determined by the spin current injected at $x = 0$,

$$I_{\pm 1} = \frac{i}{\sqrt{2}D}\left(\mp j^{(0)}_{xx} + i\,j^{(0)}_{xy}\right), \quad I_0 = -\frac{i}{D}j^{(0)}_{xz}. \tag{15c}$$

The unitary transformation,

$$\boldsymbol{\psi} = e^{i\,J_x(\pi/2 - 2y/l_s)}\boldsymbol{\phi}, \tag{16}$$

further simplifies Eq. (14) to

$$\left(i\,\partial_x + \frac{2}{l_s}J_y(y)\right)^2\boldsymbol{\phi} - \partial_y^2\boldsymbol{\phi} = 0, \tag{17}$$

where $J_y(y) = e^{-i\,J_x(\pi/2-2y/l_s)}J_y\,e^{i\,J_x(\pi/2-2y/l_s)}$, and the boundary conditions at the lateral edges of the system then read

$$\partial_y\boldsymbol{\phi}|_{y=\pm L/2} = 0. \tag{18}$$

The transformed differential equations (17) and the boundary conditions (18) are exact equivalent representations of the original problem.

For the case of a narrow strip, $L \ll l_s$, one can expand $J_y(y)$ up to second order in y/l_s to obtain $J_y(y) = J_z + 2(y/l_s)J_y - 2(y/l_s)^2 J_z$ and consider the last two terms in this expression as a perturbation. Due to Eq. (18), the solution of Eq. (17) can be represented as a Fourier expansion in $(\sin(2n+1)\pi y/L)$ and $\cos(2n\pi y/L)$, where n is an integer. Further analysis reveals that only a term uniform in y is relevant because the other Fourier components decay very quickly along the x direction. The equation for $\bar{\boldsymbol{\phi}}$, that is, $\boldsymbol{\phi}$ averaged over $-L/2 \leqslant y \leqslant L/2$, can then be derived from Eq. (17) as[18]

$$\left(i\,\partial_x + \frac{2}{l_s}J_z\right)^2\bar{\boldsymbol{\phi}} + \frac{\Gamma}{l_s^2}(2 - J_z^2)\bar{\boldsymbol{\phi}} = 0, \tag{19}$$

where $\Gamma = 2L^2/3l_s^2$. The general solution of this equation that converges for $x \to \infty$ has the form $\bar{\phi}_{\pm 1} = A_{\pm 1}\,e^{\pm 2\,i\,x/l_s}\,e^{-\sqrt{\Gamma}x/l_s}$ and $\bar{\phi}_0 = A_0\,e^{-\sqrt{2\Gamma}x/l_s}$. The coefficients A can be found from the boundary condition (15a).

If we consider a case analogous to that presented for extrinsic spin swapping in Sec. II, where a spin current $j^{(0)}_{xx}$ carrying spins polarized along x is injected, we find $I_{\pm 1} = \mp\frac{i}{\sqrt{2}D}j^{(0)}_{xx}$ and $I_0 = 0$. Applying the unitary operator (16) to this boundary condition we obtain in the leading approximation,

$$\bar{\phi}_{\pm 1}(x=0) = \pm\frac{j^{(0)}_{xx}l_s}{\sqrt{2\Gamma}D}, \quad \bar{\phi}_0(x=0) = 0. \tag{20}$$

From this it follows that

$$\bar{\phi}_{\pm 1} = \pm\frac{j^{(0)}_{xx}l_s}{\sqrt{2\Gamma}D}\,e^{\pm 2\,i\,x/l_s - \sqrt{\Gamma}x/l_s}, \quad \bar{\phi}_0 = 0. \tag{21}$$

Using Eqs. (16) and (13), we finally obtain the spin densities,

$$f_x = \frac{j^{(0)}_{xx}l_s}{\sqrt{\Gamma}D}\,e^{-\sqrt{\Gamma}x/l_s}\,\cos(2x/l_s), \tag{22a}$$

$$f_y = -2\frac{j^{(0)}_{xx}l_s}{\sqrt{\Gamma}D}\frac{y}{l_s}\,e^{-\sqrt{\Gamma}x/l_s}\,\sin(2x/l_s), \tag{22b}$$

$$f_z = -\frac{j^{(0)}_{xx}l_s}{\sqrt{\Gamma}D}\,e^{-\sqrt{\Gamma}x/l_s}\,\sin(2x/l_s), \tag{22c}$$

to first order in y/l_s. The accumulation of y spins at the lateral edges of the narrow strip caused by the intrinsic spin swapping effect reads

$$f_y(y = \pm L/2) = \mp\sqrt{\frac{3}{2}}\frac{j^{(0)}_{xx}l_s}{D}\,e^{-\sqrt{\Gamma}x/l_s}\,\sin(2x/l_s). \tag{23}$$

Since $\sqrt{\Gamma}/l_s \ll 1$, the spin accumulation oscillates and slowly decreases along x.

Considering the second case treated in Sec. III, where a spin current $j^{(0)}_{xy}$ carrying spins polarized along y is injected, a similar calculation yields

$$f_x = 0, \tag{24a}$$

$$f_y = \frac{j^{(0)}_{xy}l_s}{\sqrt{2\Gamma}D}\,e^{-\sqrt{2\Gamma}x/l_s}, \tag{24b}$$

$$f_z = -2\frac{j^{(0)}_{xy}l_s}{\sqrt{2\Gamma}D}\frac{y}{l_s}\,e^{-\sqrt{2\Gamma}x/l_s}. \tag{24c}$$

Again, the spin densities slowly decay along x but, analogous to the previous discussion, no oscillation takes place.

V. EXPERIMENTAL OBSERVATION OF SPIN SWAPPING

In order to observe spin swapping, a primary spin current needs to be injected. This can be achieved in a two terminal setup where a spin current is electrically injected into a two-dimensional diffusive metal from a ferromagnetic electrode.[16] As discussed here, spin swapping then gives rise to spin accumulations at the lateral sample edges that could be detected experimentally, for example, by optical means[10] or by measuring the interface voltage at weak contacts between the lateral boundaries and ferromagnets.[12,14,15] However, in such a setup, an electric current is present in the system as well and additional spin currents therefore emerge from the coupling of charge and spin via the spin Hall effect. In a two-dimensional system with extrinsic spin-orbit coupling, the spin accumulations resulting from spin swapping at the lateral sample edges are polarized in-plane while those generated by the electric current via the spin Hall effect are polarized out-of-plane.[2,3] This makes it possible to experimentally distinguish the two effects. On the other hand, in a diffusive system with intrinsic Rashba spin-orbit coupling, a uniform electric field gives rise to a uniform in-plane spin polarization via the Edelstein effect (while it does not produce spin currents).[22,23] In contrast, the resulting in-plane accumulation of swapped spins generated by a primary spin current with in-plane polarization is opposite at the lateral boundaries, as discussed above. This difference allows one to distinguish the intrinsic spin swapping effect and the Edelstein effect in experiment.

Another possibility is the use of a nonlocal geometry[14] where the spin swapping effects could be observed in a part of the system where there is no charge current. There, an electric current is injected from a ferromagnetic electrode on top of a diffusive metal toward a second electrode. A tunnel barrier between the electrodes and the metal assures that the current is injected uniformly and it optimizes the polarization of the injected electrons. A pure spin current is thus generated in the system, propagating in the opposite direction of the injected charge current and away from the electrodes. This spin current will give rise to spin accumulations at the lateral sample edges through the spin swapping effect that could be detected experimentally.

VI. CONCLUSION

In conclusion, we have demonstrated that there is an intrinsic analog to the extrinsic spin swapping effect in two-dimensional diffusive metals with Rashba spin-orbit coupling. We found that the intrinsic effect is drastically different because it is large for system dimensions exceeding the spin-orbit precession length and gives rise to secondary spin currents and accumulations that are of the same order of magnitude as the injected primary spin currents while leading to a long-range propagation of spin polarizations in narrow strip systems. In contrast, the extrinsic spin swapping effect is proportional to the spin-orbit coupling strength for any system size and is therefore small. Moreover, intrinsic spin swapping is more complex and richer than its extrinsic counterpart, resulting in a nontrivial dependence on the relative orientation of the injected spin flow and the spin polarization.

We derived explicit expressions for the transverse spin currents in the bulk and numerically computed the resulting spin accumulations at the lateral boundaries. In addition, we derived explicit expressions for the spin accumulations in a narrow strip when $L \ll l_s$ and found that the exponential decay of spin polarizations along the x direction is greatly reduced in such systems. We further gave a brief discussion on how the spin swapping effect could be observed in experiment.

ACKNOWLEDGMENTS

This work was partially supported by the Research Council of Norway.

[1] R. Karplus and J. M. Luttinger, Phys. Rev. **95**, 1154 (1954).
[2] M. I. Dyakonov and V. I. Perel, Sov. Phys. JETP Lett. **13**, 467 (1971).
[3] M. I. Dyakonov and V. I. Perel, Phys. Lett. A **35**, 459 (1971).
[4] J. E. Hirsch, Phys. Rev. Lett. **83**, 1834 (1999).
[5] S. Zhang, Phys. Rev. Lett. **85**, 393 (2000).
[6] S. Murakami, N. Nagaosa, and S.-C. Zhang, Science **301**, 1348 (2003).
[7] J. Sinova, D. Culcer, Q. Niu, N. A. Sinitsyn, T. Jungwirth, and A. H. MacDonald, Phys. Rev. Lett. **92**, 126603 (2004).
[8] H.-A. Engel, E. I. Rashba, and B. I. Halperin, in *Handbook of Magnetism and Advanced Magnetic Materials*, edited by H. Kronmüller and S. Parkin, Vol. 5 (Wiley, Chichester, 2007), pp. 2858–2877.
[9] Y. K. Kato, R. C. Myers, A. C. Gossard, and D. D. Awschalom, Science **306**, 1910 (2004).
[10] V. Sih, R. C. Myers, Y. K. Kato, W. H. Lau, A. C. Gossard, and D. D. Awschalom, Nat. Phys. **1**, 31 (2005).
[11] J. Wunderlich, B. Kaestner, J. Sinova, and T. Jungwirth, Phys. Rev. Lett. **94**, 047204 (2005).
[12] E. Saitoh, M. Ueda, H. Miyajima, and G. Tatara, Appl. Phys. Lett. **88**, 182509 (2006).
[13] N. P. Stern, S. Ghosh, G. Xiang, M. Zhu, N. Samarth, and D. D. Awschalom, Phys. Rev. Lett. **97**, 126603 (2006).
[14] S. Valenzuela and M. Tinkham, Nature (London) **442**, 176 (2006).
[15] T. Kimura, Y. Otani, T. Sato, S. Takahashi, and S. Maekawa, Phys. Rev. Lett. **98**, 156601 (2007).
[16] M. B. Lifshits and M. I. Dyakonov, Phys. Rev. Lett. **103**, 186601 (2009).
[17] The terms responsible for extrinsic spin swapping were already indicated in Refs. 2 and 3. However, their physical origin was not understood at the time.[16]
[18] A. G. Mal'shukov and K. A. Chao, Phys. Rev. B **61**, R2413 (2000).
[19] Y. A. Bychkov and E. I. Rashba, J. Phys. C **17**, 6039 (1984).
[20] C. S. Tang, A. G. Mal'shukov, and K. A. Chao, Phys. Rev. B **71**, 195314 (2005).
[21] A. Brataas, A. G. Mal'shukov, and Y. Tserkovnyak, New J. Phys. **9**, 345 (2007).
[22] V. Edelstein, Solid State Commun. **73**, 233 (1990).
[23] J.-I. Inoue, G. E. W. Bauer, and L. W. Molenkamp, Phys. Rev. B **67**, 033104 (2003).
[24] J. Rammer, *Quantum Field Theory of Non-Equilibrium States* (Cambridge University Press, Cambridge, 2007).
[25] R. Raimondi and P. Schwab, Physica E **42**, 952 (2010).

Paper 3

Extrinsic spin-orbit induced spin, charge, and energy transport
in diffusive superconductors.
Preprint, 2013.

Is not included due to copyright